Downloaded from orbit.dtu.dk on: May 06, 2023

DTU Library

Reconstruction Methods for Inverse Problems with Partial Data

Hoffmann, Kristoffer

Publication date:
2015

Document Version
Publisher's PDF, also known as Version of record

Link back to DTU Orbit

Citation (APA):
Hoffmann, K. (2015). *Reconstruction Methods for Inverse Problems with Partial Data*. Technical University of Denmark. DTU Compute PHD-2014 No. 344

General rights
Copyright and moral rights for the publications made accessible in the public portal are retained by the authors and/or other copyright owners and it is a condition of accessing publications that users recognise and abide by the legal requirements associated with these rights.

- Users may download and print one copy of any publication from the public portal for the purpose of private study or research.
- You may not further distribute the material or use it for any profit-making activity or commercial gain
- You may freely distribute the URL identifying the publication in the public portal

If you believe that this document breaches copyright please contact us providing details, and we will remove access to the work immediately and investigate your claim.

Reconstruction Methods for Inverse Problems with Partial Data

Kristoffer Hoffmann

PhD Thesis

2014

Reconstruction Methods for Inverse Problems with Partial Data

Kristoffer Hoffmann

Thesis submitted: July 14th, 2014

Thesis defended: August 25th, 2014

PhD degree awarded: September 25th, 2014

PhD supervisor: Associate Professor Kim Knudsen
Department of Applied Mathematics and Computer Science
Technical University of Denmark

PhD committee: Professor Dr. Bastian von Harrach
Department of Mathematics
University of Stuttgart

Professor Gunther Uhlmann
Department of Mathematics
University of Washington

Professor Steen Markvorsen
Department of Applied Mathematics and Computer Science
Technical University of Denmark

Technical University of Denmark
Department of Applied Mathematics and Computer Science
Richard Petersens Plads, Building 324
2800 Kongens Lyngby, Denmark
Phone +45 4525 3031
compute@compute.dtu.dk
www.compute.dtu.dk

PHD-2014-344
ISSN 0909-3192

Preface

This thesis was prepared in partial fulfilment of the requirements for acquiring the PhD degree at the Technical University of Denmark (DTU). The work was carried out between July 2011 and July 2014 at the Section for Scientific Computing at the Department of Applied Mathematics and Computer Science (formerly Department of Mathematics), DTU, under the supervision of Associate Professor Kim Knudsen.

During my studies I have co-authored the following papers:

- K. Hoffmann, G. Bal, and K. Knudsen
  On the Propagation of Singularities for a Class of Hybrid Inverse Problems
  To be submitted
- K. Hoffmann, and K. Knudsen
  Iterative Reconstruction Methods for Hybrid Inverse Problems in Impedance Tomography
  Sensing and Imaging, Vol. 15, 96, 2014.

The aim of this thesis has been to present and document my work, and more specifically to provide new mathematical insight for a class of hybrid inverse problems in impedance tomography. As a natural consequence, the key parts of this thesis therefore build upon the aforementioned papers. Accordingly, most of the theoretical results stated in the first paper are also presented in Chap. 4, and likewise, the numerical analyses and results of the second paper are to some extent repeated in Chap. 5. However, in this thesis I provide a much more thorough theoretical and numerical analysis, and present several unpublished results, especially related to partial data and limited-view data.

Acknowledgements

During my studies I have benefited from discussions, remarks and advice from various individuals. Foremost, I would like to thank my advisor, Associate Professor Kim Knudsen, for the continuous support during my study and research, for his motivation, and his ability to ask the right questions. He has provided me with the freedom to work independently, and I have enjoyed having him as an advisor.

I would also thank the members of the Section for Scientific Computing for all their support, help, and advice over the years. The friendly working environment among my colleagues at the Department of Applied Mathematics and Computer Science, and the former Department of Mathematics, has been a motivating factor throughout my studies.

In the last four months of 2012 I worked with the research group of Professor Guillaume Bal at the Department of Applied Physics and Applied Mathematics at Columbia University, New York. The visit was very beneficial for me, both on a professional and personal level, and I would like to thank Guillaume for being a very friendly host and for taking the time to supervise me during my stay. My thanks also goes to the rest of the research group, for interesting mathematical discussions and recommendations.

Finally, I would like to thank the Otto Mønsted Foundation for financial support in connection with conferences and during my stay in New York, and the Fields Institute at the University of Toronto for financial support during my stay at a month-long workshop in July 2012.

Kgs. Lyngby
July 14th, 2014

Kristoffer Hoffmann

Summary (English)

This thesis presents a theoretical and numerical analysis of a general mathematical formulation of hybrid inverse problems in impedance tomography. This includes problems from several existing hybrid imaging modalities such as Current Density Impedance Imaging, Magnetic Resonance Electrical Impedance Tomography, and Ultrasound Modulated Electrical Impedance Tomography.

After giving an introduction to hybrid inverse problems in impedance tomography and the mathematical tools that facilitate the related analysis, we explain in detail the stability properties associated with the classification of a linearised hybrid inverse problem. This is done using pseudo-differential calculus and theory for overdetermined boundary value problem. Using microlocal analysis we then present novel results on the propagation of singularities, which give a precise description of the distinct features of solutions in the case of a non-elliptic problem.

To conduct a numerical analysis, we develop four iterative reconstruction methods using the Picard and Newton iterative schemes, and the unified approach to the reconstruction problem encompasses several algorithms suggested in the literature. The algorithms are implemented numerically in two dimensions and the properties of the algorithms and their implementations are investigated theoretically. Novel numerical results are presented for both the full and partial data problem, and they show similarities and differences between the proposed algorithms, which are closely linked to the results of the theoretical analysis. The findings in this thesis justify that the choice of algorithm should be based on a theoretical analysis of the underlying inverse problem.

Summary (Danish)

Denne afhandling indeholder en teoretisk og numerisk analyse af en generel matematisk model for hybrid-inverse problemer i impedanstomografi. Modellen beskriver flere eksisterende metoder fra hybrid billeddannelse, såsom Current Density Impedance Imaging, Magnetic Resonance Electrical Impedance Tomography og Ultrasound Modulated Electrical Impedance Tomography.

Efter en indledende matematisk beskrivelse af problemet, og de relaterede matematiske værktøjer, beskrives stabilitetsegenskaberne af det lineariserede hybrid-inverse problem. Disse resultater er baseret på teorien for pseudodifferential-operatorer og overdeterminerede randværdiproblemer. Ved brug af mikrolokal analyse udledes herefter nye resultater, som giver en præcis beskrivelse af de særprægede egenskaber, der hører til løsningerne af et ikke-elliptisk problem.

Den numeriske analyse er baseret på fire iterative rekonstruktionsmetoder, som udvikles på baggrund af Picard- og Newton-metoden. Den generelle tilgang til det inverse problem betyder, at rekonstruktionsmetoderne i flere tilfælde generaliserer metoder, der allerede findes i litteraturen. Vi implementerer derefter de fire algoritmer og laver en teoretisk analyse af deres egenskaber. Herefter præsenteres nye numeriske rekonstruktionsresultater for det inverse problem med både komplet og begrænset data. Resultaterne påviser både ligheder og forskelle mellem metoderne, som kan forklares ved at henlede til den teoretiske analyse. Resultaterne af den numeriske analyse berettiger, at valget af rekonstruktionsmetode bør baseres på en teoretisk analyse af det tilgrundliggende inverse problem.

Contents

Chapter 1

Introduction

Mathematical modelling is often motivated by the wish to shape our understanding of physical phenomena and to predict the measurements of quantities related to known physical systems. Indeed, one can always predict the behaviour of any deterministic physical system given a sufficiently precise mathematical model. Likewise, a physical system may be identified and characterised based on measurements of its behaviour.

The mathematical formulation related to the inversion of measurements is known as an inverse problem. Here the problem is to recover certain properties of the physical system based on actual measurements of the behaviour. In situations where knowledge about such properties is not available, solving the inverse problem gives valuable information that we otherwise cannot directly observe.

Inverse problems form a multidisciplinary field combining mathematics with many branches of physics, chemistry and biology, and covers a wide range of applications. Examples are problems from medical imaging, geophysics and astronomy, where abstract mathematical formulations can be used to devise procedures to convert exterior measurements into information about interior properties [28, 33, 88]. Despite their similar appearance, inverse problems can be based on entirely different mathematical formulations, and there are inevitably problem dependent challenges associated with both their theoretical and numerical analysis [41, 48, 73].

Within the field of medical imaging there exists a variety of popular imaging techniques, and there is a constant development and refinement of such non-invasive methods. A new generation of imaging methods formulate procedures based on measurements obtained from several existing modalities. These are called *hybrid imaging methods*. An analysis of the corresponding mathematical models, described by *hybrid inverse problems*, can predict how well such methods will perform and, from the perspective of applications, provides a general guideline for further development [8, 11, 83].

The primary subject of this thesis is to present a theoretical and numerical analysis of a class of hybrid inverse problems related to applications in medical imaging; or more precisely, impedance tomography. We present many interesting novel theoretical results, primarily concerned with the propagation of singularities for the non-elliptic linearised inverse problem. Another major contribution is the development, analysis, implementation and comparison of several iterative reconstruction methods, among which some are new.

In this chapter we present a short and general introduction to the mathematics behind inverse problems and give some examples of existing methods from medical imaging. We introduce hybrid inverse problems, by formulating a simple mathematical model for impedance tomography, and then give two examples of hybrid modalities. These work as models for the more general mathematical formulation of a hybrid inverse problem, which will be the main subject of analysis in this thesis. In the end of this chapter we provide a reading guide.

1.1 Inverse problems

The mathematical formulation of an inverse problem is often based on a map between function spaces

$$\mathcal{F}_\sigma : x \mapsto y.$$

Here $\mathcal{F}_\sigma$ is an operator that models the physical system, which depends on an underlying function σ usually modelling an unknown physical property, x represents a chosen physical disturbance, and y the corresponding physical reaction. Based on knowledge of $\mathcal{F}_\sigma$ and pairs $\{x, y\}$, the inverse problem is to find the function σ. This corresponds to an inversion of the map

$$\sigma \mapsto \mathcal{F}_\sigma.$$

In mathematical terms, $\mathcal{F}_\sigma$ could be a differential or integral operator, or in more abstract formulations, say, a Poincaré-Steklov operator.

Most inverse problems are not difficult to formulate because the physical system can often be described in terms of mathematical notion and language, but usually their analysis turns out to be difficult and relies on advanced techniques from several fields of mathematics. This is an interesting feature of inverse problems.

The mathematical analysis of often related to qualitative features such as existence, uniqueness and stability of solutions. The question of existence is related to existence of a physical property that generates the observed data. From the perspective of a physical system, this is of course always satisfied, but the existence of solutions to the mathematical model is always questionable. In particular, this could be the case if the observed data for some reason is imprecise. In mathematical terms, this corresponds to data outside the range of the map that models the physical system. In the mathematical context, one should also pay close attention to the use of the word *solution*, because this is often defined in a specific formulation of the original problem.

Uniqueness is typically expressed as necessary or sufficient conditions for which the observed data uniquely determines the physical property. How to actually reconstruct the physical property, given the observed data, is a completely different question, but seen from the perspective of applications, this is often the most important one.

Stability is a measure of how sensitive the model of the physical system is to changes in the unknown property. A common challenge for inverse problems is bad stability properties, such that small changes in the observed data, can correspond to large changes in the physical property. If the observed data is contaminated by noise, this property is of course a critical element. If an inverse problem has either bad stability properties, or does not have a unique solution, then the problem is said to be *ill-posed*, and special care needs to be taken in the development of reconstruction methods. Additional challenges are related to practical limitations of the physical system, which need to be included in the model and analysis.

This thesis will consider the analysis of certain inverse problems related to medical imaging, where the recovery of interior properties provides valuable information that could help in diagnostics, treatment monitoring and response evaluation. These problems describe methods based on exterior measurements that in some way quantify how externally imposed physical fields are affected by an unknown physical property as they propagate inside a given object. This naturally leads to mathematical models expressed by inverse problems.

1.1.1 Examples from medical imaging

Within the class of mathematical models from medical imaging we find several examples of inverse problems. A few of these are:

- X-ray tomography, also known as radiography, or the related method of Computerised Tomography (CT). Here one measures attenuation of a collimated beam of radiation that passes through an object and this is used to reconstruct the spatially varying interior absorption coefficient, called the radiodensity [46]. The inverse problem from CT is based on the inversion of the Radon transform, which is a well-known example of a mildly ill-posed problem [77].
- Magnetic Resonance Imaging (MRI), that uses an oscillating magnetic field to manipulate the magnetic properties of hydrogen atoms inside an object. The exited atoms emit material dependent radio-frequency signals which are then recorded. This can be used to generate an image representing the material composition of the interior. The basic physics and mathematics behind MRI is explained in detail by Buxton [21]. Note that the inversion process does not amplify noise, since it is based on a discrete Fourier transform. The inverse problem in MRI is therefore not ill-posed [66].
- Medical ultrasound, a well-known method for diagnostic sonography. Ultrasonic waves are produced with the purpose of penetrating a chosen medium. As the waves propagate, some are scattered and reflected at interior interfaces. This wave response is measured and provides information about the inner structure of the medium. The mathematical formulation is based on the inverse scattering problem which is generally ill-posed [26]. We refer to Duck et al. [30] for an introduction to medical ultrasound.
- Electrical Impedance Tomography (EIT), which recovers the interior conductivity distribution of an object, based on current and voltage pairs measured on electrodes attached on the boundary. The inverse problem from EIT is known as the Calderón problem, and mathematically it corresponds to reconstructing the coefficient of a second-order divergence form elliptic differential operator from an associated boundary data map. This is an example of an inverse problem, where the physical system, which depends on the unknown interior conductivity distribution, is described by a Poincaré-Steklov operator. Much work has been used on the theoretical and numerical analysis of this problem in order to describe this dependence. An introduction to the methods, history and applications of EIT can be found in many texts [19, 44, 73]. Note that the inverse problem from EIT is severly ill-posed.

Because the presented imaging methods reconstruct different physical properties, they all have individual advantages and disadvantages as stand-alone modalities, and their practicality depends on the specific application in mind. In medical imaging, the goal is to obtain high contrast and high spatial resolution interior information that makes it possible to classify different parts of the image and identify small details, which often is necessary for early diagnostics. Note that contrast is a feature of the reconstructed physical quantity, while the spatial resolution is determined entirely by the choice of reconstruction method. The cost and safety of the method is of course also an important parameter.

The ability of an imaging method to produce a high resolution reconstruction is closely linked the type of physics that the measurements are based on. High resolution methods often rely on electromagnetic or mechanical waves that, to a certain extend, can be focused in space and thereby generate measurements that include spatial information. In the other hand, methods based on electrical measurements are usually of low resolution, since electric fields are diffusive by nature and therefore impossible to focus.

As an example of the individual advantages and disadvantages, we can mention that medical ultrasound, which is considered a high resolution modality, cannot be used to detect early stage breast tumours, simply because the behaviour of acoustic waves is very similar in healthy and cancerous breast tissue; that is, the contrast in the acoustic property is too low. On the other hand, the electrical properties between healthy and cancerous breast tissue can differ by several factors, which speaks in favour of EIT [54].

Conductivity reconstructions from EIT are typically of low resolution, because the method is based on a model of the diffusive nature of electric fields. Furthermore, the inverse problem from EIT is ill-posed, which makes the reconstruction very sensitive to noise and modelling errors. Reconstruction methods for ill-posed inverse problems, such as the one from EIT, therefore rely on mathematical constructions to reduce the effects of the ill-posedness. A common choice is to impose additional smoothness assumptions or utilise certain a priori knowledge. This process is known as regularisation [32]. It is not possible to develop a well-performing reconstruction method for EIT without such procedures, simply because the ill-posedness of the problem is inherited directly from the physics it models. A different approach is to consider another physical setting, for which the mathematical model inherits better stability properties and the reconstruction obtains the best possible contrast and resolution. This is the motivation behind the development of hybrid imaging methods.

1.2 Hybrid inverse problems

If a single imaging method does not provide an acceptable reconstruction, it seems natural to utilise information from multiple modalities. Of course, the methods should then be chosen such that they complement each other; that is, they should not share the same disadvantages. If the chosen imaging methods complement each other, it is possible to increase the contrast, resolution, and stability of the reconstruction.

A simple approach would be to draw conclusions based on a collection of different recovered properties. The combined PET/CT scan is an example of such a procedure [54]. Another possibility is to derive a reconstruction scheme based on measurements from multiple imaging methods. Here a physical field related to one method, is measured by other methods. In this setting the modelling is based on existing physical descriptions, but the inverse problem is different and a new reconstruction scheme has to be developed. Magnetic Resonance EIT (MREIT) is an example of such a problem. Here the two individual modalities are used simultaneously to obtain additional interior data, for which a new reconstruction scheme is developed. We explain the basic idea behind MREIT on p. 9.

Finally, it is possible to formulate a new model based on an interaction between certain physical properties and high intensity physical fields. Here a physical coupling makes it possible, at least in theory, to obtain very good approximations of interior physical quantities. This could theoretically produce interior data with both high resolution and high contrast, if it is based on well-chosen coupled modalities that include a high resolution method and measurements of a physical property of high contrast. Again, a new inverse problem is formulated for the interior data. Ultrasound modulated EIT (UMEIT) is an imaging method that utilises such a coupling to measure additional interior data. We will explain the basic idea behind UMEIT on p. 10.

The particular field of imaging modalities, that combines two or more existing methods, is often called *hybrid imaging* and the associated inverse problems are called *hybrid inverse problems*. In some parts of the literature, these methods are also called multi-physics, coupled physics or multi-wave techniques. Some choose to use the term hybrid imaging exclusively for methods that rely on coupled-physics phenomena. A survey of hybrid imaging methods can be found in the review papers on the subject [8, 12, 54].

A hybrid imaging modality can often mathematically be considered as a two-step process: The first step is related to the modelling of experimental apparatus and the physical fields and couplings, and provides a strategy on how to recover

the interior data. The second step is the reconstruction of the relevant physical parameters using the available mathematical models, the exterior measurements and the recovered interior data sets. In this thesis we only consider the second step and present a theoretical and numerical analysis of a specific class of non-linear hybrid inverse problems augmented with interior data of infinite precision. These problems are generalisations of hybrid imaging modalities related to impedance tomography.

The mathematical model of impedance tomography is based on the fundamental concepts of electricity and magnetism, being static or time-dependent, which are naturally related by Maxwell's equations. These equations defines the electromagnetic properties of materials by the constitutive relations between the electric field quantities and the magnetic field quantities [47]. Electrically charged particles exert a force on other electrically charged objects. This phenomena is explained using the concept of electric fields. The size of the electric field is defined as the electric force per unit charge and the direction of the field is defined to be the direction of the force it would exert on a *stationary* positive charge. In the same way, an electric field that changes over time introduces a local magnetic field defined by the (Lorentz) force it would exert on a *moving* electrically charged particle.

Table 1: Electrical properties of biological tissues at 10 kHz [19].

Tissue type	**Conductivity** [S/m]	**Permittivity** [μF m^{-1}]
Muscle	0.131	0.49
Liver	0.146	0.49
Heart	0.167	0.88
Fat	< 0.1	0.18
Lung	0.105	0.22

On a macroscopic level, the electrical properties of any biological tissue can be expressed using the notions of conductivity and permittivity. In the presence of an external applied electric field, the conductivity is a measure of the ability to *transport* charge and the permittivity is a measure of the ability to *store* charge. In other words, these properties determine the exact pattern flow of current. Attributes like cell concentration, cellular structure, molecular composition and membrane capacitance, all influence the electrical properties of tissues [58]. As an example of this, the conductivity and permittivity of five types of biological tissue are listed in Tab. 1. From this we see that spatial information about the interior distribution of the electrical properties could make it possible to characterise and localise the type of tissue. The macroscopic electrical properties

of biological tissues, is explained in detail in a paper by Miklavčič et al. [68].

The object in question is modelled by a conducting body Ω, an open, bounded subset of $\mathbb{R}^n, n = 2, 3$, having a sufficiently smooth boundary $\partial\Omega$. Note that the two-dimensional setting is a mathematical abstraction, and does not represent any real physical object. The conductivity inside Ω is then modelled by the function σ, which for simplicity is assumed to be a scalar function bounded above and below in Ω by a positive constant. Thus, we assume that permittivity is negligible. An imposed fixed boundary potential, expressed by the function f, generates an interior scalar electric potential u. The current density field is defined as $\boldsymbol{J} := -\sigma\nabla u$ following Kirchhoff's reformulation of Ohm's law for stationary conductors [80]. The continuity condition on the current density field is

$$\nabla \cdot \boldsymbol{J} = 0 \quad \text{in } \Omega,$$

since no current sources exist inside the object. The electrical potential u can therefore be modelled as the solution to the generalised Laplace problem

$$\begin{cases} \nabla \cdot \sigma\nabla u = 0 & \text{in } \Omega, \\ u = f & \text{on } \partial\Omega. \end{cases} \tag{1.1}$$

This is the boundary value problem behind most mathematical models of impedance tomography. The inverse problem from EIT is to reconstruct σ from knowledge of the boundary data operator which relates a boundary potential f and a boundary current $\sigma\nabla u \cdot \boldsymbol{\nu}$, where $\boldsymbol{\nu}$ denotes the exterior unit normal to $\partial\Omega$.

This formulation is clearly a very simplified model of any real experiment. It might be necessary to also model the effect of the electrodes that are attached to the boundary, the possible anisotropy of the conductivity and the presence of measurement noise. We choose not to include any of such properties in this model, such that mathematical formulation of the inverse problem is as simple as possible.

We now give two examples of how an additional modality can be used to recover interior data that allows us to formulate a hybrid inverse problem.

1.2.1 Magnetic Resonance EIT and Current Density Impedance Imaging

The first example is related to the use of EIT together with MRI. It is based on Ampere's law from classical electromagnetism that can be expressed in the differential form

$$\boldsymbol{J} = \nabla \times \boldsymbol{B}/\mu_0,$$

where $\boldsymbol{B}$ is the magnetic flux density vector and μ_0 is the vacuum permeability. Thus, full knowledge of $\boldsymbol{B}$ in the interior, gives full knowledge of the current density field $\boldsymbol{J}$.

An MRI scan measures a single component of the magnetic flux density vector $\boldsymbol{B}$ inside an object. If we assume that we can rotate the object such that all components can be measured it is possible to measure the full vector $\boldsymbol{B}$. Imagine that these measurements are done during an EIT measurement. Then the use of MRI allows us to augment the EIT inverse problem with additional interior data given by the current density field, which can be calculated using Ampere's law. Thus, for any EIT measurement, expressed mathematically by (1.1), we can augment the inverse problem with additional interior data given by the current density field

$$\boldsymbol{J} = \sigma \nabla u.$$

The inverse problem of MREIT is then to reconstruct σ from the knowledge of this data, corresponding to a number of solutions $\{u_j\}_{j=1}^J$ to (1.1) for a chosen set of boundary conditions $\{f_j\}_{j=1}^J$

The assumption that all components of $\boldsymbol{B}$ can be measured, is often not true. In many situations, only one or two components can be measured due to practical limitations in the MRI setup. In this setting the inverse problem is of course different, and relies on different reconstruction schemes [58, 79, 85]. Note that some authors reserve the name MREIT for such methods. A related method that relies on knowledge of the magnitude of $\boldsymbol{J}$ is Current Density Impedance Imaging (CDII). In this thesis, the analysis will cover the inverse problem for EIT, where interior knowledge of the magnitude of the current density field is available; thus we treat the problem from CDII.

1.2.2 Ultrasound Modulated EIT

The second example of a hybrid inverse problem in impedance tomography, is Ultrasound Modulated EIT. Here one utilises a physical coupling called the acousto-electric effect, that describes the conversion of acoustical energy into electrical energy; or equivalently, the transfer of momentum from the imposed acoustic wave to the electrons of the conducting material. This means that high intensity acoustic pressure waves create a local deformation of the electronic structure which changes the electrical properties. The effect is also partially caused by changes in the ionic mobility, and changes in the so-called dissociation equilibrium of partially dissociated ionic species. However, experiments have showed that the bulk compressibility is responsible for most of the acousto-electric effect [49]. Experiments also show that the acousto-electric effect seems to be rather small [61, 98], and the feasibility of utilising this effect in an imaging method is therefore questionable.

The idea in UMEIT is to conduct a classical EIT measurement, while an known ultrasonic wave travels through the object. Due to the acousto-electric effect, the EIT boundary measurements will record changes in the electrical properties. This is now done for a family of known ultrasonic waves, which corresponds to EIT boundary measurements reflecting different interior conductivity perturbations.

If the ultrasonic signal is assumed to be in the form of a plane wave with a chosen amplitude, the following derivation, based on the presentation by Bal [12], shows how a mathematical expression of the interior power density can be recovered from boundary measurements. For this we need to make the assumption that the wave speed is constant.

The acousto-electric effect which perturbs the conductivity is modelled by the relation

$$\sigma_\epsilon(x) = \sigma(x)\left(1 + \epsilon e^{i(k\cdot x)}\right) + \mathcal{O}(\epsilon^2),$$

where $\epsilon \ll 1$ is the product of a measure of the acousto-electric coupling between the wave and the electrical conductivity, and the amplitude of the plane wave. Note that $\sigma_{-\epsilon}$ can be obtained by simply shifting the phase of the wave. We denote by u_ϵ a solution to (1.1), where σ has been replaced by σ_ϵ. Using integration by parts, we find the relation

$$\int_\Omega (\sigma_\epsilon - \sigma_{-\epsilon})\nabla u_\epsilon \cdot \nabla u_{-\epsilon}\, dx = \int_{\partial\Omega} \sigma_\epsilon u_{-\epsilon}\partial_{\boldsymbol{\nu}} u_\epsilon - \sigma_{-\epsilon}u_\epsilon\partial_{\boldsymbol{\nu}} u_{-\epsilon}\, ds, \qquad (1.2)$$

where $\partial_{\boldsymbol{\nu}} u := \boldsymbol{\nu}\cdot\nabla u$. The integral on the right-hand side can be calculated from

the measured EIT boundary data for different values of ϵ. We can therefore make the polynomial expansion in ϵ

$$\int_{\partial\Omega} \sigma_\epsilon u_{-\epsilon} \partial_{\boldsymbol{\nu}} u_\epsilon - \sigma_{-\epsilon} u_\epsilon \partial_{\boldsymbol{\nu}} u_{-\epsilon} \, ds = \epsilon J_1(k) + \epsilon^2 J_2(k) + \mathcal{O}(\epsilon^3),$$

by changing the amplitude of the acoustic wave. Here $J_1(k)$ and $J_2(k)$ are coefficients in the polynomial expansion.

We are interested in an expression of the first-order coefficient $J_1(k)$. First note that a simple perturbation argument for (1.1) shows that

$$\sigma \nabla u = \sigma \left(1 + \epsilon e^{i(k\cdot x)}\right) \nabla u_\epsilon + \mathcal{O}(\epsilon^2),$$

which for $\epsilon \ll 1$ implies

$$\nabla u_\epsilon = \nabla u - \epsilon e^{i(k\cdot x)} \nabla u + \mathcal{O}(\epsilon^2).$$

Therefore the first-order terms of (1.2) are given by the simple relation

$$\int_\Omega 2\epsilon\sigma \nabla u \cdot \nabla u \, e^{i(k\cdot x)} \, dx = \epsilon J_1(k).$$

We recognise $\frac{1}{2} J_1(k)$ as the Fourier transform of $\sigma|\nabla u|^2$ extended to zero outside Ω. In theory we can measure $J_1(k)$ for all $k \in \mathbb{R}^n$, and by the inverse Fourier transform this corresponds to interior knowledge of $\sigma|\nabla u|^2$.

This interior data models the electrical power density distribution inside Ω. The inverse problem of UMEIT is then to reconstruct σ from the knowledge of this data, corresponding to a number of solutions $\{u_j\}_{j=1}^J$ to (1.1) for a chosen set of boundary conditions $\{f_j\}_{j=1}^J$.

Note that if one uses perfectly focused waves or spherical waves instead of plane waves, it is also possible to recover the electrical power density distribution, by a similar mathematical construction [55].

The feasibility and practicality of both of the presented hybrid methods is of course questionable, since many assumptions and simplifications have been made. A further analysis of this question is beyond the scope of this thesis, but it is important to note that the presented methods indeed are based on models that are way to simple to model any real applications. It should also be noted that some hybrid inverse problems actually have been shown to work in real-life applications. Examples are the aforementioned combined PET/CT scan and so-called Photoacoustic Tomography [97].

1.2.3 Hybrid inverse problems in impedance tomography

In this thesis we will analyse a hybrid inverse problem from impedance tomography, augmented with interior data of the type $\sigma|\nabla u_j|^p, p > 0$. This is a more general problem which covers CDII and UMEIT as two special cases. By considering the inverse problem for a general parameter $p > 0$, we take a unified approach that accounts for many modalities in a single formulation. We will therefore not limit the analysis to the values of p which correspond to a mathematical model of certain physical quantities. However, from a practical perspective, the cases $p = 1$ and $p = 2$ seem to be the most interesting. Note that for $p \leq 0$ the corresponding problem is closely related to the so-called p-Laplacian which has already been thoroughly analysed in the literature [64].

To sum up, this thesis is concerned with the mathematical analysis of the following hybrid inverse problem:

Let Ω be an open, bounded subset of $\mathbb{R}^n, n = 2, 3$ with a sufficiently smooth boundary $\partial\Omega$ and let σ be a scalar function uniformly bounded above and below by positive constants in Ω. Consider the set of generalised Laplace problems

$$\begin{cases} \nabla \cdot \sigma \nabla u_j = 0 & \text{in } \Omega, \\ u_j = f_j & \text{on } \partial\Omega, \end{cases} \quad 1 \leq j \leq J, \tag{1.3}$$

and the scalar interior data of the type

$$H_j = \sigma|\nabla u_j|^p \text{ in } \Omega, \quad p > 0. \tag{1.4}$$

For a chosen set of boundary conditions $\{f_j\}_{j=1}^J$ and knowledge of the corresponding interior data $\{H_j\}_{j=1}^J$ we want to reconstruct σ.

1.3 Reading guide

This thesis contributes to the area of theoretical and applied mathematics for hybrid inverse problems. Specifically, it introduces novel results and approaches for the analysis of hybrid inverse problems in impedance tomography.

The primary contributions are:

- A precise theoretical explanation of how non-ellipticity affects the properties of solutions to the linearised hybrid inverse problem.

- The development, analysis, implementation, and comparison of iterative reconstruction methods for hybrid inverse problems with full and partial data.

The thesis is organised around topics that build upon each other and the aim has been to present the work in a clear structure that provides a logical progression of ideas from chapter to chapter.

In the previous part of this chapter, we gave an introduction to inverse problems, and the field of hybrid inverse problems. Based on a simple model for impedance tomography, we formulated two hybrid inverse problems related to physical models. We generalised these problems to a purely mathematical inverse problem, which is the problem analysed in this thesis.

In Chap. 2 we will introduce the mathematical concepts that facilitates the analysis of linear differential problems that is being conducted in this thesis. This includes the linearisation of maps in Banach spaces, an introduction to pseudo-differential calculus, theory related to the stability of boundary value problems, and microlocal analysis, here related to the propagation of singularities.

A precise mathematical formulation of the inverse problem, given by a system of non-linear PDEs and an approximation given by a linear system of PDEs is presented in Chap. 3.

The theoretical analysis is conducted in Chap. 4. Here we show how the stability properties of the hybrid inverse problem is related to the value of the parameter p and the chosen boundary conditions. Novel results on the propagation of singularities for the non-elliptic linearised hybrid inverse problem are presented in Sec. 4.4. In the end of the chapter, we shortly explain how certain qualitative properties of solutions to the forward problem (1.3) can be obtained in two dimensions, discuss the implications of such properties, and model the situations of partial and limited-view data.

In Chap. 5 we develop and analyse four iterative reconstruction methods for the inverse problem. For each method, we analyse and compare their performance and relate this to the stability results obtained in Chap. 4. We also show how the loss of ellipticity manifest itself as propagating singularities, exactly as predicted by the presented theory. Finally, we test the robustness of the developed reconstruction methods using noisy data, and show how the reconstruction is affected by partial data and limited-view data.

Concluding remarks are found in Chap 6, were we also discuss the results in relation to other inverse problems.

A short note on the used notation and symbols can be found in Appendix A.

Chapter 2

Strategies for studying hybrid inverse problems

In this chapter, we introduce the mathematical concepts that facilitates the analysis of linear differential problems that is being conducted in this thesis. The presentation is not entirely self-contained; the intention is merely to introduce the reader to the fields and approaches needed for a systematic treatment of the relevant mathematical problems, and to focus the attention on typical structures and properties of systems of linear differential equations. We state important definitions and explain the motivation in a suitable context, but do not include proofs. Instead we leave room for examples, which should help the reader to understand the more abstract concepts.

The motivation is the analysis of linear formulations of certain types of hybrid inverse problems, but the presented methods are formulated without restrictions to a specific approach and can therefore be applied to most mathematical problems based on differential operator equations and related boundary value problems.

2.1 Linearisation of non-linear maps in Banach spaces

Inverse problems can often be formulated in terms of a non-linear map between Banach spaces. Non-linear maps are by definition a class of map, that does not share the simple structure of linear maps, and as a result their corresponding analysis often relies on completely different mathematical techniques. For linear maps we can rely on a well-developed theory, and utilise their characteristic properties such as additivity and homogeneity, and the fact that linearity is conserved in compositions. Also if a linear operator has an inverse, we know that this is also linear [53]. Similar properties does not exist for non-linear maps, and therefore non-linear maps are considered more difficult to analyse.

In the study of non-linear inverse problems expressed by non-linear maps, an analysis of the corresponding linearisation provides a simple framework for studying the properties of the problem in the vicinity of some reference solution. Linear problems are, by nature, simpler to understand and numerical methods for linear problems are typically faster, the implementation is often straightforward, and the robustness and efficiency of linear solvers are second to none.

A standard approach is therefore to consider a non-linear problem from the field of differential calculus in infinite-dimensional space; that is to consider a linear map that in some suitable sense approximates the non-linear map. By analogy, for a real or complex smooth function, it is well-known that the first-order Taylor expansion is a linear function representing the change in the function value under infinitesimal changes in the argument. We can generalise the notion of derivatives, such that this type of representation can be extended to non-linear maps between function spaces. If these function spaces are Banach spaces, the corresponding linearisation is a linear map denoted the Fréchet derivative.

Definition 2.1 (Fréchet derivative)**.** *Let V and W be Banach spaces, and $U \subset V$ be open. A map $\mathcal{F} : U \to W$ is called Fréchet differentiable at $u \in U$ if there exists a bounded linear operator $\mathrm{d}\mathcal{F}|_u : V \to W$ such that*

$$\lim_{h \to 0} \frac{\|\mathcal{F}(u+h) - \mathcal{F}(u) - \mathrm{d}\mathcal{F}|_u(h)\|_W}{\|h\|_V} = 0.$$

The linear map $\mathrm{d}\mathcal{F}|_u$ is called the Fréchet derivative of $\mathcal{F}$ at u, and its value at $h \in V$ is denoted by $\mathrm{d}\mathcal{F}|_u(h)$. We say that $\mathcal{F}$ is Fréchet differentiable in an open domain, if it is differentiable at every point in this domain [63].

Remark 2.2. *For more general function spaces a similar theory has been developed using a so-called functional derivative. In locally convex topological vector*

spaces, that are not Banach spaces, the functional derivative is often defined by a so-called Gâteaux derivative. Note that such a derivative is not necessarily a linear map [63].

In Chapter 3, this type of linearisation will be applied to a non-linear inverse problem, to obtain a linear inverse problem on which most of the analysis in this thesis is done.

2.2 Analysis of linear differential operators and boundary value problems

We now give an introduction to the, somewhat abstract, field of pseudo-differential calculus, the related operators and an algebra that facilitates convenient symbolic manipulations. Motivated by the wish to analyse operator equations and boundary value problems on open bounded subsets of Euclidean space, we continue by defining the concept of ellipticity for scalar pseudo-differential operator equations. We extend the theory to determined and overdetermined boundary value problems under certain additional requirements on the prescribed boundary conditions. For such boundary value problems, we explain the concept of parametrices and the closely related a priori stability estimates. After this, we give a short introduction to microlocal analysis, in order to state the classical result on the propagation of singularities for real principal type pseudo-differential operators, and the less known extension to scalar pseudo-differential operators of constant multiplicity.

2.2.1 Pseudo-differential calculus

This section is a very brief introduction to the field of pseudo-differential calculus, which is among the most powerful tools for analysing partial differential operators. We include the definitions and theorems needed for the analysis of hybrid inverse problems that we conduct in the next chapter. The presentation is not self-contained and many non-trivial details are skipped. We recommend the reader to consult some of the many text books on the subject for a more general introduction to the subject [45, 87, 93, 95]. Note that most literature treat the concept of pseudo-differential operators on euclidean space, and then afterwards extend the theory to open bounded subsets by the use of certain cut-off functions. For brevity, we define it exclusively for open bounded subsets, since this is what we need for our analysis.

Consider a linear partial differential operator of order m expressed in the form

$$P(x,D) = \sum_{|\alpha|\leq m} c_\alpha(x) D^\alpha, \tag{2.1}$$

where $c_\alpha \in C^\infty(\Omega)$. For the analysis of such partial differential operators, the Fourier integral representation can provide a remarkable simplification, since in the Fourier domain differentiation is replaced by polynomial multiplication in the dual Fourier variable. For $u \in C_0^\infty(\Omega)$ let its Fourier transform $\hat{u}$ be defined by

$$\hat{u}(\xi) = \int_{\mathbb{R}^n} u(x) e^{-ix\cdot\xi} dx, \tag{2.2}$$

and the corresponding inverse Fourier transform by

$$u(x) = \int_{\mathbb{R}^n} \hat{u}(\xi) e^{ix\cdot\xi} đ\xi,$$

where u has been extended by zero in $\mathbb{R}^n \setminus \Omega$ and $đ\xi := (2\pi)^{-n} d\xi$.

For operators of the form (2.1), the Fourier inversion formula provides the relation

$$P(x,D)u(x) = \int_{\mathbb{R}^n} \mathfrak{p}(x,\xi)\hat{u}(\xi) e^{ix\cdot\xi} đ\xi,$$

where

$$\mathfrak{p}(x,\xi) = \sum_{|\alpha|\leq m} c_\alpha(x)\xi^\alpha$$

is called the *symbol* of $P(x,D)$ and is a polynomial in ξ of order m. In this way all partial differential operators with smooth coefficients can be represented by symbols which are polynomials in ξ and the associated operator calculus is by the Fourier transform carried over to algebraic manipulations of the associated symbol. It is clear that this construction can be generalised to functions in the dual variable which are not polynomials. Such a function, or symbol, then becomes a Fourier representation of an operator which is not a differential operator. Thus, by considering functions $\mathfrak{p}(x,\xi)$ in appropriate function spaces we get integral expressions of operators that generalises the concept of differential operators and have a related behaviour. These operators are what we call *pseudo-differential operators*.

It will be beneficial to consider symbol classes which provide a convenient algebra that facilitates standard symbolic manipulations. We begin by introducing the

symbol class $S^m_{1,0}$ which is defined relative to a growth condition.

Definition 2.3 (Symbol class $S^m_{1,0}(\Omega\times\mathbb{R}^n)$)**.** *The space $S^m_{1,0}(\Omega\times\mathbb{R}^n)$ of symbols of degree m and type $1,0$ is defined as the set of functions $\mathfrak{p}\in C^\infty(\Omega\times\mathbb{R}^n)$ with the property that for any compact $K\subset\Omega$ and any multi-indices $\alpha,\beta\in\mathbb{N}_0^n$, there exists a constant $C_{K,\alpha,\beta}$ such that*

$$|D_x^\beta D_\xi^\alpha \mathfrak{p}(x,\xi)|\le C_{K,\alpha,\beta}(1+|\xi|^2)^{\frac{m-|\alpha|}{2}}.$$

When $\mathfrak{p}\in S^m_{1,0}(\Omega\times\mathbb{R}^n)$ and there exists a sequence of symbols $\mathfrak{p}_{m_j}, j\in\mathbb{N}_0$, with $\mathfrak{p}_{m_j}\in S^{m_j}_{1,0}(\Omega\times\mathbb{R}^n)$, $m_j\searrow-\infty$, such that $\mathfrak{p}-\sum_{j<M}\mathfrak{p}_{m_j}\in S^{m_M}_{1,0}(\Omega\times\mathbb{R}^n)$ for all M, we say that $\mathfrak{p}$ has the asymptotic expansion $\sum_{j\in\mathbb{N}_0}\mathfrak{p}_{m_j}$, in short, $\mathfrak{p}\sim\sum_j\mathfrak{p}_{m_j}$ in $S^{m_0}_{1,0}(\Omega\times\mathbb{R}^n)$ [38, Def. 7.1].

Remark 2.4. *Related symbol classes, often denoted by $S^m_{\varrho,\delta}$, where $0\le\varrho,\delta\le1$, turn out to be more appropriate in certain settings, but we will not introduce these types of symbol classes in this presentation. The definition of these spaces can be found in most text books on pseudo-differential calculus [45, 87].*

Polynomials of order m with smooth coefficients are elements of $S^m_{1,0}(\Omega\times\mathbb{R}^n)$ and therefore this symbol class is a generalisation of Fourier representations of standard differential operators of order m with smooth coefficients. Note that the definition also directly implies the embeddings

$$S^m_{1,0}(\Omega\times\mathbb{R}^n)\subset S^{m'}_{1,0}(\Omega\times\mathbb{R}^n)\text{ when }m'>m.$$

For every symbol $\mathfrak{p}(x,\xi)\in S^m_{1,0}(\Omega\times\mathbb{R}^n)$ we can express a corresponding operator P by the integral formulation

$$Pu(x)=\int_{\mathbb{R}^n}\mathfrak{p}(x,\xi)\hat{u}(\xi)e^{ix\cdot\xi}đ\xi,\quad u\in C_0^\infty(\Omega).\tag{2.3}$$

This integral is absolutely convergent, since $\hat{u}\in\mathscr{S}(\mathbb{R}^n)$ for any $u\in C_0^\infty(\Omega)$. Differentiation can therefore be performed under the integration sign and it follows that $Pu\in C^\infty(\Omega)$. Thus, the integral formulation (2.3) defines a continuous linear map

$$P: C_0^\infty(\Omega)\to C^\infty(\Omega).$$

By a duality argument (see e.g. [38, p. 171]), we can uniquely extend P to a continuous linear map

$$P:\mathscr{E}'(\Omega)\to\mathscr{D}'(\Omega).$$

The operator $P : \mathscr{E}'(\Omega) \to \mathscr{D}'(\Omega)$ of the form (2.3) with symbol in $S^m_{1,0}(\Omega \times \mathbb{R}^n)$ is called a *pseudo-differential operator* of order m, and is said to belong to the class $\Psi^m_{1,0}(\Omega)$.

For $P \in \Psi^m_{1,0}(\Omega)$ we can also define the adjoint operator $P^* \in \Psi^m_{1,0}(\Omega)$ by the integral formulation

$$P^*u(x) = \int_{\mathbb{R}^n} \mathfrak{p}^*(x,\xi)\hat{u}(\xi)e^{ix\cdot\xi}\,đ\xi, \quad u \in C_0^\infty(\Omega),$$

where

$$\mathfrak{p}^*(x,\xi) \sim \sum_{\alpha\in\mathbb{N}_0^n} \frac{1}{\alpha!}\partial_x^\alpha D_\xi^\alpha \mathfrak{p}(x,\xi)^* \text{ in } S^m_{1,0}(\Omega) \text{ [38, Thm. 7.13]}.$$

Also P^* can be extended to a bounded linear map $P^* : \mathscr{E}'(\Omega) \to \mathscr{D}'(\Omega)$.

A certain type of pseudo-differential operators admits a composition with other pseudo-differential operators and these are called *properly supported*.

Definition 2.5 (Properly supported pseudo-differential operator)**.** *A pseudo-differential operator P is properly supported in Ω when both P and P^* have the property: For each compact $K \subset \Omega$ there is a compact $K' \subset \Omega$ such that distributions supported in K are mapped into distributions supported in K' [38, Def. 7.6].*

Note that this implies that if P is properly supported, P and P^* are maps $C_0^\infty(\Omega) \to C_0^\infty(\Omega)$ and P and P^* therefore both extend to maps $\mathscr{D}'(\Omega) \to \mathscr{D}'(\Omega)$. An example of a properly supported pseudo-differential operator, is a partial differential operator [38, p. 173].

For a properly supported pseudo-differential operator, we can define its composition with another pseudo-differential operator.

Theorem 2.6 (Composition)**.** *Let $P \in \Psi^m_{1,0}(\Omega)$ and $P' \in \Psi^{m'}_{1,0}(\Omega)$ and let P or P' be properly supported. Then the composition PP' makes sense and $PP' \in \Psi^{m+m'}_{1,0}(\Omega)$ [38, Thm. 7.13].*

Also, it is not difficult to show that the composition of two properly supported pseudo-differential operators is again a properly supported pseudo-differential operator.

A subclass of symbols are the *classical* symbols which is later shown to facilitate a convenient symbolic calculus.

Definition 2.7 (Classical symbols $S^m(\Omega \times \mathbb{R}^n)$)**.** *The space $S^m(\Omega \times \mathbb{R}^n)$ of classical symbol of degree m is defined as the set of symbols $\mathfrak{p}(x,\xi) \in S^m_{1,0}(\Omega \times \mathbb{R}^n)$ for which there exists a sequence of functions $\mathfrak{p}_{m-l} \in C^\infty(\Omega \times \mathbb{R}^n)$ for $l \in \mathbb{N}_0$, satisfying (i) and (ii):*

(i) Each $\mathfrak{p}_{m-l}$ satisfies

$$\mathfrak{p}_{m-l}(x,t\xi) = t^{m-l}\mathfrak{p}_m(x,\xi), \text{ for } |\xi| \geq 1, t \geq 1.$$

(ii) p has the asymptotic expansion

$$\mathfrak{p}(x,\xi) \sim \sum_{l \in \mathbb{N}_0} \mathfrak{p}_{m-l}(x,\xi) \text{ in } S^m_{1,0}(\Omega \times \mathbb{R}^n) \text{ [38, Def. 7.2].}$$

Note that the definition implies that

$$S^m(\Omega \times \mathbb{R}^n) \subset S^{m'}(\Omega \times \mathbb{R}^n) \text{ when } m' - m \in \mathbb{N}_0.$$

Classical symbols are sometimes also called *polyhomogeneous symbols* in the literature.

We denote by $\Psi^m(\Omega)$ the class of classical pseudo-differential operators of order m, i.e. operators with classical symbols of order m. From the definition, clearly the partial differential operators of order m expressed in the form (2.1) are elements of $\Psi^{m'}(\Omega)$ for $m' - m \in \mathbb{N}_0$. The leading term $\mathfrak{p}_m$ in the asymptotic expansion of the symbol is called the principal symbol of a classical pseudo-differential operator P and we will denote this by $\mathfrak{p}^{(0)}$. We will denote by $\mathfrak{P}$ an operator that relates a classical pseudo-differential operator P with its principal symbol $\mathfrak{p}^{(0)}$, i.e. $\mathfrak{P}(P) = \mathfrak{p}^{(0)}$. One motivation behind introducing classical pseudo-differential operators is that the principal symbol of an operator composed of such operators has a very simple form.

Theorem 2.8 (Principal symbol of composition)**.** *If $P \in \Psi^m(\Omega)$ and $P' \in \Psi^{m'}(\Omega)$, and the composition $PP' \in \Psi^{m+m'}(\Omega)$ makes sense, then $\mathfrak{P}(PP') = \mathfrak{P}(P)\mathfrak{P}(P') \in S^{m+m'}(\Omega \times \mathbb{R}^n)$ [38, Thm. 7.13].*

For the set of classical symbols of arbitrary high order, defined by

$$S^\infty(\Omega \times \mathbb{R}^n) := \bigcup_{m \in \mathbb{R}} S^m(\Omega \times \mathbb{R}^n),$$

and any properly supported pseudo-differential operator P, there exists a cor-

responding unique symbol given by

$$\mathfrak{p}(x,\xi) = e^{-ix\cdot\xi}P(e^{ix\cdot\xi}) \in S^{\infty}(\Omega\times\mathbb{R}^n) \text{ [38, Lem. 7.7]}.$$

However, the correspondence between general symbols in $S^m_{1,0}(\Omega)$ and operators in $\Psi^m_{1,0}(\Omega)$ is not necessarily unique. It is possible that different symbols can represent the same operator, and in these situations, the previous treatment of the symbol classes is not entirely fulfilling. This ambiguity can be studied using the set of symbols and operators of arbitrary low orders, defined by the relations

$$S^{-\infty}(\Omega\times\mathbb{R}^n) \coloneqq \bigcap_{m\in\mathbb{R}} S^m(\Omega\times\mathbb{R}^n) = \bigcap_{m\in\mathbb{R}} S^m_{1,0}(\Omega\times\mathbb{R}^n),$$
$$\Psi^{-\infty}(\Omega) \coloneqq \bigcap_{m\in\mathbb{R}} \Psi^m(\Omega) = \bigcap_{m\in\mathbb{R}} \Psi^m_{1,0}(\Omega).$$

It can be shown that if, and only if, a pseudo-differential operator can be extended to a linear mapping $\mathscr{E}'(\Omega) \to C^{\infty}(\Omega)$ then it is an element of $\Psi^{-\infty}(\Omega\times\mathbb{R}^n)$ [38, p. 183]. Such operators are, for obvious reasons, called *smoothing operators*. We will identify two pseudo-differential operators P and Q with each other, written as $P\sim Q$, if $P-Q$ is a smoothing operator. In some parts of the literature, smoothing operators are also called negligible operators or regularising operators.

Many interesting properties follows by the definition of smoothing operators. For example, any pseudo-differential operator can be decomposed as the sum of a properly supported pseudo-differential operator and a smoothing operator [38, Prop. 7.8]. Also, the composition of a properly supported pseudo-differential operator and a smoothing operator gives a smoothing operator [38, Lem. 7.12].

2.2.2 Stability of determined and overdetermined boundary value problems

Much of the developed theory in pseudo-differential calculus was motivated by the wish to analyse and solve pseudo-differential operator equations of the type

$$Pu = f \quad \text{in } \Omega, \tag{2.4}$$

perhaps under additional constraints on the solution u. In appropriate function spaces, the Fourier transform provides the relation

$$\mathfrak{p}(x,\xi)\hat{u}(\xi) = \hat{f}(\xi), \quad (x,\xi)\in\Omega\times\mathbb{R}^n.$$

This suggest that the function u can, at least formally, be expressed by the integral

$$u(x) = \int_{\mathbb{R}^n} \mathfrak{p}(x,\xi)^{-1} \hat{f}(\xi) e^{ix\cdot\xi} \, d\xi.$$

However, this approach is likely to fail, simply because the expression on the right is not well-defined.

The previous example illustrates that any zeros of $\mathfrak{p}(x,\xi)$ in $\Omega \times \mathbb{R}^n$ is problematic in the inversion of P. A pseudo-differential operator for which the principal symbol has no non-trivial roots allows for an inversion of the highest order term, and this distinct feature characterises the so-called elliptic pseudo-differential operators.

Definition 2.9 (Ellipticity)**.** *$P \in \Psi^m(\Omega)$ is called elliptic, if its principal symbol $\mathfrak{p}^{(0)}$ satisfies*

$$\mathfrak{p}^{(0)}(x,\xi) \neq 0 \quad \textit{for all} \quad (x,\xi) \in \Omega \times (\mathbb{R}^n \setminus 0) \textit{ [38, Def. 7.17].}$$

The simplest example of an elliptic partial differential operator is the Laplace operator. For $P = \Delta$, we have $\mathfrak{p}^{(0)} = -|\xi|^2$ which clearly satisfies the requirement for ellipticity in any dimension. Another example is the first-order operator $\partial_{x_1} + i\partial_{x_2}$ which is elliptic for $\Omega \subset \mathbb{R}^2$.

The definition of ellipticity has a natural extension to matrices of classical pseudo-differential operators of the same order.

Definition 2.10 (Ellipticity for systems)**.** *An $(k \times k')$-system P of classical pseudo-differential operators of order m is called elliptic, if the $(k \times k')$-matrix of principal symbols $\mathfrak{p}^{(0)}$ satisfies*

$$\textit{rank } \mathfrak{p}^{(0)}(x,\xi) = k' \quad \textit{for all} \quad (x,\xi) \in \Omega \times (\mathbb{R}^n \setminus 0) \textit{ [38, Def. 7.17].}$$

When P is an $(k \times k')$-system and elliptic, it is called injectively elliptic if $k > k'$.

A great deal of the theoretical work on elliptic pseudo-differential operators is based on quantifying the properties of an approximate inversion of the symbol. For $P \in \Psi^m(\Omega)$ elliptic, it can be shown that there exits $Q \in \Psi^{-m}(\Omega)$ properly supported and elliptic, such that

$$QP \sim PQ \sim I.$$

Such an operator Q is called a *parametrix* to the elliptic operator P and a

symbol of Q can be constructed explicitly from the symbol of P. One can show that Q is defined uniquely upto a smoothing operator, and the ellipticity of P is indeed a requirement for such a construction [38, Thm. 7.18].

The concept of ellipticity especially becomes relevant in the analysis of scalar operators equation of the type (2.4). For instance, with P being an elliptic pseudo-differential operator, all possible solutions are equal modulo smooth functions and regularity results in certain Sobolev spaces follows as a natural consequence of the parametrix construction [38, Cor. 7.20].

We now continue with the definition of ellipticity for determined and overdetermined systems of linear partial differential operators. This also covers scalar operators as a special case and is a natural extension of the concept of ellipticity for scalar pseudo-differential operators, and systems of pseudo-differential operators of the same order. For boundary value problems, the presented theory provides important information regarding the stability, and in certain situations uniqueness, of solutions. The results are mainly based on the work on overdetermined boundary value problems by Solonnikov [89], on determined boundary value problems by Agmon, Douglis, and Nirenberg [3, 4], a review paper on the subject by Agranovich [5], and the somewhat simpler presentation following Bal's work on hybrid inverse problems [13].

Consider a boundary value problem in the general form

$$\begin{cases} \mathcal{L}\boldsymbol{u} = \boldsymbol{f} & \text{in } \Omega, \\ \mathcal{B}\boldsymbol{u} = \boldsymbol{g} & \text{on } \partial\Omega, \end{cases} \tag{2.5}$$

where $\mathcal{L} := \mathcal{L}(x, D)$ is an $(I \times J)$-matrix of partial differential operators in Ω and $\mathcal{B} := \mathcal{B}(x, D)$ is a $(K \times J)$-matrix of partial differential operators on $\partial\Omega$. We assume that $I \geq J$, denote by $\mathcal{L}_{ij}, \mathcal{B}_{kj}, i = 1, \ldots, I,\ j = 1, \ldots, J,\ k = 1, \ldots, K$ the respective elements of $\mathcal{L}$ and $\mathcal{B}$, and consider the problem represented by the vector functions

$$\boldsymbol{u} = \begin{pmatrix} u_1 \\ \vdots \\ u_J \end{pmatrix}, \quad \boldsymbol{f} = \begin{pmatrix} f_1 \\ \vdots \\ f_I \end{pmatrix}, \quad \text{and} \quad \boldsymbol{g} = \begin{pmatrix} g_1 \\ \vdots \\ g_K \end{pmatrix},$$

where $\boldsymbol{f}$ and $\boldsymbol{g}$ are given.

We want to give qualitative information, such as regularity results, for possible solutions $\boldsymbol{u}$ to the boundary value problem (2.5) under certain conditions on $\mathcal{L}$ and $\mathcal{B}$. The results are based on concepts from pseudo-differential calculus, such as principal symbols, here limited to the special case of linear partial

differential operators. We begin with the definition of the principal symbol of matrix differential operators, which is defined relative to two sets of integers.

Definition 2.11 (Principal symbol of matrix differential operators)**.** *Let $\mathcal{L}$ be the $(I \times J)$-matrix of partial differential operators in* (2.5)*. To each row we assign integers, $\{s_i\}_{i=1}^{I}$, normalised such that $\max s_i = 0$, and to each column integers, $\{t_j\}_1^J$, such that the order of $\mathcal{L}_{ij}$ is not greater than $s_i + t_j$; and if $s_i + t_j < 0$ then $\mathcal{L}_{ij} = 0$. Consider the matrix $\mathcal{L}^{(0)}$ with elements $\mathcal{L}_{ij}^{(0)}$ that are the terms of order exactly $s_i + t_j$ of $\mathcal{L}_{ij}$. $\mathcal{L}^{(0)}$ is called the principal part of the matrix $\mathcal{L}$, and we denote by $\mathfrak{l}^{(0)}$ the principal symbol of the $\mathcal{L}$, i.e. the symbol of $\mathcal{L}^{(0)}$ [89].*

It is often possible to choose the integers $\{s_i\}_{i=1}^{I}$ and $\{t_j\}_{j=1}^{J}$ in multiple ways and this will naturally result in different expressions of the principal symbol. As we will see in a moment, the analysis is based on *existence* of a set of integers, for which the principal symbol satisfies certain conditions.

The concept of ellipticity for matrix differential operators is defined relative to the principal symbol.

Definition 2.12 (Douglis–Nirenberg ellipticity of matrix differential operators)**.** *Let $\mathcal{L}$ be the $(I \times J)$-matrix of partial differential operators in* (2.5)*. $\mathcal{L}$ is called Douglis–Nirenberg (DN) elliptic in $\bar{\Omega}$ if there exist two sets of integers $\{s_i\}_{i=1}^{I}, \{t_j\}_{j=1}^{J}$, such that the principal symbol $\mathfrak{l}^{(0)}$ (see Def. 2.11) satisfies*

$$\textit{rank}\ \mathfrak{l}^{(0)}(x,\xi) = J \quad \textit{for all} \quad (x,\xi) \in \bar{\Omega} \times (\mathbb{R}^n \setminus 0)\ \textit{[89]}.$$

The existence of sets of integers $\{s_i\}_{i=1}^{I}$ and $\{t_j\}_{j=1}^{J}$ such that $\mathfrak{l}^{(0)}$ has rank J, allows one to transform $\mathcal{L}$ into a matrix of partial differential operators all being first-order by differentiating equations such that each column in $\mathcal{L}$ becomes of the same order, and then introducing additional equations to express higher order derivatives by coupled first-order derivatives.

For the boundary operator $\mathcal{B}$, the principal symbol is defined relative to a set of integers $\{\kappa_k\}_{k=1}^{K}$, which depends on $\{t_j\}_{j=1}^{J}$.

Definition 2.13 (Principal part of boundary operator)**.** *Consider the boundary value problem* (2.5)*, and a chosen set of integers $\{t_j\}_{j=1}^{J}$. Denote by b_{kj} the order of $\mathcal{B}_{kj}$, and define $\kappa_k := \max_j(b_{kj} - t_j)$. The principal part of $\mathcal{B}_{kj}$ is denoted by $\mathcal{B}^{(0)}$, and has entries $\mathcal{B}_{kj}^{(0)}$ defined as the elements of $\mathcal{B}_{kj}$ of degree exactly equal to $\kappa_k + t_j$ [89].*

For boundary value problems, the boundary condition is, by nature, a constraint

on the solution space and the concept of ellipticity therefore depends on the properties shared by $\mathcal{L}$ and $\mathcal{B}$. Therefore an additional condition need to be satisfied for $(\mathcal{L}, \mathcal{B})$.

Definition 2.14 (Lopatinskii condition for $(\mathcal{L}, \mathcal{B})$)**.** *Consider the boundary value problem* (2.5)*, three sets of integers* $\{s_i\}_{i=1}^{I}$,$\{t_j\}_{j=1}^{J}$,$\{\kappa_k\}_{k=1}^{K}$ *and the associated principal parts* $\mathcal{L}^{(0)}, \mathcal{B}^{(0)}$*. For each* $x \in \partial\Omega$*, denote by* $\boldsymbol{v}$ *the inward unit normal to* Ω *at* $x \in \partial\Omega$*, and let* z *be the parametrisation of the half line* $x + z\boldsymbol{v}$ *for* $z \geq 0$*. Let* $\boldsymbol{\zeta} \in \mathbb{S}^{n-1}$ *with* $\boldsymbol{\zeta} \cdot \boldsymbol{v} = 0$*, and consider the system of ordinary differential equations given by*

$$\begin{cases} \mathcal{L}^{(0)}\left(x, i\boldsymbol{\zeta} + \boldsymbol{v}\dfrac{d}{dz}\right)\boldsymbol{w}(z) = 0 \quad \text{for } z > 0, \\ \mathcal{B}^{(0)}\left(x, i\boldsymbol{\zeta} + \boldsymbol{v}\dfrac{d}{dz}\right)\boldsymbol{w}(z) = 0 \quad \text{for } z = 0. \end{cases}$$

The Lopatinskii condition is satisfied for $(\mathcal{L}, \mathcal{B})$*, if for each* $x \in \partial\Omega, \boldsymbol{\zeta} \in \mathbb{S}^{n-1}$*, the only solution to the above system, such that* $\boldsymbol{w}(z) \to \mathbf{0}$ *as* $z \to +\infty$*, is* $\boldsymbol{w}(z) = \mathbf{0}$ *[89].*

If the Lopatinskii condition is satisfied for $(\mathcal{L}, \mathcal{B})$, it is said that $\mathcal{B}$ covers $\mathcal{L}$. If $\mathcal{L}$ is DN elliptic, (2.5) is then said to be an elliptic boundary value problem. In the literature, the Lopatinskii condition is also known as the Shapiro–Lopatinskii condition, the coerciveness condition or the covering condition [45]. Note that if a boundary value problem is elliptic, imposing additional boundary conditions on the solution does not change this property.

At first sight, the Lopatinskii condition might seem a bit abstract, but it can be formulated in the following non-algebraic way [4]: Consider a point $x \in \partial\Omega$, and make a coordinate transformation in a neighbourhood Γ of x into a portion of a plane, represented by $z = 0$, with the transformed image of $\Gamma \cap \Omega$ contained in a half-plane represented by $z \geq 0$. Then consider the boundary value problem under this transformation, keeping only the principal parts of the differential operator and the boundary operator, and fix the coefficient of the operators at their values at x. Now, consider the corresponding homogeneous problem and let $\boldsymbol{y}$ represent the coordinates in the plane given by $z = 0$. For any real $\boldsymbol{\zeta} \in \mathbb{S}^{n-1}$ in this hyperplane, consider separated solution of the form $e^{i\boldsymbol{y}\cdot\boldsymbol{\zeta}}\boldsymbol{w}(z)$, where $\boldsymbol{w}(z)$ is a solution to ordinary differential equations with constant coefficients. The Lopatinskii condition then requires that the for all $\boldsymbol{\zeta}$, the only solution $\boldsymbol{w}$, bounded for $z \geq 0$, is $\boldsymbol{w}(z) = \mathbf{0}$.

As an example of how the Lopatinskii condition can be applied on a specific

problem, consider the scalar boundary value problem

$$\begin{cases} \Delta u = f & \text{in } \Omega, \\ \boldsymbol{\mu} \cdot \nabla u = g & \text{on } \partial\Omega, \end{cases}$$

for some real $\boldsymbol{\mu} \in \mathbb{S}^{n-1}$. The governing ODE problem related to the Lopatinskii condition is then

$$\begin{cases} \left(-1 + \dfrac{d^2}{dz^2}\right) w(z) = 0 & \text{for } z > 0, \\ \boldsymbol{\mu} \cdot \left(i\boldsymbol{\zeta} + \boldsymbol{v}\dfrac{d}{dz}\right) w(z) = 0 & \text{for } z = 0. \end{cases}$$

For $z > 0$, we find that the only solutions satisfying $w(z) \to 0$ as $z \to +\infty$ are of the type

$$w(z) = ce^{-z},$$

where c is a constant. The ODE for $z = 0$ implies that

$$(\boldsymbol{\mu} \cdot (i\boldsymbol{\zeta} - \boldsymbol{v}))c = 0.$$

For $n = 2$, clearly $c = 0$ is the only way to satisfy this equation and the Lopatinskii condition is therefore satisfied for any vector $\boldsymbol{\mu} \in \mathbb{S}^{n-1}$. For $n \geq 3$, the Lopatinskii condition is satisfied if, and only if, $\boldsymbol{\mu} \cdot \boldsymbol{v} \neq 0$, i.e. if $\boldsymbol{\mu}$ is not tangent to the boundary.

In view of the general boundary value problem (2.5), we will now recast it in the form of the equivalent operator equation

$$\mathcal{A}\boldsymbol{u} = \boldsymbol{h},$$

where $\mathcal{A}$ and $\boldsymbol{h}$ are defined by the relations

$$\mathcal{A}\boldsymbol{u} = \begin{pmatrix} \mathcal{L}\boldsymbol{u} \\ \mathcal{B}\boldsymbol{u} \end{pmatrix}, \quad \boldsymbol{h} = \begin{pmatrix} \boldsymbol{f} \\ \boldsymbol{g} \end{pmatrix}.$$

Following this construction, we define $\mathcal{A}$ on the Sobolev spaces

$$D(q, l) := W^{l+t_1,q}(\Omega) \times \cdots \times W^{l+t_J,q}(\Omega),$$

where $q > 1$ and $l \geq 0$ is an integer. It can be shown that if the coefficients of

$\mathcal{A}$ are sufficiently smooth, then $\mathcal{A}$ is a bounded operator from $D(q,l)$ in

$$R(q,l) := W^{l-s_1,q}(\Omega) \times \cdots \times W^{l-s_I,q}(\Omega) \\ \times W^{l-\kappa_1-\frac{1}{q},q}(\partial\Omega) \times \cdots \times W^{l-\kappa_K-\frac{1}{q},q}(\partial\Omega) \text{ [89].}$$

For non-integer order Sobolev spaces, these spaces should be understood as Bessel potential spaces [1].

Furthermore, we denote by $\mathcal{L}_{ij}^{(m)}, \mathcal{B}_{ij}^{(m)}$ the parts of $\mathcal{L}_{ij}, \mathcal{B}_{kj}$ that are exactly of order $s_i + t_j - m$ and $\kappa_k + t_j - m$, respectively, such that

$$\mathcal{L}_{ij} = \sum_{m=0}^{s_i+t_j} \mathcal{L}_{ij}^{(m)} \qquad \text{and} \qquad \mathcal{B}_{kj} = \sum_{m=0}^{\kappa_k+t_j} \mathcal{B}_{kj}^{(m)}.$$

We are now ready to state the fundamental stability theorem for elliptic boundary value problem.

Theorem 2.15 (Fundamental stability theorem for elliptic boundary value problems)**.** *Let $q > 1$ and $l \geq 0$ be an integer such that $q(l+1) > n$ and $q(l-\kappa_k+1) > n$ for $1 \leq k \leq K$. Consider the boundary value problem (2.5), where the coefficients of the operators $\mathcal{L}_{ij}^{(m)}, \mathcal{B}_{kj}^{(m)}$ belong to $W^{l-s_i,q}(\Omega)$ and $W^{l-\kappa_k-\frac{1}{q},q}(\partial\Omega)$, respectively. Furthermore, let the coefficients of the operators $\mathcal{L}_{ij}^{(0)}, \mathcal{B}_{kj}^{(0)}$ be continuous. Then the three following statements are equivalent:*

1. *$\mathcal{L}$ is DN elliptic in $\bar{\Omega}$ and the Lopatinskii condition is satisfied for $(\mathcal{L}, \mathcal{B})$.*
2. *The operator $\mathcal{A} := \begin{pmatrix} \mathcal{L} \\ \mathcal{B} \end{pmatrix}$ has a left parametrix; i.e there exits a bounded operator $\mathcal{P} : R(q,l) \to D(q,l)$ such that*

$$\mathcal{P}A = I - T,$$

   where T is a smoothing operator in $D(q,l)$.

3. *The following a priori estimate holds:*

$$\sum_{j=1}^{J} \|u_j\|_{W^{l+t_j,q}(\Omega)} \leq c_1 \left(\sum_{i=1}^{I} \|f_i\|_{W^{l-s_i,q}(\Omega)} + \sum_{k=1}^{K} \|g_k\|_{W^{l-\kappa_k-\frac{1}{q},q}(\partial\Omega)} \right) \\ + c_2 \sum_{t_j>0} \|u_j\|_{L^q(\Omega)} \text{ [89, Thm. 1.1].}$$

Remark 2.16. *This theorem is a slight simplification of the original theorem [89, Thm. 1.1]. In the original paper the requirements on l are less strict.*

We choose to simplify the theorem to avoid the use of so-called Besov spaces.

Note that the possible non-uniqueness of solutions to the elliptic boundary value problem is clear from the fact that u_j is present on the right-hand side of the a priori estimate. Also, the theorem implies that a uniqueness result for smooth solutions can be extended to a uniqueness result for all functions.

The presented analysis of ellipticity, and the associated regularity properties, is done modulo smoothing terms and this motivates a finer characterisation of the non-smoothness of solutions to operator equations and boundary value problems, even in the non-elliptic case. First, note that the differential operator D is local in the sense that it preserves support, i.e.

$$\operatorname{supp} Du \subseteq \operatorname{supp} u, \quad u \in \mathscr{D}'(\Omega).$$

The property that D is local is also clear from the fact that $(Du)(x_0)$ only depends on u evaluated in a neighbourhood around $x_0 \in \Omega$. Not all pseudo-differential operators share this local property, but pseudo-differential operators are pseudo-local in the sense that they preserve the so-called *singular support* [38, Prop. 7.11]. This property has motivated the development of various techniques to analyse how the application of pseudo-differential operators actually change the non-smoothness of functions. These techniques make up microlocal analysis, which is used to study operators in the pseudo-differential framework. As we will see in the next subsection, this can for instance be used to provide qualitative information about solutions to both elliptic and non-elliptic boundary value problems.

2.2.3 Microlocal analysis and propagation of singularities

A compactly supported distribution $u \in \mathscr{E}'(\Omega)$ is smooth if, and only if, it satisfies the bound

$$|\hat{u}(\xi)| \leq C_N(1 + |\xi|)^{-N}, \tag{2.6}$$

for some constants $C_N < \infty$ and all $\xi \in \mathbb{R}^n, N \in \mathbb{N}_0$. This result is known as Schwartz's Paley–Wiener theorem [45, Thm. 7.3.1], [82, Thm. 7.22]. It shows the equivalence of smoothness of a compactly supported distribution and a Fourier transform that is rapidly decreasing in all directions. The set of points at which a distribution fails to be smooth is characterised by its singular support.

Definition 2.17 (Singular support)**.** *For a distribution $u \in \mathscr{D}'(\Omega)$ the singular support of u, denoted* $\operatorname{sing\,supp} u$*, is the set of points in Ω having no open neighbourhood to which the restriction of u is a smooth function [45, Def. 2.2.3].*

Distributions being non-smooth will violate the bound (2.6) at every point in the singular support. However, the singular support only gives information about the spatial localisation of singularities of a given distribution and does not provide information about in which directions it fails to be smooth. The directions turn out to be very important in the analysis of pseudo-differential operators applied to non-smooth distributions. This motivates the construction of a set which besides the spatial localisation of singularities includes the directions in which smoothness is lost. This set is called *the wave front set*.

To determine the microlocal smoothness of a distribution $u \in \mathscr{D}'(\Omega)$ at a point $x_0 \in \Omega$ we first localise in space. For this we multiply the distribution with smooth cut-off functions $\phi \in C_0^\infty(\Omega)$ supported in a neighbourhood around x_0. This creates a distribution having compact support around x_0 and the same local smoothness properties as u, and can thus be analysed using the bound (2.6). This makes it possible to define microlocal smoothness at a point $x_0 \in \Omega$, in direction $\xi_0 \in \mathbb{R}^n \setminus 0$.

Definition 2.18 (Microlocal smoothness)**.** *A distribution $u \in \mathscr{D}'(\Omega)$ is microlocally smooth at (x_0, ξ_0) if there exists $\phi \in C_0^\infty(\Omega)$ with $\phi(x_0) \neq 0$ and an open cone Γ containing ξ_0 such that $v = \phi u$ satisfies* (2.6) *for all $\xi \in \Gamma$ [91, Sec. 8.6].*

To localise the directions in which smoothness is lost we introduce the cone $\Sigma(u)$ of all $\xi_0 \in \mathbb{R}^n \setminus 0$ having no conic neighbourhood Γ such that (2.6) is satisfied when $\xi \in \Gamma$. At every point $x_0 \in \Omega$ we can define the set

$$\Sigma_{x_0}(u) = \bigcap_{\phi} \Sigma(\phi u); \quad \phi \in C_0^\infty(\Omega), \quad \phi(x_0) \neq 0.$$

Note that $\Sigma_{x_0}(u)$ is empty if, and only if, $x_0 \notin \operatorname{sing\,supp} u$ and otherwise closed in $\mathbb{R}^n \setminus 0$. At $x_0 \in \Omega$ the conic set $\Sigma_{x_0}(u)$ defines the directions where u is non-smooth, and this is the information which defines the wave front set.

Definition 2.19 (Wave front set)**.** *If $u \in \mathscr{D}'(\Omega)$, then the closed subset of $\Omega \times (\mathbb{R}^n \setminus 0)$ defined by*

$$\mathrm{WF}(u) = \{(x, \xi) \in \Omega \times (\mathbb{R}^n \setminus 0); \xi \in \Sigma_x(u)\}$$

is called the wave front set *of u [45, Def. 8.1.2].*

Note that the wave front set consist of points and directions and is therefore a subset of the cartesian product of the two sets Ω and $\mathbb{R}^n \setminus 0$.

For $u \in \mathscr{D}'(\Omega)$ the projection of $\mathrm{WF}(u)$ in Ω is $\operatorname{sing\,supp} u$, and for $u \in \mathscr{E}'(\mathbb{R}^n)$ the projection of $\mathrm{WF}(u)$ in $\mathbb{R}^n \setminus 0$ is $\Sigma(u)$ [45, Def. 8.1.2; Prop. 8.1.3]. Thus, the

wave front set is a finer characteristic of the singularities of u than $\operatorname{sing\,supp} u$ and $\Sigma(u)$.

In the analysis of pseudo-differential operators applied to non-smooth distributions, the characteristic set plays an important role.

Definition 2.20 (Characteristic set)**.** *Let P be a classical pseudo-differential operator of order m on Ω. The characteristic set is defined by*

$$\operatorname{Char}(P) = \{(x,\xi) \in \Omega \times (\mathbb{R}^n \setminus 0),\ \mathfrak{p}^{(0)}(x,\xi) = 0\},$$

where $\mathfrak{p}^{(0)}(x,\xi)$ is the principal symbol of P [87, Cor. A.1.2.].

Note that if P is an elliptic operator then $\operatorname{Char}(P)$ is the empty set. In the following we will denote by $(\mathfrak{p}^{(0)})^{-1}(0)$ the set of points in $\Omega \times (\mathbb{R}^n \setminus 0)$ for which $\mathfrak{p}^{(0)} = 0$.

The definitions of the wave front set for distributions and the characteristic set for pseudo-differential operators are very useful in the analysis of both global and local properties of solution to certain classes of PDEs. An important part of microlocal analysis is concerned with the extent to which the wave front set of a solution to a PDE is determined by the wave front set of the right-hand side and the characteristic set of the governing partial differential operator. For a classical pseudo-differential operator, the following theorem provides an important relation, in which the first embedding shows the pseudo-local nature of pseudo-differential operators.

Theorem 2.21 (Pseudo-local nature)**.** *Let P be a classical pseudo-differential operator of order m on Ω and let $u \in \mathscr{D}'(\Omega)$. If either P is properly supported or $u \in \mathscr{E}'(\Omega)$, then*

$$\operatorname{WF}(Pu) \subset \operatorname{WF}(u) \subset \operatorname{WF}(Pu) \cup \operatorname{Char}(P) \text{ [87, Cor. A.1.4.].}$$

Note that if P is an elliptic differential operator then $\operatorname{Char}(P)$ is the empty set and it follows directly that $\operatorname{WF}(u) = \operatorname{WF}(Pu)$.

It is possible to give a finer description of the wave front set of u by considering so-called *bicharacteristics*.

Definition 2.22 (Bicharacteristics)**.** *For a smooth real valued function $a(x,\xi)$ defined on an open subset of $\Omega \times (\mathbb{R}^n \setminus 0)$, an integral curve $(x(t),\xi(t))$ of the*

system of equations

$$\begin{cases} \dfrac{d}{dt}x(t) = \dfrac{\partial}{\partial \xi}a(x,\xi), \\ \dfrac{d}{dt}\xi(t) = -\dfrac{\partial}{\partial x}a(x,\xi), \end{cases}$$

is called a bicharacteristic of $a(x,\xi)$ *[87, Def. 17.1.].*

A bicharacteristic of a function $a(x,\xi)$ is called a *null bicharacteristic* if

$$a(x(t),\xi(t)) = 0,$$

and the projections of bicharacteristics into x-space are called the bicharacteristic curves or rays.

For a classical pseudo-differential operator P, the null bicharacteristic curves of the principal symbol are only proper curves (i.e. not just a point) if the operator is of principal type.

Definition 2.23 (Principal type operators)**.** *A classical pseudo-differential operator* P *(or its principal symbol* $\mathfrak{p}^{(0)}$*) is said to be of principal type if, and only if,* $\frac{\partial}{\partial \xi}\mathfrak{p}^{(0)} \neq 0$ *at each point* $(x,\xi) \in (\mathfrak{p}^{(0)})^{-1}(0)$ *[45, Def. 26.1.8].*

We can now state one of the most remarkable results in microlocal analysis, originally formulated by Duistermaat and Hörmander [31], which is the theorem on propagation of singularities.

Theorem 2.24 (Propagation of singularities for operators of real principal type)**.** *Let* P *be a classical pseudo-differential operator having a real principal symbol* $\mathfrak{p}^{(0)}$ *and let* $u \in \mathscr{D}'(\Omega)$*. Let either* P *be properly supported or* $u \in \mathscr{E}'(\Omega)$*, such that* Pu *makes sense. Then if* Γ *is any connected interval of a null bicharacteristic of the function* $\mathfrak{p}^{(0)}(x,\xi)$ *not intersecting* $\mathrm{WF}(Pu)$ *then either* $\Gamma \subset \mathrm{WF}(u)$ *or* $\Gamma \cap \mathrm{WF}(u) = \emptyset$ *[87, Thm. A.1.1.].*

This theorem tells us that if some point along a null bicharacteristic is part of $\mathrm{WF}(u)$, then the whole bicharacteristic is part of $\mathrm{WF}(u)$ as long as it does not intersect $\mathrm{WF}(Pu)$.

The stated theorem of propagation of singularities does only cover the case where P has a principal symbol of real principal type. A similar result can also be stated for classical pseudo-differential operators of constant multiplicity that satisfies a so-called *Levi condition*; that is a condition on the lower order terms.

We first give the definition of operators of constant multiplicity.

Definition 2.25 (Constant multiplicity). *$P \in \Psi^m(\Omega)$ is said to have constant multiplicity if its principal symbol $\mathfrak{p}^{(0)}$ can be factorised in the form*

$$\mathfrak{p}^{(0)} = \prod_{j=1}^{s} \mathfrak{q}_j^{r_j},$$

where $\mathfrak{q}_j$ are smooth symbols of real principal type and the curves defined by $\mathfrak{q}_j^{-1}(0)$ are mutually disjoint in $\Omega \times (\mathbb{R}^n \setminus 0)$ [23, Def. 2.5.].

The relevant Levi condition for this analysis takes the following form.

Definition 2.26 (Levi condition). *Let $P \in \Psi^m(\Omega)$ have a real principal symbol $\mathfrak{p}^{(0)}$ of constant multiplicity. We say that P satisfies the* Levi condition *at a point $(x_0, \xi_0) \in (\mathfrak{p}^{(0)})^{-1}(0) \subset \Omega \times (\mathbb{R}^n \setminus 0)$ if for every solution φ to the equation*

$$\mathfrak{q}_j(x, \nabla\varphi(x)) = 0, \quad \textit{(for those } j \textit{ where } \mathfrak{q}_j(x_0, \xi_0) = 0\textit{)}$$

in a neighbourhood of x_0 where $\nabla\varphi(x_0) = \xi_0$ satisfies

$$e^{-it\phi} P(\alpha e^{it\phi}) = \mathcal{O}(t^{m-r_j}) \quad t \to \infty,$$

for all $\alpha \in C_0^\infty(\Omega)$ with support in a neighbourhood x_0 where $\nabla\varphi \neq \mathbf{0}$. An operator that satisfies the Levi condition at a point $(x_0, \xi_0) \in (\mathfrak{p}^{(0)})^{-1}(0)$ satisfies the condition for all points in $(\mathfrak{p}^{(0)})^{-1}(0)$ [24, Def. 1.2.].

For a specific operator it can be difficult to check if it satisfies the stated Levi condition. A certain type of operators with constant multiplicity can be decomposed, which makes the analysis of the Levi condition much more simple.

Definition 2.27 (Decomposition of operators). *Let $P \in \Psi^m(\Omega)$ have constant multiplicity. We say that P can be decomposed relative to the factor $\mathfrak{q}_j$ of $\mathfrak{p}^{(0)}$ if*

$$P = \sum_{k=0}^{r_j} B_k Q_j^k,$$

for certain operators $B_k \in \Psi^{m-r_j}(\Omega)$ and where Q_j denotes an operator with principal symbol $\mathfrak{q}_j(x, \xi)$ [23, Def. 2.9.].

The following lemma shows how the presented decomposition is related to the Levi condition.

Lemma 2.28. *(Levi condition and decomposable operators) Let $P \in \Psi^m(\Omega)$ have constant multiplicity. Then P satisfies the Levi condition for the factor $\mathfrak{q}_j$ if, and only if, P can be decomposed relative to the factor $\mathfrak{q}_j$ [23, Thm. 2.10.].*

We end this chapter with the theorem on the propagation of singularities for operators of constant multiplicity.

Theorem 2.29 (Propagation of singularities for operators of constant multiplicity)**.** *Let $P \in \Psi^m(\Omega)$ be an operator with a real principal symbol $\mathfrak{p}^{(0)}$ of constant multiplicity satisfying the Levi condition and let $u \in \mathscr{D}'(\Omega)$. Let either P be properly supported or $u \in \mathscr{E}'(\Omega)$, such that Pu makes sense. Then if $\Gamma \in \Omega \times (\mathbb{R}^n \setminus 0)$ is any connected interval of a null bicharacteristic of one of the factors $\mathfrak{q}_j(x,\xi)$ not intersecting $\mathrm{WF}(Pu)$, then either $\Gamma \subset \mathrm{WF}(u)$ or $\Gamma \cap \mathrm{WF}(u) = \emptyset$ [24, Thm. 1.1.].*

Chapter 3

Mathematical formulations of the hybrid inverse problem

In this chapter we present two formulations of the hybrid inverse problem that was presented in Sec. 1.2.3. By a simple substitution at the PDE level, it is possible to formulate the problem as a system of non-linear PDE problems. Another approach is to make a linearisation of a non-linear map and thereby formulate the inverse problem as a system of linear PDE problems. Both problems will be analysed theoretically and numerically in Chap. 4 and 5.

3.1 Non-linear formulation

A way to formulate the problem described by (1.3)-(1.4) is to recast the set of generalised Laplace problems (1.3) as non-linear PDE problems. For this, we eliminate the unknown function σ from the PDEs using the interior measurements, $\sigma = \frac{H_j}{|\nabla u_j|^p}$. This gives the set of non-linear PDE problems

$$\begin{cases} \nabla \cdot \dfrac{H_j}{|\nabla u_j|^p} \nabla u_j = 0 & \text{in } \Omega, \\ u_j = f_j & \text{on } \partial\Omega, \end{cases} \qquad 1 \leq j \leq J, \tag{3.1}$$

for known functions $\{H_j\}_{j=1}^J$. In this setting the procedure for solving the inverse problem would be to first solve the problems for $\{u_j\}_{j=1}^J$ and then use the knowledge of $\{H_j\}_{j=1}^J$ to determine σ. Note that the problems (3.1) are actually quasi-linear, but in this text we will not distinguish between quasi-linear and non-linear problems.

In Sec. 4.1 we classify the problems expressed by (3.1) and discuss the implications. Later, in Sec. 5.2.1, we explain how to construct an iterative reconstruction method based on this non-linear formulation, and in Sec. 5.3.1 we present related numerical results.

3.2 Linear formulation

Consider the non-linear interior data map defined by

$$\mathcal{H}_j : \sigma \mapsto \sigma |\nabla u_j|^p, \; p > 0. \tag{3.2}$$

In this section we use the theory of linearisations of non-linear maps in Banach spaces (see Sec. 2.1) to derive a linear approximation of this operator. This will ultimately lead to a linear inverse problem, expressed by a linear system of PDE problems, which is the starting point for the classification of the linearised inverse problem and the analysis of the propagation of singularities which are presented in the next chapter.

Let $C_+^\infty(\bar{\Omega})$ be the smooth functions in $\bar{\Omega}$ uniformly bounded below by a strictly positive constant. We denote the function $\tilde{\sigma} \in C_+^\infty(\bar{\Omega})$ the *reference* conductivity, and denote the corresponding *reference* potential by $\tilde{u}_j \in H^1(\Omega)$, which is the solution to (1.3), when σ is replaced by $\tilde{\sigma}$. Furthermore we define by

$$\tilde{H}_j := \tilde{\sigma} |\nabla \tilde{u}_j|^p, \quad p > 0,$$

the *reference* interior data.

The interior map operator (3.2) can relate the difference $\sigma - \tilde{\sigma}$ to the corresponding difference in interior data $H_j - \tilde{H}_j$ by the simple relation

$$\mathcal{H}_j(\sigma) - \mathcal{H}_j(\tilde{\sigma}) = H_j - \tilde{H}_j. \tag{3.3}$$

The Fréchet derivative of $\mathcal{H}_j$ at $\tilde{\sigma}$ evaluated at $\sigma - \tilde{\sigma}$ is a function that approximates $\mathcal{H}_j(\sigma) - \mathcal{H}_j(\tilde{\sigma})$ to first-order in $\sigma - \tilde{\sigma}$. In this way, (3.3) is transformed into a linear relation.

We begin the derivation by establishing the functional setting. The following lemma implies that $\mathcal{H}_j$ can be considered as a mapping

$$\mathcal{H}_j : L^\infty_+(\Omega) \to L^2(\Omega),$$

under certain regularity assumptions on Ω and the imposed boundary conditions. Here $L^\infty_+(\Omega)$ denotes the space of functions in $L^\infty(\Omega)$ that are uniformly bounded below by a strictly positive constant in Ω.

Lemma 3.1. *Let $\sigma \in L^\infty_+(\Omega)$, $f_j \in C^\infty(\partial\Omega)$ and assume that $\partial\Omega$ is smooth. For the solution u_j to the problem (1.3), the interior data expressed by $\sigma|\nabla u_j|^p$ is an $L^2(\Omega)$-function for any $0 < p < \infty$.*

Proof. Standard elliptic regularity theory implies that $u_j \in H^1(\Omega)$ and therefore $|\nabla u_j| \in L^2(\Omega)$. By the embedding of Lebesgue spaces, this is sufficient to conclude that $\sigma|\nabla u_j|^p \in L^2(\Omega)$ for any $0 < p \leq 1$, since $\sigma \in L^\infty_+(\Omega)$.

For the case $p > 1$, define by $F \in C^\infty(\bar{\Omega})$ a function that satisfies $F|_{\partial\Omega} = f$. An example of such a function would be the (harmonic) solution to the problem (1.3) for some constant σ. By introducing the function $v = u_j - F \in H^1_0(\Omega)$ the problem (1.3) can be recast as the homogeneous problem

$$\begin{cases} \nabla \cdot \sigma \nabla v = -\nabla \cdot \sigma \nabla F & \text{in } \Omega, \\ v = 0 & \text{on } \partial\Omega. \end{cases}$$

By the uniform ellipticity of the problem, and the fact that $\sigma|\nabla F| \in L^{2p}(\Omega)$, the results of Meyers [67, Chap. 3] imply that there exists a unique solution $v \in H^1_0(\Omega)$ for which $|\nabla v| \in L^{2p}(\Omega)$. This is clearly sufficient to conclude that $\sigma|\nabla u_j|^p \in L^2(\Omega)$ for $1 < p < \infty$. □

The linearisation of $\mathcal{H}_j$ is simplified if we consider it is a two-step mapping

$$\mathcal{H}_j : \sigma \mapsto \{\sigma, u_j\} \mapsto \sigma|\nabla u_j|^p.$$

First we will analyse how the first step can be linearised. For this we linearise the solution operator

$$\mathcal{U}_j : \sigma \mapsto u_j(\sigma),$$

for the problem (1.3), near the reference conductivity $\tilde{\sigma} \in C^\infty_+(\bar{\Omega})$.

Lemma 3.2. *The solution operator $\mathcal{U}_j : \sigma \mapsto u_j(\sigma)$ for the problem (1.3) is Fréchet differentiable as an operator from $L^\infty(\Omega) \to H^1_0(\Omega)$ at $\tilde{\sigma} \in C^\infty_+(\bar{\Omega})$. The*

Fréchet derivative in the direction $\delta\sigma \in L^\infty(\Omega)$ is given by

$$\mathrm{d}\mathcal{U}_j|_{\tilde{\sigma}}(\delta\sigma) = \delta u_j, \tag{3.4}$$

where $\delta u \in H_0^1(\Omega)$ is the unique weak solution to the homogeneous problem

$$\begin{cases} \nabla \cdot \tilde{\sigma}\nabla\delta u_j = -\nabla \cdot \delta\sigma\nabla\tilde{u}_j & \text{in } \Omega, \\ \delta u_j = 0 & \text{on } \partial\Omega, \end{cases} \tag{3.5}$$

where $\tilde{u}_j \in H^1(\Omega)$ denotes the solution to (1.3), when σ is replaced by $\tilde{\sigma}$.

Proof. It is sufficient to show that $\mathrm{d}\mathcal{U}_j|_{\tilde{\sigma}}$ given by (3.4) is a bounded linear operator from $L^\infty(\Omega) \to H_0^1(\Omega)$ satisfying

$$\lim_{\delta\sigma\to 0} \frac{\|\mathcal{U}_j(\tilde{\sigma}+\delta\sigma) - \mathcal{U}_j(\tilde{\sigma}) - \mathrm{d}\mathcal{U}_j|_{\tilde{\sigma}}(\delta\sigma)\|_{H^1(\Omega)}}{\|\delta\sigma\|_{L^\infty(\Omega)}} = 0. \tag{3.6}$$

The linearity of $\mathrm{d}\mathcal{U}_j|_{\tilde{\sigma}}$ is obvious, since by definition (see (3.5)) δu_j is linear in $\delta\sigma$. To prove boundedness, note that $\delta\sigma|\nabla\tilde{u}_j| \in L^2(\Omega)$. By the results of Meyers [67, Chap. 3] this is sufficient to conclude that $\delta u \in H_0^1(\Omega)$.

We are left to show that (3.6) is satisfied. Now, consider the weak form of the homogeneous problem (3.5) given by

$$\int_\Omega \tilde{\sigma}\nabla\delta u_j \cdot \nabla\phi\, dx = -\int_\Omega \delta\sigma\nabla\tilde{u}_j \cdot \nabla\phi\, dx, \quad \forall\, \phi \in H_0^1(\Omega).$$

By choosing δu_j as the test function and since $\tilde{\sigma} \in C_+^\infty(\bar{\Omega})$ and $\delta\sigma \in L^\infty(\Omega)$, we get the relation

$$\|\nabla\delta u_j\|_{L^2(\Omega)}^2 \leq c\|\delta\sigma\|_{L^\infty(\Omega)}\|\nabla\tilde{u}_j \cdot \nabla\delta u_j\|_{L^1(\Omega)},$$

for some positive constant c. We abuse notation a bit and use the letter c throughout the proof to symbolise some sufficiently large positive constant. Because $\tilde{u}_j \in H^1(\Omega)$ we get using Hölder's inequality

$$\|\nabla\delta u_j\|_{L^2(\Omega)} \leq c\|\delta\sigma\|_{L^\infty(\Omega)}. \tag{3.7}$$

By the definition of $\mathcal{U}_j$, we get the relation

$$\nabla \cdot (\tilde{\sigma}+\delta\sigma)\nabla(\mathcal{U}_j(\tilde{\sigma}+\delta\sigma) - \mathcal{U}_j(\tilde{\sigma}) - \mathrm{d}\mathcal{U}_j|_{\tilde{\sigma}}(\delta\sigma)) = -\nabla \cdot \delta\sigma\nabla\delta u_j,$$

which in weak form can be expressed as

$$\int_\Omega (\tilde{\sigma}+\delta\sigma)\nabla(\mathcal{U}_j(\tilde{\sigma}+\delta\sigma)-\mathcal{U}_j(\tilde{\sigma})-\mathrm{d}\mathcal{U}_j|_{\tilde{\sigma}}(\delta\sigma))\cdot\nabla\phi\,dx = \\ -\int_\Omega \delta\sigma\nabla\delta u_j\cdot\nabla\phi\,dx, \quad \forall\,\phi\in H_0^1(\Omega).$$

Since $\mathcal{U}_j(\tilde{\sigma}+\delta\sigma)-\mathcal{U}_j(\tilde{\sigma})-\mathrm{d}\mathcal{U}_j|_{\tilde{\sigma}}(\delta\sigma)\in H_0^1(\Omega)$ we can use it as a test function. Together with the theorem of absolutely integrable functions [25, Lem. 1.7.2] we get the relation

$$\|\nabla(\mathcal{U}_j(\tilde{\sigma}+\delta\sigma)-\mathcal{U}_j(\tilde{\sigma})-\mathrm{d}\mathcal{U}_j|_{\tilde{\sigma}}(\delta\sigma))\|^2_{L^2(\Omega)}\leq \\ \frac{\|\delta\sigma\|_{L^\infty(\Omega)}}{\|\tilde{\sigma}+\delta\sigma\|_{L^\infty(\Omega)}}\|\nabla\delta u_j\cdot\nabla(\mathcal{U}_j(\tilde{\sigma}+\delta\sigma)-\mathcal{U}_j(\tilde{\sigma})-\mathrm{d}\mathcal{U}_j|_{\tilde{\sigma}}(\delta\sigma))\|_{L^1(\Omega)}. \tag{3.8}$$

Now, for $\|\delta\sigma\|_{L^\infty(\Omega)}$ sufficiently small (i.e. $\|\delta\sigma\|_{L^\infty(\Omega)} < \frac{1}{2}\|\tilde{\sigma}\|_{L^\infty(\Omega)}$), the inequality

$$\|\tilde{\sigma}+\delta\sigma\|_{L^\infty(\Omega)} > \frac{1}{2}\|\tilde{\sigma}\|_{L^\infty(\Omega)},$$

is satisfied following the reverse triangle inequality, thus

$$\frac{\|\delta\sigma\|_{L^\infty(\Omega)}}{\|\tilde{\sigma}+\delta\sigma\|_{L^\infty(\Omega)}}\leq c\|\delta\sigma\|_{L^\infty(\Omega)}.$$

When applying Hölder's inequality to the right-hand side of (3.8) we end up with the expression

$$\|\nabla(\mathcal{U}_j(\tilde{\sigma}+\delta\sigma)-\mathcal{U}_j(\tilde{\sigma})-\mathrm{d}\mathcal{U}_j|_{\tilde{\sigma}}(\delta\sigma))\|_{L^2(\Omega)}\leq c\|\delta\sigma\|_{L^\infty(\Omega)}\|\nabla\delta u_j\|_{L^2(\Omega)}.$$

Now, Poincaré's inequality [34, Thm. 5.6.1.3] can be applied because

$$\mathcal{U}_j(\tilde{\sigma}+\ \delta\sigma)-\mathcal{U}_j(\tilde{\sigma})-\mathrm{d}\mathcal{U}_j|_{\tilde{\sigma}}(\delta\sigma)$$

has zero trace, and together with (3.7) this gives the desired relation

$$\|\mathcal{U}_j(\tilde{\sigma}+\delta\sigma)-\mathcal{U}_j(\tilde{\sigma})-\mathrm{d}\mathcal{U}_j|_{\tilde{\sigma}}(\delta\sigma)\|_{H^1(\Omega)}\leq c\|\delta\sigma\|^2_{L^\infty(\Omega)},$$

which proves that (3.6) is satisfied. □

Under the stated regularity assumptions, and if $|\nabla\tilde{u}_j|$ is bounded below by a positive constant in Ω, we can now show that the operator $\mathcal{H}_j$ is Fréchet differentiable at $\tilde{\sigma}$ as a mapping $L^\infty(\Omega)\to L^2(\Omega)$. The assumption on $|\nabla\tilde{u}_j|$ to be bounded below by a positive constant is a general assumption when analysing

the presented problem. How to ensure that this assumption is satisfied, will be discussed shortly in Sec. 4.5.

Theorem 3.3. *Let $\tilde{\sigma} \in C_+^\infty(\bar{\Omega})$ and denote by $\tilde{u}_j \in H^1(\Omega)$ the solution to (1.3), when σ is replaced by $\tilde{\sigma}$. Also let $|\nabla \tilde{u}|$ be bounded below by a positive constant in Ω. The map*

$$\mathcal{H}_j : \sigma \mapsto \sigma |\nabla u_j|^p, \quad p > 0,$$

is then Fréchet differentiable as a map $L^\infty(\Omega) \to L^2(\Omega)$ at $\tilde{\sigma}$ and the Fréchet derivative in the direction $\delta\sigma \in L^\infty(\Omega)$ is given by

$$\mathrm{d}\,\mathcal{H}_j|_{\tilde{\sigma}}(\delta\sigma) = \delta\sigma |\nabla \tilde{u}|^p + p\tilde{\sigma} \frac{\nabla \tilde{u}_j \cdot \nabla \delta u_j}{|\nabla \tilde{u}_j|^{2-p}}, \tag{3.9}$$

where $\delta u_j \in H_0^1(\Omega)$ is defined as in Lem. 3.2.

Proof. It is sufficient to show that $\mathrm{d}\,\mathcal{H}_j|_{\tilde{\sigma}}$ given by (3.9) is a bounded linear operator from $L^\infty(\Omega) \to L^2(\Omega)$ satisfying

$$\lim_{\delta\sigma \to 0} \frac{\|\mathcal{H}_j(\tilde{\sigma} + \delta\sigma) - \mathcal{H}_j(\tilde{\sigma}) - \mathrm{d}\,\mathcal{H}_j|_{\tilde{\sigma}}(\delta\sigma)\|_{L^2(\Omega)}}{\|\delta\sigma\|_{L^\infty(\Omega)}} = 0.$$

The linearity of $\mathrm{d}\,\mathcal{H}_j|_{\tilde{\sigma}}$ is obvious, since by definition (see Lem. 3.2) δu_j is linear in $\delta\sigma$. Standard elliptic regularity theory implies that $\tilde{u} \in C^\infty(\Omega)$, which together with the triangle inequality and the inequality from (3.7) gives

$$\|\mathrm{d}\,\mathcal{H}_j|_{\tilde{\sigma}}(\delta\sigma)\|_{L^2(\Omega)} = \left\| \delta\sigma |\nabla \tilde{u}|^p + p\tilde{\sigma} \frac{\nabla \tilde{u} \cdot \nabla \delta u}{|\nabla \tilde{u}|^{2-p}} \right\|_{L^2(\Omega)} \leq c\|\delta\sigma\|_{L^\infty(\Omega)}.$$

This proves the boundedness. For sufficiently small $\delta\sigma$ we find by Taylor expansion of $|\cdot|^p$ away from zero that

$$\mathcal{H}_j(\tilde{\sigma} + \delta\sigma) - \mathcal{H}_j(\tilde{\sigma}) = \delta\sigma |\nabla \tilde{u}_j|^p + p\tilde{\sigma} \frac{\nabla \tilde{u}_j \cdot \nabla \delta u_j}{|\nabla \tilde{u}_j|^{2-p}} + \mathcal{O}(|\delta\sigma|^2).$$

This implies that

$$\|\mathcal{H}_j(\tilde{\sigma} + \delta\sigma) - \mathcal{H}_j(\tilde{\sigma}) - \mathrm{d}\,\mathcal{H}_j|_{\tilde{\sigma}}(\delta\sigma)\|_{L^2(\Omega)} \leq c\|\delta\sigma\|^2_{L^\infty(\Omega)},$$

which proves that (3.9) is satisfied. □

From the previous lemma, we see that the Fréchet derivative of $\mathcal{H}_j$ at $\tilde{\sigma}$ in

direction $\delta\sigma \in L^\infty(\Omega)$ is given by

$$\mathrm{d}\,\mathcal{H}_j|_{\tilde{\sigma}}(\delta\sigma) = \delta\sigma|\nabla\tilde{u}_j|^p + p\tilde{\sigma}\frac{\nabla\tilde{u}_j\cdot\nabla\delta u_j}{|\nabla\tilde{u}_j|^{2-p}} \qquad \text{in } \Omega,$$

where $\delta u_j \in H_0^1(\Omega)$ solves

$$\begin{cases} \nabla\cdot\tilde{\sigma}\nabla\delta u_j = -\nabla\cdot\delta\sigma\nabla\tilde{u}_j & \text{in } \Omega, \\ \delta u_j = 0 & \text{on } \partial\Omega. \end{cases} \tag{3.10}$$

It follows that a solution $\delta\sigma \in L^\infty(\Omega)$ to

$$\mathrm{d}\,\mathcal{H}_j|_{\tilde{\sigma}}(\delta\sigma) = H_j - \tilde{H}_j \ \text{ in } \Omega, \tag{3.11}$$

is a first-order approximation of $\sigma - \tilde{\sigma}$. Note that this equation is only in the appropriate functional setting under the regularity assumption $H_j \in L^2(\Omega)$, which in turn imposes additional regularity conditions on σ.

The equations (3.10) and (3.11) form a collection of linear PDE problems for $\{\delta\sigma, \{\delta u_j\}_{j=1}^J\}$ which can be expressed in the matrix form of a boundary value problem

$$\begin{cases} \mathcal{L}\boldsymbol{u} = \boldsymbol{f} & \text{in } \Omega, \\ \mathcal{B}\boldsymbol{u} = \boldsymbol{0} & \text{on } \partial\Omega, \end{cases} \tag{3.12}$$

where $\mathcal{L}$ is the sparse $2J \times (J+1)$ matrix of partial differential operators

$$\mathcal{L}(x,\nabla) = \begin{bmatrix} \nabla\cdot([\cdot]\nabla\tilde{u}_1) & \nabla\cdot(\tilde{\sigma}\nabla[\cdot]) & \cdots & 0 \\ \vdots & \vdots & \ddots & \vdots \\ \nabla\cdot([\cdot]\nabla\tilde{u}_J) & 0 & \cdots & \nabla\cdot(\tilde{\sigma}\nabla[\cdot]) \\ |\nabla\tilde{u}_1|^p & p\tilde{\sigma}\frac{\nabla\tilde{u}_1\cdot\nabla[\cdot]}{|\nabla\tilde{u}_1|^{2-p}} & \cdots & 0 \\ \vdots & \vdots & \ddots & \vdots \\ |\nabla\tilde{u}_J|^p & 0 & \cdots & p\tilde{\sigma}\frac{\nabla\tilde{u}_J\cdot\nabla[\cdot]}{|\nabla\tilde{u}_J|^{2-p}} \end{bmatrix},$$

$\mathcal{B}$ is the boundary operator

$$\mathcal{B} = \begin{bmatrix} 0 & 0 & \cdots & 0 \\ 0 & 1 & \cdots & 0 \\ \vdots & \vdots & \ddots & \vdots \\ 0 & 0 & \cdots & 1 \end{bmatrix},$$

and the solution vector $\boldsymbol{u}$ and right-hand side $\boldsymbol{f}$ are given by

$$\boldsymbol{u} = \begin{bmatrix} \delta\sigma \\ \delta u_1 \\ \vdots \\ \delta u_J \end{bmatrix} \quad \text{and} \quad \boldsymbol{f} = \begin{bmatrix} 0 \\ \vdots \\ 0 \\ H_1 - \tilde{H}_1 \\ \vdots \\ H_J - \tilde{H}_J \end{bmatrix}.$$

The boundary value problem (3.12) is the PDE formulation of the linearised inverse problem, which will be analysed in the next chapter.

Chapter 4

Stability of hybrid inverse problems in impedance tomography

The analysis of linear and non-linear PDEs are often considered as separate mathematical fields and this is simply a consequence of the different methods needed for their respective theoretical and numerical analysis. Along with the distinction between the linear and non-linear formulation, many PDEs can be classified.

The point of classification is to find categories of PDEs for which the overall qualitative properties of their respective solutions are similar. Such properties is often closely tied to concepts like existence, uniqueness and regularity. L.C. Evans, in his preface to his AMS text on PDEs [94], mentions that he finds it unsatisfactory to classify PDEs, since it creates the false impression that a general classification scheme exists. In fact, several equations cannot be classified, for instance equations that abruptly change behaviour in time or space (e.g. the Euler–Tricomi equation) and many PDEs of interest do not fall into the standard categories. However, if we indeed can classify a partial differential operator or a related boundary value problem, it is possible to state very powerful results on the properties of any solutions.

Certain PDEs can be classified as elliptic, parabolic or hyperbolic, by analogy with the three conic sections. We already gave a mathematical description of elliptic operators in Chap. 2, and results from pseudo-differential calculus showed that elliptic PDEs give raise to smooth solutions; at least as smooth as coefficients of the equation. Hyperbolic operators are very different, since they are direction dependent, and they allow discontinuous solutions with distinct behaviour along certain directions. Parabolic PDEs are the borderline case between elliptic and hyperbolic PDEs. Elliptic and parabolic PDEs correspond to global phenomena, such that any local change in a coefficient can potentially change the solution globally. In the hyperbolic setting, a local change will only change the solution locally, but not necessary limited to the same position in space.

Classification of PDEs has close bonds to the modelling of physical systems. An elliptic PDE often models a physical system that has reached an equilibrium state. Parabolic PDEs usually model processes of a diffusive nature, such as the distribution of heat in a given region over time. Hyperbolic PDEs model wave-like behaviour from, say, oscillating mechanical systems. Therefore, two PDEs that are classified differently are, in some sense, related to two mathematical models of systems that describe very different physical phenomena. Note, that we only study time-independent problems in this thesis, but the close coupling to time-dependent physical problems is still true, if one spatial dimension in the mathematical setting corresponds to the direction of time in the physical setting.

Note that one can experience problems that can be classified differently in space or time, or based on certain directions in the Fourier domain. The latter situation should mathematically be seen from the perspective of pseudo-differential calculus. Also, for an operator to be classified as elliptic in all but one direction, or to be classified as parabolic, is based on an equivalent property of the highest order term. However, the latter type of classification seems to be used exclusively for operators in time-dependent problems that are second-order and elliptic in space and first-order in time.

In this chapter we classify and analyse the stability properties of the specific type of non-linear and linear hybrid inverse problems that was formulated in Chap. 3. To be more specific, we analyse how the classification and the related stability properties are related to the value of p and the choice of boundary conditions. This type of analysis is closely related to the works of Kuchment and Steinhauer [57], and Bal [13], and to some extent recent work by Moltalto and Stefanov [71].

4.1 Classification of the non-linear problem

A simple derivation shows that the non-linear PDE problems (3.1) can be recast in the equivalent form of a system of non-linear problems

$$\begin{cases} \left(I - p\dfrac{\nabla u_j \otimes \nabla u_j}{|\nabla u_j|^2}\right) : \nabla \otimes \nabla u_j + \nabla \ln H_j \cdot \nabla u_j = 0 & \text{in } \Omega, \\ u_j = f_j & \text{on } \partial\Omega, \end{cases} \qquad 1 \le j \le J,$$

where I is the identity in $\mathbb{R}^n$, $\boldsymbol{\xi}_1 \otimes \boldsymbol{\xi}_2$ denotes the outer product of the vectors $\boldsymbol{\xi}_1$ and $\boldsymbol{\xi}_2$, and $\boldsymbol{M}_1 : \boldsymbol{M}_2$ denotes the Frobenius inner product of the matrices $\boldsymbol{M}_1$ and $\boldsymbol{M}_2$.

The classification is determined by the eigenvalues of the matrix in front of the second-order term. As we now show, these eigenvalues have a very simple form.

Theorem 4.1. *For $|\nabla u_j| \neq 0$, the matrix*

$$I - p\frac{\nabla u_j \otimes \nabla u_j}{|\nabla u_j|^2},$$

has eigenvalues $(1-p, 1, \cdots, 1)$.

Proof. First note that

$$\left(I - p\frac{\nabla u_j \otimes \nabla u_j}{|\nabla u_j|^2}\right) \nabla u_j = (1-p)\nabla u_j.$$

Therefore $1-p$ is an eigenvalue for the eigenvector ∇u_j. Now, pick $n-1$ non-zero vectors $\{\boldsymbol{v}_i\}_{i=1}^{n-1}$ all mutually orthogonal and orthogonal to ∇u_j. For such vectors

$$\left(I - p\frac{\nabla u_j \otimes \nabla u_j}{|\nabla u_j|^2}\right) \boldsymbol{v}_i = \boldsymbol{v}_i, \quad 1 \le i \le n-1.$$

Thus, 1 is an eigenvalue for all the $n-1$ eigenvectors $\{\boldsymbol{v}_i\}_{i=1}^{n-1}$. □

This implies that the matrix in front of the second-order term is either (positive) definite, has a one-dimensional kernel or has signature $(1, n-1)$. From the usual classification scheme for quasi-linear PDEs [94], it follows that each problem in (3.1) is elliptic for $p < 1$, degenerate elliptic for $p = 1$ and hyperbolic for $p > 1$. A similar result was found by Bal [13].

For $p < 1$, the ellipticity implies that perturbations stay local and the stability is optimal. In the degenerate elliptic case, ∇u_j is the direction of degeneracy and we cannot expect optimal stability, due to the presence of so-called characteristic directions aligned with ∇u_j. In the hyperbolic case, ∇u_j is the time-like direction and even if each problem in (3.1) is equipped with additional Neumann boundary data, uniqueness can only be guaranteed in parts of Ω [14]. The hyperbolic nature of the problem gives rise to solutions with wave-like behaviour, possibly allowing singularities to propagate along specific curves. Actually, in the non-elliptic case, the so-called light cone, related to the structure of the corresponding (Lorentzian) metric defined by the non-definite matrix coefficient, consists of the vectors $\boldsymbol{v}$ for which $\boldsymbol{v}^T \left(I - p \frac{\nabla u_j \otimes \nabla u_j}{|\nabla u_j|^2} \right) \boldsymbol{v} = 0$. These can be considered as the directions in which the problem is non-elliptic and play an important role in the stability properties of the solution to the quasi-linear PDE; see also the discussion on this topic by Bal [13]. This is of course closely linked to the performance of the numerical algorithms working on the non-linear formulation and we will see an example of this in Sec. 5.3.1.

We should also mention that for $p \leq 1$ the non-linear PDEs in (3.1) are each a Euler–Lagrange equation for the problem of minimizing the functional

$$\int_\Omega H_j |\nabla u_j|^{2-p} dx, \quad 1, \leq j \leq J.$$

In this way, u_j can be characterised as a minimiser of a variational problem in an appropriate function space. For $p < 1$ the functional is strictly convex and one can actually show that a unique minimiser exists [64].

4.2 Stability and classification of the linear problem

Based on the derivation of the linearised inverse problem in Sec. 3.2, we now analyse the stability properties of the solution $\boldsymbol{u}$ to the boundary value problem

$$\begin{cases} \mathcal{L}\boldsymbol{u} = \boldsymbol{f} & \text{in } \Omega, \\ \mathcal{B}\boldsymbol{u} = \boldsymbol{0} & \text{on } \partial\Omega. \end{cases} \tag{4.1}$$

We follow the scheme that was developed in Sec. 2.2. We first show exactly when the operator $\mathcal{L}$ is elliptic in the DN sense for well-chosen DN numbers and present a geometrical interpretation of the ellipticity condition. We then show that $\mathcal{B}$ covers $\mathcal{L}$, i.e. the Lopatinskii condition is satisfied, if $\mathcal{L}$ is DN elliptic and then state the associated stability properties which follows from the fundamental

stability theorem for elliptic boundary value problems; see Thm. 2.15.

Based on the definition of the principal symbol of matrix differential operators (Def. 2.11), we find that the only possible way to choose the DN numbers for $\mathcal{L}$ is

$$\{s_i\}_{i=1}^{J} = 0, \{s_i\}_{i=J+1}^{2J} = -1, t_1 = 1, \{t_j\}_{j=2}^{J+1} = 2.$$

The DN numbers for $\mathcal{B}$ are then

$$\kappa = \{-1, -2, \cdots, -2\}.$$

The principal parts of $\mathcal{L}$ and $\mathcal{B}$ are then found to be

$$\mathcal{L}^{(0)} = \begin{bmatrix} \nabla\tilde{u}_1 \cdot \nabla[\cdot] & \tilde{\sigma}\Delta[\cdot] & \cdots & 0 \\ \vdots & \vdots & \ddots & \vdots \\ \nabla\tilde{u}_J \cdot \nabla[\cdot] & 0 & \cdots & \tilde{\sigma}\Delta[\cdot] \\ |\nabla\tilde{u}_1|^p & p\tilde{\sigma}\frac{\nabla\tilde{u}_1\cdot\nabla[\cdot]}{|\nabla\tilde{u}_1|^{2-p}} & \cdots & 0 \\ \vdots & \vdots & \ddots & \vdots \\ |\nabla\tilde{u}_J|^p & 0 & \cdots & p\tilde{\sigma}\frac{\nabla\tilde{u}_J\cdot\nabla[\cdot]}{|\nabla\tilde{u}_J|^{2-p}} \end{bmatrix} \quad \text{and} \quad (4.2)$$

$$\mathcal{B}^{(0)} = \begin{bmatrix} 0 & 0 & \cdots & 0 \\ 0 & 1 & \cdots & 0 \\ \vdots & \vdots & \ddots & \vdots \\ 0 & 0 & \cdots & 1 \end{bmatrix}.$$

The associated principal symbol of $\mathcal{L}^{(0)}$ is therefore

$$\mathfrak{l}^{(0)} = \begin{bmatrix} \nabla\tilde{u}_1 \cdot i\xi & -\tilde{\sigma}|\xi|^2 & \cdots & 0 \\ \vdots & \vdots & \ddots & \vdots \\ \nabla\tilde{u}_J \cdot i\xi & 0 & \cdots & -\tilde{\sigma}|\xi|^2 \\ |\nabla\tilde{u}_1|^p & p\tilde{\sigma}\frac{\nabla\tilde{u}_1\cdot i\xi}{|\nabla\tilde{u}_1|^{2-p}} & \cdots & 0 \\ \vdots & \vdots & \ddots & \vdots \\ |\nabla\tilde{u}_J|^p & 0 & \cdots & p\tilde{\sigma}\frac{\nabla\tilde{u}_J\cdot i\xi}{|\nabla\tilde{u}_J|^{2-p}} \end{bmatrix}.$$

For $\mathfrak{l}^{(0)}$ to have full rank (here $J+1$), it is a necessary and sufficient condition that at least one $((J+1)\times(J+1))$-subdeterminant of $\mathfrak{l}^{(0)}$ is non-zero. A simple analysis of the matrix structure shows that all these subdeterminants are either zero or take the form

$$\pm(\tilde{\sigma}|\xi|^2)^J \left(1 - p\frac{(\nabla\tilde{u}_j \cdot \xi)^2}{|\nabla\tilde{u}_j|^2|\xi|^2}\right), \quad 1 \le j \le J.$$

This makes it possible to state the following theorem.

Theorem 4.2. *Consider the boundary value problem given by* (4.1). *$\mathcal{L}$ is DN elliptic if, and only if, for all $(x,\xi) \in \Omega \times \mathbb{R}^n \setminus 0$ there exists $\nabla \tilde{u}_j \neq \mathbf{0}$ such that*

$$\frac{(\nabla \tilde{u}_j \cdot \xi)^2}{|\nabla \tilde{u}_j|^2 |\xi|^2} \neq \frac{1}{p}.$$

The implication of Thm. 4.2 is that the ellipticity of $\mathcal{L}$ is determined by the set $\{\nabla \tilde{u}_j\}_{j=1}^J$. Clearly $\mathcal{L}$ is always DN elliptic for $p < 1$. For $p \geq 1$, choosing $J \geq n$ is necessary to obtain an elliptic operator. A simple geometrical interpretation gives the following results [13, 57]: Loss of ellipticity corresponds to the intersection of the cones (in the ξ-variable) given by the equations $\frac{(\nabla \tilde{u}_j \cdot \xi)^2}{|\nabla \tilde{u}_j|^2 |\xi|^2} - \frac{1}{p} = 0$ at some point away from the apex. In Sec. 4.5 we discuss how ellipticity is related to the choice of boundary conditions.

We now show that the Lopatinskii condition is satisfied for the problem (4.1) if $\mathcal{L}$ is DN elliptic.

Theorem 4.3. *Consider the boundary value problem given by* (4.1). *If $\mathcal{L}$ is DN elliptic, i.e. it satisfies the condition in Thm. 4.2, then $\mathcal{B}$ covers $\mathcal{L}$.*

Proof. We have to show that the requirements of Def. 2.14 is satisfied. Based on the principal parts $\mathcal{L}^{(0)}, \mathcal{B}^{(0)}$ given by (4.2), we find that the relevant system of ODE problems takes the form

$$\begin{cases} \nabla \tilde{u}_j \cdot \left(i\boldsymbol{\zeta} + \boldsymbol{v} \dfrac{d}{dz} \right) w_1 + \tilde{\sigma} \left(i\boldsymbol{\zeta} + \boldsymbol{v} \dfrac{d}{dz} \right) \cdot \left(i\boldsymbol{\zeta} + \boldsymbol{v} \dfrac{d}{dz} \right) w_{j+1} = 0 & \text{for } z > 0, \\ |\nabla \tilde{u}_j|^p w_1 + p\tilde{\sigma} \dfrac{\nabla \tilde{u}_j \cdot \left(i\boldsymbol{\zeta} + \boldsymbol{v} \frac{d}{dz} \right)}{|\nabla \tilde{u}_j|^{2-p}} w_{j+1} = 0 & \text{for } z > 0, \\ w_{j+1} = 0 & \text{for } z = 0, \end{cases}'$$

for $1 \leq j \leq J$. In this system we can eliminate w_1, to get the ODE problems

$$\begin{cases} \alpha_j(x) \dfrac{d^2}{dz^2} w_{j+1} - \beta_j(x) \dfrac{d}{dz} w_{j+1} + \gamma_j(x) w_{j+1} = 0 & \text{for } z > 0, \\ w_{j+1} = 0 & \text{for } z = 0, \end{cases} \tag{4.3}$$

where

$$\alpha_j(x) = 1 - p\frac{(\nabla\tilde{u}_j \cdot \boldsymbol{v})^2}{|\nabla\tilde{u}_j|^2},$$
$$\beta_j(x) = 2ip\frac{(\nabla\tilde{u}_j \cdot \boldsymbol{\zeta})(\nabla\tilde{u}_j \cdot \boldsymbol{v})}{|\nabla\tilde{u}_j|^2} \quad \text{and}$$
$$\gamma_j(x) = p\frac{(\nabla\tilde{u}_j \cdot \boldsymbol{\zeta})^2}{|\nabla\tilde{u}_j|^2} - 1.$$

Since $\mathcal{L}$ is DN elliptic, we have that $\alpha_{j_0}(x) \neq 0$ for some $1 \leq j_0 \leq J$. Thus, we have a second-order ODE with constant coefficients for w_{j_0+1}.

First, we notice that β is purely imaginary and both α and γ are real. This implies that the corresponding characteristic polynomial has a purely imaginary root of multiplicity two, or two roots of the form $\pm k_1 + ik_2$, for some $k_1, k_2 \in \mathbb{R}$. It follows by a simple calculation that $w_{j_0+1} = 0$ is then the only possible solution to the ODE problem, satisfying the additional requirement $w_{j_0+1} \to 0$ for $z \to +\infty$. From this it follows by the relation

$$|\nabla\tilde{u}_j|^p w_1 + p\tilde{\sigma}\frac{\nabla\tilde{u}_j \cdot \left(i\boldsymbol{\zeta} + \boldsymbol{v}\frac{d}{dz}\right)}{|\nabla\tilde{u}_{j_0}|^{2-p}} w_{j_0+1} = 0 \quad \text{for } z > 0,$$

that also $w_1 = 0$. We are then left with the problems

$$\begin{cases} \left(i\boldsymbol{\zeta} + \boldsymbol{v}\frac{d}{dz}\right) \cdot \left(i\boldsymbol{\zeta} + \boldsymbol{v}\frac{d}{dz}\right) w_{j+1} = 0 & \text{for } z > 0, \\ w_{j+1} = 0 & \text{for } z = 0, \end{cases} \qquad 1 \leq j \leq J.$$

Since $\boldsymbol{\zeta} \cdot \boldsymbol{v} = 0$ we can recast this as

$$\begin{cases} \frac{d^2}{dz^2} w_{j+1} - w_{j+1} = 0 & \text{for } z > 0, \\ w_{j+1} = 0 & \text{for } z = 0, \end{cases}$$

for which the only solutions satisfying $w_{j+1} \to 0$ for $z \to +\infty$ are $w_{j+1} = 0$ for $1 \leq j \leq J$. Thus, we can conclude that $\{w_j\}_{j=1}^{J+1} = 0$ and therefore the Lopatinskii condition is satisfied. □

Remark 4.4. *In a paper by Bal [13], the solutions to the ODE problem* (4.3) *seem to be compared to the solutions to the corresponding ODE setting for the Laplace problem with Dirichlet boundary conditions, to show that the Lopatinski condition is satisfied. But it is not sufficient to consider only the highest order term in the ODE problem to analyse the vector space of possible solutions, because lower order terms can influence the asymptotic behaviour. A simple*

example is the ODE problem

$$\begin{cases} \dfrac{d^2}{dz^2}w + 2\dfrac{d}{dz}w + 2w = 0 & \text{for } z > 0, \\ w = 0 & \text{for } z = 0, \end{cases}$$

which has the non-zero solution $w = e^{-z}\sin(z)$ *that indeed satisfies* $w \to 0$ *for* $z \to +\infty$.

Now that we have shown the condition for DN ellipticity of $\mathcal{L}$ and shown that this implies that the Lopatinskii condition is satisfied for the problem (4.1), we can state a stability estimate for the inverse problem, based on the results of Thm. 2.15.

Theorem 4.5. *Consider the boundary value problem given by* (4.1)*, where* $\mathcal{L}$ *is DN elliptic. Let* $q > 1$ *and* $l \geq 0$ *be an integer such that* $q(l+1) > n$*. If* $\mathcal{L}_{ij}^{(k)} \in W^{l-s_i,q}(\Omega), \mathcal{L}_{ij}^{(0)}$ *are continuous functions and* $H_j - \tilde{H}_j \in W^{l+1,q}(\Omega)$*, then the following a priori estimate holds:*

$$\|\delta\sigma\|_{W^{l+1,q}(\Omega)} + \sum_{j=1}^{J} \|\delta u_j\|_{W^{l+2,q}(\Omega)} \leq c_1 \sum_{j=1}^{J} \|H_j - \tilde{H}_j\|_{W^{l+1,q}(\Omega)} + c_2 \left(\|\delta\sigma\|_{L^q(\Omega)} + \sum_{j=1}^{J} \|\delta u_j\|_{L^q(\Omega)} \right).$$

The implication of the stated stability result is that a DN elliptic problem gives optimal stability properties for the reconstruction, since we can reconstruct $\delta\sigma$ with exactly the same regularity as the given data. Of course, this is only applicable to an inverse problem where the given data has the required regularity.

4.3 Stability and classification of the normal form

The symbolic calculus, and especially operator compositions, becomes less complicated if we express the linearised inverse problem as a first-order system. As proved by Cosner [27], a DN elliptic matrix operator can always be expressed by an equivalent first-order matrix that is elliptic in the classical sense; see Def. 2.10. The transformation is done by differentiation of rows and by introducing additional variables, related to the two sets of DN numbers $\{s_i\}$ and $\{t_j\}$, respectively.

In our case, we take the gradient of the equations in (3.11), but as a technicality we first multiply the equations by $(|\nabla\tilde{u}_1|^{-p},\cdots,|\nabla\tilde{u}_J|^{-p})^T$ to make the calculation of the principal symbol more simple. For this, we assume that the interior data has the required regularity, such that the performed operations make sense. Furthermore, we introduce $\{\nabla\delta u_j\}_{j=1}^J$ as unknowns. We can then express the second-order linear problem in terms of the equivalent first-order problem

$$\begin{cases} \acute{\mathcal{L}}\acute{\boldsymbol{u}} = \acute{\boldsymbol{f}} & \text{in } \Omega, \\ \acute{\mathcal{B}}\acute{\boldsymbol{u}} = \mathbf{0} & \text{on } \partial\Omega, \end{cases} \tag{4.4}$$

where $\acute{\mathcal{L}}$ is the sparse $3J\times(2J+1)$ matrix of operators

$$\acute{\mathcal{L}} = \begin{bmatrix} \nabla\cdot([\cdot]\nabla\tilde{u}_1) & \nabla\cdot(\tilde{\sigma}[\cdot]) & \cdots & 0 & 0 & \cdots & 0 \\ \vdots & \vdots & \ddots & \vdots & \vdots & \ddots & \vdots \\ \nabla\cdot([\cdot]\nabla\tilde{u}_J) & 0 & \cdots & \nabla\cdot(\tilde{\sigma}[\cdot]) & 0 & \cdots & 0 \\ \nabla & \nabla\left(p\tilde{\sigma}\frac{\nabla\tilde{u}_1\cdot[\cdot]}{|\nabla\tilde{u}_1|^2}\right) & \cdots & 0 & 0 & \cdots & 0 \\ \vdots & \vdots & \ddots & \vdots & \vdots & \ddots & \vdots \\ \nabla & 0 & \cdots & \nabla\left(p\tilde{\sigma}\frac{\nabla\tilde{u}_J\cdot[\cdot]}{|\nabla\tilde{u}_J|^2}\right) & 0 & \cdots & 0 \\ 0 & -I & \cdots & 0 & \nabla & \cdots & 0 \\ \vdots & \vdots & \ddots & \vdots & \vdots & \ddots & \vdots \\ 0 & 0 & \cdots & -I & 0 & \cdots & \nabla \end{bmatrix} \tag{4.5}$$

and the solution vector $\acute{\boldsymbol{u}}$ and right-hand side $\acute{\boldsymbol{f}}$ are given by

$$\acute{\boldsymbol{u}} = \begin{bmatrix} \delta\sigma \\ \nabla\delta u_1 \\ \vdots \\ \nabla\delta u_J \\ \delta u_1 \\ \vdots \\ \delta u_J \end{bmatrix} \quad \text{and} \quad \acute{\boldsymbol{f}} = \begin{bmatrix} 0 \\ \vdots \\ 0 \\ \nabla(|\nabla\tilde{u}_1|^{-p}(H_1-\tilde{H}_1)) \\ \vdots \\ \nabla(|\nabla\tilde{u}_J|^{-p}(H_J-\tilde{H}_J)) \\ \mathbf{0} \\ \vdots \\ \mathbf{0} \end{bmatrix}.$$

With this notation, the boundary operator $\acute{\mathcal{B}}$ is defined by the relation

$$\acute{\mathcal{B}}\acute{\boldsymbol{u}} = (0,\cdots,0,\delta u_1,\cdots,\delta u_J)^T.$$

We use the acute accent (´) as the notation for operators and vector functions in this first-order setting. Note that the transformation into the first-order system has not introduced additional boundary conditions. Also note that when we take the gradient of the equations in (3.11) we differentiate the data. This should, if possible, always be avoided in practical applications, where measurement noise could be present.

The first part of the analysis concerns the ellipticity of $\acute{\mathcal{L}}$, and this follows directly by the construction that leads to the definition of DN ellipticity [27]. Therefore we state the following theorem without a proof.

Theorem 4.6. *$\acute{\mathcal{L}}$ is elliptic at $(x, \xi) \in \Omega \times (\mathbb{R}^n \setminus 0)$ if, and only if, $\mathcal{L}$ is DN elliptic.*

For $J > 1$, the linearised inverse problem (4.4) is not a square system of equations, and such a system is difficult to analyse. In this case, it is the standard approach to define a solution of such overdetermined systems using the method of least squares.

A simple analysis of the operator $\acute{\mathcal{L}}$ shows that it acts as an operator

$$\acute{\mathcal{L}} : H^1(\Omega) \times [H_{\mathrm{div}}(\Omega)]^J \times [H^1(\Omega)]^J \to [L^2(\Omega)]^{(1+2n)J},$$

for sufficiently smooth $\tilde{\sigma}$. Here $H_{\mathrm{div}}(\Omega)$ denote the usual (Hilbert) space of vector functions in $[L^2(\Omega)]^n$ for which the divergence is also an $L^2(\Omega)$ function; see e.g. [92, Chap. 20]. Thus, it specifies the appropriate function space setting which satisfies the homogeneous boundary conditions:

$$\acute{\boldsymbol{u}} \in H^1(\Omega) \times [H_{\mathrm{div}}(\Omega)]^J \times [H_0^1(\Omega)]^J.$$

To this formulation we assign the energy functional

$$I(\acute{\boldsymbol{u}}) = \|\acute{\mathcal{L}}\acute{\boldsymbol{u}} - \acute{\boldsymbol{f}}\|^2_{L^2(\Omega)}.$$

A least squares solution to the linearised inverse problem (4.4) is then a function

$$\acute{\boldsymbol{u}}^\star = \operatorname*{argmin}_{\acute{\boldsymbol{u}}} I(\acute{\boldsymbol{u}}), \tag{4.6}$$

for $\acute{\boldsymbol{u}}$ satisfying the previously defined homogeneous boundary conditions in appropriate function spaces. We want to classify and state stability results for solutions to this least squares formulation. In order to do so, we want to transform it into a boundary value problem for $\acute{\boldsymbol{u}}^\star$.

It is a classical result from quadratic minimisation that for a standard matrix equation, a solution to the normal equation is a solution that minimises the

residual in the least squares sense [62]. For a matrix operator equation, this is often also the case, but additional boundary conditions might need to be imposed on the solution space.

For $\acute{\boldsymbol{u}}^\star$ to be a minimiser of (4.6), a necessary condition is that the first variation vanishes, which means that

$$\lim_{t\to 0}\frac{d}{dt}I(\acute{\boldsymbol{u}}^\star + t\boldsymbol{\phi}) = 0, \quad \forall\, \boldsymbol{\phi} \in H^1(\Omega)\times[H_{\mathrm{div}}(\Omega)]^J \times [H_0^1(\Omega)]^J.$$

This leads to the least squares weak formulation of (4.4). We want to find $\acute{\boldsymbol{u}}^\star \in H^1(\Omega)\times[H_{\mathrm{div}}(\Omega)]^J \times [H_0^1(\Omega)]^J$ such that

$$\int_\Omega \acute{\mathcal{L}}\acute{\boldsymbol{u}}^\star\, \acute{\mathcal{L}}\boldsymbol{\phi} dx = \int_\Omega \acute{\boldsymbol{f}}\, \acute{\mathcal{L}}\boldsymbol{\phi}\, dx,\ \forall\, \boldsymbol{\phi} \in H^1(\Omega)\times[H_{\mathrm{div}}(\Omega)]^J \times [H_0^1(\Omega)]^J. \quad (4.7)$$

We now show how the solutions to this weak formulation are related to the solutions of a certain boundary value problem. For this we need an expression for the adjoint $\acute{\mathcal{L}}^*$ in a suitable functional setting.

Lemma 4.7. *Denote by V and W the function spaces $H^1(\Omega)\times[H_{div}(\Omega)]^J \times [H^1(\Omega)]^J$ and $[L^2(\Omega)]^{(1+2n)J}$, respectively, and denote the scalar and vector elements of the functions $\boldsymbol{v}\in V, \boldsymbol{w}\in W$ by*

$$\boldsymbol{v} = (v_1, \boldsymbol{v}_2, \cdots, \boldsymbol{v}_{J+1}, v_{J+2}, \cdots, v_{2J+1})^T,$$
$$\boldsymbol{w} = (w_1, \cdots, w_J, \boldsymbol{w}_{J+1}, \cdots, \boldsymbol{w}_{3J})^T.$$

Let the operator $\acute{\mathcal{L}}\colon V\to W$ be given by (4.5). If $\boldsymbol{v}=\boldsymbol{0}$ on $\partial\Omega$, then the adjoint $\acute{\mathcal{L}}^*\colon W^*\to V^*$ can then be identified by the L^2-inner product

$$\langle \boldsymbol{v}, \acute{\mathcal{L}}^*\boldsymbol{w}\rangle_{V,V^*} = (\acute{\mathcal{L}}\boldsymbol{v}, \boldsymbol{w})_W,\ \forall\, \boldsymbol{v}\in V, \boldsymbol{w}\in V,$$

where

$$\acute{\mathcal{L}}^*\boldsymbol{w} = \begin{bmatrix} \sum_{j=1}^J -\nabla\tilde{u}_j\cdot\nabla w_j - \nabla\cdot\boldsymbol{w}_{J+j} \\ -\tilde{\sigma}\nabla w_1 - p\tilde{\sigma}\frac{\nabla\tilde{u}_1\nabla\cdot\boldsymbol{w}_{J+1}}{|\nabla\tilde{u}_1|^2} - \boldsymbol{w}_{2J+1} \\ \vdots \\ -\tilde{\sigma}\nabla w_J - p\tilde{\sigma}\frac{\nabla\tilde{u}_J\nabla\cdot\boldsymbol{w}_{2J}}{|\nabla\tilde{u}_J|^2} - \boldsymbol{w}_{3J} \\ -\nabla\cdot\boldsymbol{w}_{2J+1} \\ \vdots \\ -\nabla\cdot\boldsymbol{w}_{3J} \end{bmatrix} \in V^*.$$

Proof. The adjoint of $\acute{\mathcal{L}}$ is defined as a mapping $\acute{\mathcal{L}}^*\colon W^* \to V^*$ satisfying

$$(\acute{\mathcal{L}}\boldsymbol{v}, \boldsymbol{w})_W = \langle \boldsymbol{v}, \acute{\mathcal{L}}^* \boldsymbol{w} \rangle_{V,V^*},\ \forall\, \boldsymbol{v} \in V, \boldsymbol{w} \in W.$$

Note that $W^* = \left([L^2(\Omega)]^{(1+2n)J}\right)^*$ can be identified by W. By integration by parts we find that

$$\begin{aligned}
(\acute{\mathcal{L}}\boldsymbol{v}, \boldsymbol{w})_W &= \int_\Omega (\acute{\mathcal{L}}\boldsymbol{v}) \cdot \boldsymbol{w}\, dx \\
&= \sum_{j=1}^{J} \int_\Omega \Big[(\nabla \cdot v_1 \nabla \tilde{u}_j + \nabla \cdot \tilde{\sigma} \boldsymbol{v}_{j+1}) w_j \\
&+ \nabla \left(v_1 + p\tilde{\sigma} \frac{\nabla \tilde{u}_j \cdot \boldsymbol{v}_{j+1}}{|\nabla \tilde{u}_j|^2} \right) \cdot \boldsymbol{w}_{J+j} \\
&+ (-\boldsymbol{v}_{j+1} + \nabla v_{J+j+1}) \cdot \boldsymbol{w}_{2J+j} \Big]\, dx \\
&= \sum_{j=1}^{J} \int_\Omega \Big[v_1 (-\nabla \tilde{u}_j \cdot \nabla w_j - \nabla \cdot \boldsymbol{w}_{J+j}) \\
&+ \boldsymbol{v}_{j+1} \cdot \left(-\tilde{\sigma} \nabla w_j - p\tilde{\sigma} \frac{\nabla \tilde{u}_j \nabla \cdot \boldsymbol{w}_{J+j}}{|\nabla \tilde{u}_j|^2} - \boldsymbol{w}_{2J+j} \right) \\
&+ v_{J+j+1} \left(-\nabla \cdot \boldsymbol{w}_{2J+j} \right) \Big]\, dx \\
&+ \int_{\partial\Omega} \Big[\left(v_1 (\nabla \tilde{u}_j \cdot \boldsymbol{n}) + \tilde{\sigma} (\boldsymbol{v}_{j+1} \cdot \boldsymbol{n}) \right) w_j \\
&+ \left(v_1 + p\tilde{\sigma} \frac{\nabla \tilde{u}_j \cdot \boldsymbol{v}_{j+1}}{|\nabla \tilde{u}_j|^2} \right) (\boldsymbol{w}_{J+j} \cdot \boldsymbol{n}) + v_{J+j+1} (\boldsymbol{w}_{2J+j} \cdot \boldsymbol{n}) \Big]\, ds, \\
&\forall\, \boldsymbol{v} \in V, \boldsymbol{w} \in W.
\end{aligned}$$

If $\boldsymbol{v} = 0$ on $\partial\Omega$ all boundary terms vanish, and we are left with

$$\begin{aligned}
(\acute{\mathcal{L}}\boldsymbol{v}, \boldsymbol{w})_W = \sum_{j=1}^{J} \int_\Omega \Big[& v_1 (-\nabla \tilde{u}_j \cdot \nabla w_j - \nabla \cdot \boldsymbol{w}_{J+j}) \\
& + \boldsymbol{v}_{j+1} \cdot \left(-\tilde{\sigma} \nabla w_j - p\tilde{\sigma} \frac{\nabla \tilde{u}_j \nabla \cdot \boldsymbol{w}_{J+j}}{|\nabla \tilde{u}_j|^2} - \boldsymbol{w}_{2J+j} \right) \\
& + v_{J+j+1} \left(-\nabla \cdot \boldsymbol{w}_{2J+j} \right) \Big]\, dx, \quad \forall\, \boldsymbol{v} \in V, \boldsymbol{w} \in W,
\end{aligned}$$

and we can therefore give a precise description of $\acute{\mathcal{L}}^*$ using the L^2-inner product.

In this setting we can identify the duality pairing, such that

$$\langle \boldsymbol{v}, \acute{\mathcal{L}}^* \boldsymbol{w} \rangle_{V,V^*} := (\boldsymbol{v}, \acute{\mathcal{L}}^* \boldsymbol{w})_W, \, \forall \, \boldsymbol{v} \in V, \boldsymbol{w} \in W,$$

where

$$\acute{\mathcal{L}}^* \boldsymbol{w} = \begin{bmatrix} \sum_{j=1}^{J} -\nabla \tilde{u}_j \cdot \nabla w_j - \nabla \cdot \boldsymbol{w}_{J+j} \\ -\tilde{\sigma} \nabla w_1 - p\tilde{\sigma} \frac{\nabla \tilde{u}_1 \nabla \cdot \boldsymbol{w}_{J+1}}{|\nabla \tilde{u}_1|^2} - \boldsymbol{w}_{2J+1} \\ \vdots \\ -\tilde{\sigma} \nabla w_J - p\tilde{\sigma} \frac{\nabla \tilde{u}_J \nabla \cdot \boldsymbol{w}_{2J}}{|\nabla \tilde{u}_J|^2} - \boldsymbol{w}_{3J} \\ -\nabla \cdot \boldsymbol{w}_{2J+1} \\ \vdots \\ -\nabla \cdot \boldsymbol{w}_{3J} \end{bmatrix} \in V^*.$$

□

From the definition of the adjoint $\acute{\mathcal{L}}^*$ it is possible to show a correspondence between solutions to the normal form and the weak form of the least squares formulation.

Lemma 4.8. *A solution* $\acute{\boldsymbol{u}}^\star$ *to*

$$\begin{cases} \acute{\mathcal{L}}^* \acute{\mathcal{L}} \acute{\boldsymbol{u}}^\star = \acute{\mathcal{L}}^* \acute{\boldsymbol{f}} & \text{in } \Omega, \\ \acute{\boldsymbol{u}}^\star = \boldsymbol{0} & \text{on } \partial\Omega, \end{cases} \tag{4.8}$$

is also a solution to the weak form of the least squares formulation (4.7)*, for* $\boldsymbol{\phi} = \boldsymbol{0}$ *on* $\partial\Omega$*.*

Proof. Let $\acute{\boldsymbol{u}}^\star \in H^1(\Omega) \times [H_{\text{div}}(\Omega)]^J \times [H^1(\Omega)]^J$ satisfy the boundary condition $\acute{\boldsymbol{u}}^\star = \boldsymbol{0}$ on $\partial\Omega$. From the definition of $\acute{\mathcal{L}}^*$ (see Lem. 4.7), we can then express the boundary value problem (4.8) in the weak form:

$$(\acute{\mathcal{L}} \acute{\boldsymbol{u}}^\star, \acute{\mathcal{L}} \acute{\boldsymbol{\phi}}) = (\acute{\boldsymbol{f}}, \acute{\mathcal{L}} \acute{\boldsymbol{\phi}}), \, \forall \, \acute{\boldsymbol{\phi}} \in H^1(\Omega) \times [H_{\text{div}}(\Omega)]^J \times [H^1(\Omega)]^J,$$

where $\acute{\boldsymbol{\phi}} = \boldsymbol{0}$ on $\partial\Omega$. Thus, a weak solution to the normal equation equipped with homogeneous Dirichlet boundary conditions corresponds to a solution to the weak form of the least squares formulation. □

Now we will continue the analysis of the boundary value problem

$$\begin{cases} \acute{\mathcal{L}}^* \acute{\mathcal{L}} \acute{\boldsymbol{u}} = \acute{\mathcal{L}}^* \acute{\boldsymbol{f}} & \text{in } \Omega, \\ \acute{\boldsymbol{u}} = \mathbf{0} & \text{on } \partial\Omega. \end{cases} \tag{4.9}$$

We will now show that the ellipticity results for $\acute{\mathcal{L}}$ can be extended to the normal operator $\acute{\mathcal{L}}^* \acute{\mathcal{L}}$.

Theorem 4.9. *The normal operator $\acute{\mathcal{L}}^* \acute{\mathcal{L}}$ is elliptic if, and only if, $\acute{\mathcal{L}}$ is elliptic, or equivalently $\mathcal{L}$ is DN elliptic.*

Proof. Because the differential equations that constitutes $\acute{\mathcal{L}}$ are all first-order, we have $(\acute{\mathfrak{l}}^* \acute{\mathfrak{l}})^{(0)} = (\acute{\mathfrak{l}}^*)^{(0)} \acute{\mathfrak{l}}^{(0)} = (\acute{\mathfrak{l}}^{(0)})^* \acute{\mathfrak{l}}^{(0)}$. Since all elements of $\acute{\mathfrak{l}}^{(0)}$ are complex expressions we have that $(\acute{\mathfrak{l}}^{(0)})^* = (\overline{\acute{\mathfrak{l}}^{(0)}})^T$, where $\bar{\cdot}$ denotes complex conjugation. The determinant $\det(\acute{\mathfrak{l}}^* \acute{\mathfrak{l}})^{(0)}$ can then be calculated using the Cauchy–Binet formula [36, p. 119]

$$\det((\acute{\mathfrak{l}}^* \acute{\mathfrak{l}})^{(0)}) = \det((\overline{\acute{\mathfrak{l}}^{(0)}})^T \acute{\mathfrak{l}}^{(0)}) = \sum_{\alpha=2J+1} |\det_{\alpha} \acute{\mathfrak{l}}^{(0)}|^2,$$

where the sum is taken over all $(2J+1)\times(2J+1)$ subdeterminants of the matrix $\acute{\mathfrak{l}}^{(0)}$. Thus, $(\acute{\mathfrak{l}}^* \acute{\mathfrak{l}})^{(0)}$ is invertible if, and only if, at least one of the subdeterminants of $\acute{\mathfrak{l}}^{(0)}$ is non-zero, and this is exactly the necessary and sufficient condition for ellipticity of $\acute{\mathcal{L}}$. □

We continue to show that the Lopatinskii condition is satisfied for (4.9) if $\acute{\mathcal{L}}$ is elliptic.

Theorem 4.10. *If $\acute{\mathcal{L}}$ is elliptic, or equivalently if $\mathcal{L}$ is DN elliptic, then the Lopatinskii condition is satisfied for the problem* (4.9).

Proof. If $\acute{\mathcal{L}}$ is elliptic, then $\acute{\mathcal{L}}^* \acute{\mathcal{L}}$ is an elliptic second-order square matrix operator. For such an operator, the corresponding Dirichlet problem satisfies the Lopatinskii condition [6, Sec. 1.1.4]. □

When $\acute{\mathcal{L}}^* \acute{\mathcal{L}}$ is elliptic it is therefore possible to state the associated stability properties of solutions to (4.9), which follows from the fundamental theorem for elliptic boundary value problems; see Thm. 2.15.

Theorem 4.11. *Consider the boundary value problem given by* (4.9)*, where $\acute{\mathcal{L}}$ is elliptic. Let $q > 1$ and $l \geq 0$ be an integer such that $q(l+1) > n$. If*

$(\acute{\mathcal{L}}^*\acute{\mathcal{L}})^{(k)}_{ij} \in W^{l,q}(\Omega), (\acute{\mathcal{L}}^*\acute{\mathcal{L}})^{(0)}_{ij}$ are continuous functions and $\acute{\mathcal{L}}^*\acute{\boldsymbol{f}} \in W^{l,q}(\Omega)$, then the following a priori estimate holds:

$$\|\acute{\boldsymbol{u}}\|_{W^{l+2,q}(\Omega)} \leq c_1 \sum_{j=1}^{J} \|\acute{\mathcal{L}}^*\acute{\boldsymbol{f}}\|_{W^{l,q}(\Omega)} + c_2\|\acute{\boldsymbol{u}}\|_{L^q(\Omega)}.$$

Note that $\acute{\mathcal{L}}^*\acute{\boldsymbol{f}}$ includes two differentiations of the data, thus again we see that this implies optimal stability for $\delta\sigma$. But in terms of regularity, we need one addition derivative for $\delta\sigma, \delta u_j$ and $H_j - \tilde{H}_j$.

Again, ellipticity is not a sufficient condition for injectivity of the operator. However, for the problem (4.9), injectivity of $\acute{\mathcal{L}}^*\acute{\mathcal{L}}$ can be proved under certain conditions. If $\acute{\mathcal{L}}$ is a matrix of differential operators with coefficients that are analytic, or sufficiently close to being analytic, or if the domain Ω is sufficiently small, then if $\acute{\mathcal{L}}^*\acute{\mathcal{L}}$ is elliptic it is also invertible with a bounded inverse. If the domain is large or the coefficients are not sufficiently close to being analytic, the unique continuation principle can be applied to state uniqueness when the principal symbol of $\acute{\mathcal{L}}$ satisfies certain requirements. This is explained in detail by Bal [13].

4.4 Propagation of singularities

Even though the concept of ellipticity can be extended to over-determined systems of PDEs, any established theory on the propagation of singularities for over-determined systems does not seem to exist in the literature. To circumvent this challenge, we are going to analyse a third type of formulation of the linearised inverse problem.

4.4.1 Transformation into a system of scalar problems

For this analysis, the symbolic calculus becomes less complicated if we express the linearised inverse problem by a system of scalar equations. Looking at the boundary value problem (3.12), we see that it consists of J equations which, by the Frechét derivative of $\mathcal{H}_j$, express how $\delta\sigma$ and $\{\delta u_j\}_{j=1}^J$ are related to perturbations in the interior data and J equations which relate $\delta\sigma$ and $\{\delta u_j\}_{j=1}^J$.

An elimination of $\{\delta u_j\}_{j=1}^J$ gives the set of scalar pseudo-differential equations

$$P_j \delta\sigma = H_j - \tilde{H}_j, \quad 1 \leq j \leq J, \tag{4.10}$$

where P_j is the non-local pseudo-differential operator

$$P_j = |\nabla \tilde{u}_j|^p + p\tilde{\sigma} \frac{\nabla \tilde{u}_j \cdot \nabla L_\sigma^{-1}(\nabla \cdot ([\cdot]\nabla \tilde{u}_j))}{|\nabla \tilde{u}_j|^{2-p}}. \tag{4.11}$$

Here L_σ^{-1} denotes a parametrix of the elliptic operator $L_\sigma := -\nabla \cdot (\tilde{\sigma}\nabla[\cdot])$.

Note that a parametrix is not unique, but only unique modulo smoothing terms [95, Cor. 4.3]. Since smoothing terms can be discarded in the analysis of ellipticity and propagation of singularities, the non-uniqueness is not of concern in this context.

The following theorem shows that P_j is both classical and properly supported.

Theorem 4.12. *Let $\tilde{\sigma} \in C_+^\infty(\Omega)$ and $\partial\Omega$ be smooth. Then the pseudo-differential operator P_j given by* (4.11) *is a classical and properly supported pseudo-differential operator in Ω of order zero with principal symbol*

$$\mathfrak{p}_j^{(0)} = |\nabla \tilde{u}_j|^p \left(1 - p\frac{(\nabla \tilde{u}_j \cdot \xi)^2}{|\nabla \tilde{u}_j|^2 |\xi|^2}\right). \tag{4.12}$$

Proof. It follows from standard elliptic regularity that $\tilde{\sigma} \in C_+^\infty(\Omega)$ implies $\tilde{u}_j \in C^\infty(\Omega)$. Therefore $\nabla \cdot [\cdot]\nabla \tilde{u}_j$ and $\nabla \tilde{u}_j \cdot \nabla[\cdot]$ are first-order differential operators with smooth coefficients and as a result both classical and properly supported pseudo-differential operators in $\Psi^1(\Omega)$ [52, p. 11],[87, p. 16]. Because L_σ is a second-order elliptic differential operator, it follows that there exists a parametrix, denoted by L_σ^{-1}, which is a classical and properly supported pseudo-differential elliptic operator and an element of $\Psi^{-2}(\Omega)$ [38, Thm. 7.18]. The operator

$$\nabla \tilde{u}_j \cdot \nabla L_\sigma^{-1}(\nabla \cdot ([\cdot]\nabla \tilde{u}_j))$$

is therefore a composition of pseudo-differential operators that are both classical and properly supported in Ω and therefore also such an operator. It follows that $P_j \in \Psi^0(\Omega)$ is also both classical and properly supported. The principal symbol of P_j is then the product of the principal symbols of each operator in the composition and this is easily found to be the expression given by (4.12). □

The linear scalar equations (4.10) are for $J > 1$ a redundant set of equations for $\delta\sigma$. In this case we are going to analyse the normal form of (4.10) given by the

single scalar equation

$$\sum_{j=1}^{J} P_j^* P_j \delta\sigma = \sum_{j=1}^{J} P_j^* (H_j - \tilde{H}_j). \tag{4.13}$$

Here $P_j^* \in \Psi^0(\Omega)$ denotes the formal adjoint of P_j [95, p. 21]. Note that by Thm. 4.12, P_j is classical and properly supported, which means that the composition $P_j^* P_j$ makes sense.

4.4.2 Classification of the scalar operator and the scalar normal operator

The microlocal analysis is related to the properties of the principal symbol of P_j. As we now show, the ellipticity of P_j depends on the parameter p.

Theorem 4.13. *Suppose $|\nabla \tilde{u}_j| \neq 0$. Then P_j is elliptic in Ω if, and only if, $p < 1$.*

Proof. P_j is elliptic in Ω if, and only if, its principal symbol is non-zero for all $(x, \xi) \in \Omega \times (\mathbb{R}^n \setminus 0)$. When $|\nabla \tilde{u}_j| \neq 0$ a vanishing principal symbol is equivalent to

$$\frac{(\nabla \tilde{u}_j(x) \cdot \xi)^2}{|\nabla \tilde{u}_j(x)|^2 |\xi|^2} = \frac{1}{p},$$

for some $(x, \xi) \in \Omega \times (\mathbb{R}^n \setminus 0)$. The expression of the left-hand side is clearly bounded by 1. Thus if $p < 1$ the equality is never satisfied and P_j is therefore elliptic in Ω. If $p \geq 1$, set $\xi = v(x)$ where $v(x)$ is the vector $\nabla \tilde{u}_j(x)$ rotated by an angle α_j, satisfying $\cos \alpha_j = \frac{1}{\sqrt{p}}$. Then the principal symbol vanishes for all $(x, v(x)) \in \Omega \times (\mathbb{R}^n \setminus 0)$ and P_j is therefore nowhere elliptic; see also the discussion after Thm. 4.2. □

A similar result has been found by Kuchment and Steinhauer [57], and Bal [13]. The theorem implies that if $p \geq 1$, more than one measurement of the interior data is necessary to get an elliptic operator. In this situation it makes sense to consider the problem formulated in the scalar normal form presented in (4.13). The condition that ensures ellipticity of the operator associated with the normal equation is stated in the following theorem.

Theorem 4.14. *$\sum_{j=1}^{J} P_j^* P_j$ is elliptic at $(x, \xi) \in \Omega \times (\mathbb{R}^n \setminus 0)$ if, and only if, there exists $|\nabla \tilde{u}_j(x)| \neq 0$ such that $\frac{(\nabla \tilde{u}_j(x) \cdot \xi)^2}{|\nabla \tilde{u}_j(x)|^2 |\xi|^2} \neq \frac{1}{p}$.*

Proof. Since all P_j are classical, the principal symbol of $\sum_{j=1}^{J} P_j^* P_j$ is the sum of squares of the modulus of the principal symbols of each operator P_j. Therefore the principal symbol is given by

$$\sum_{j=1}^{J} |\nabla \tilde{u}_j|^{2p} \left(1 - p\frac{(\nabla \tilde{u}_j \cdot \xi)^2}{|\nabla \tilde{u}_j|^2 |\xi|^2}\right)^2. \tag{4.14}$$

This expression is clearly positive at $(x, \xi) \in \Omega \times (\mathbb{R}^n \setminus 0)$ if, and only if, at least one of the operators P_j is elliptic. The result then follows by the proof of Thm. 4.13. □

4.4.3 Propagation of singularities for two operators

When a scalar problem is not elliptic it is possible that the solution has singularities besides those present in the right-hand side. However, the additional singularities can only be present along curves where the principal symbol vanishes. This is a simple interpretation of the classical result on the propagation of singularities; see Thm. 2.24. As we will see in the following analysis, it is possible to calculate these curves for the linearised inverse problem and state necessary conditions for the presence of singularities along such curves.

4.4.3.1 The scalar operator

When only a single interior data set is available, the relevant equation to analyse is

$$P_1 \delta\sigma = H_1 - \tilde{H}_1.$$

Thus, the propagation of singularities depends on the principal symbol of P_1. As seen from Thm. 4.12, the principal symbol of P_1 is given by

$$\mathfrak{p}_1^{(0)} = |\nabla \tilde{u}_1|^p \left(1 - p\frac{(\nabla \tilde{u}_1 \cdot \xi)^2}{|\nabla \tilde{u}_1|^2 |\xi|^2}\right).$$

We now show that P_1 is a real principal type operator if $p \neq 1$.

Lemma 4.15. *P_1 is of real principal type if, and only if, $p \neq 1$.*

Proof. Elliptic operators are trivially of principal type, so it suffices to consider

the case $p \geq 1$. Clearly $\mathfrak{p}_1^0$ is real and we find that

$$\mathfrak{p}_1^{(0)}(x,\xi) = 0 \Leftrightarrow \frac{(\nabla \tilde{u}_1 \cdot \xi)^2}{|\nabla \tilde{u}_1|^2 |\xi|^2} = \frac{1}{p}, \tag{4.15}$$

and therefore

$$\frac{\partial}{\partial \xi} \mathfrak{p}_1^{(0)}(x,\xi)\Big|_{\mathfrak{p}_1^{(0)}=0} = \frac{2|\nabla \tilde{u}_1|^p}{|\xi|^2} \left(\xi - p \frac{\nabla \tilde{u}_1 \cdot \xi}{|\nabla \tilde{u}_1|^2} \nabla \tilde{u}_1 \right).$$

This means that $\mathfrak{p}_1^{(0)}$ is of real principal type if, and only if, $\mathfrak{p}_1^{(0)}(x,\xi) = 0$ implies

$$\xi - p \frac{\nabla \tilde{u}_1 \cdot \xi}{|\nabla \tilde{u}_1|^2} \nabla \tilde{u}_1 \neq \mathbf{0}. \tag{4.16}$$

When $p = 1$, it can be seen from (4.15) that the vectors ξ and $\nabla \tilde{u}_j$ are parallel when ellipticity is lost and one finds that the inequality is not satisfied. When $p > 1$, the non-zero vectors $\nabla \tilde{u}_1$ and ξ cannot be parallel, and this is sufficient to conclude that (4.16) is satisfied. □

The classical theorem on the propagation of singularities for pseudo-differential operators of real principal type, Thm. 2.24, explains how singularities will propagate along the bicharacteristics. In the following theorem we show that the bicharacteristic curves are perpendicular to the direction in which ellipticity is lost.

Lemma 4.16. *For $p > 1$, the bicharacteristic curves of P_1 are perpendicular to the directions in which ellipticity is lost.*

Proof. By Def. 2.22, we find the bicharacteristics $(x(t), \xi(t)) \in \Omega \times (\mathbb{R}^n \setminus 0), t \in \mathbb{R}$ as integral curves of the system of equations

$$\begin{cases} \dfrac{dx(t)}{dt} &= \dfrac{\partial}{\partial \xi} \mathfrak{p}_1^{(0)}(x(t)), \xi(t)), \\ \dfrac{d\xi(t)}{dt} &= -\dfrac{\partial}{\partial x} \mathfrak{p}_1^{(0)}(x(t)), \xi(t)), \end{cases}$$

where $\mathfrak{p}_1^{(0)}(x,\xi) = 0$. We find that

$$\frac{dx(t)}{dt} = \frac{2|\nabla \tilde{u}_1(x(t))|^p}{|\xi(t)|^2} \left(\xi(t) - p \frac{\nabla \tilde{u}_1(x(t)) \cdot \xi(t)}{|\nabla \tilde{u}_1(x(t))|^2} \nabla \tilde{u}_1(x(t)) \right).$$

Note that $\frac{dx(t)}{dt} \cdot \xi(t) = 0$, when $\mathfrak{p}_1^{(0)}(x,\xi) = 0$, which means that $x(t)$ is a curve perpendicular to the direction in which ellipticity is lost. □

The previous lemma implies that singularities can only propagate in directions perpendicular to the direction in which ellipticity is lost. Thus, by Thm. 2.24, we can state the following theorem.

Theorem 4.17. *For $p > 1$, a solution $\delta\sigma$ to the equation*

$$P_1 \delta\sigma = H_1 - \tilde{H}_1,$$

has singularities propagating in directions perpendicular to the direction in which ellipticity is lost.

4.4.3.2 The normal operator

For the analysis of propagation of singularities for the normal operator we restrict ourselves to the situation with two measurements ($J = 2$) in two dimensions ($n = 2$). If one had a single measurement ($J = 1$) the normal formulation would not need to be introduced and if more than two measurements were available ($J > 2$), then one can ensure that the normal operator is elliptic by a specific choice of boundary conditions. This will also be discussed briefly in Section 4.5.

When $J = 2$, the normal formulation is the equation

$$(P_1^* P_1 + P_2^* P_2)\delta\sigma = P_1^*(H_1 - \tilde{H}_1) + P_2^*(H_2 - \tilde{H}_2). \tag{4.17}$$

The propagation of singularities depends on the symbol of $P_1^* P_1 + P_2^* P_2$. The normal form increases the order of the zeros of the principal symbol, as seen by (4.14). As a result, the principal symbol of $P_1^* P_1 + P_2^* P_2$ is *not* of principal type, and the classical propagation theory does not provide any information on the propagation of singularities. Instead we are going to use the theory for principal symbols of constant multiplicity.

We first show that the operator $P_1^* P_1 + P_2^* P_2$ can be decomposed in the form of a polynomial of an operator of real principal type. Then we show that this implies that $P_1^* P_1 + P_2^* P_2$ is of constant multiplicity and that it satisfies the relevant Levi condition. We then calculate the bicharacteristic curves along which the singularities propagate.

Theorem 4.18. *Let $p > 1$, $\Omega \subset \mathbb{R}^2$ and let $P_1^* P_1 + P_2^* P_2$ be the pseudo-differential operator from the scalar normal equation* (4.17)*. Assume that ellipticity is lost in the direction $\boldsymbol{v}(x) \in \mathbb{R}^2, |\boldsymbol{v}| = 1$, in a neighbourhood of a point $x_0 \in \Omega$. Define by $\boldsymbol{v}^T$ a unit vector perpendicular to $\boldsymbol{v}$. Then in a neighbourhood of $(x_0, \boldsymbol{v}(x_0))$, the pseudo-differential operator $P_1^* P_1 + P_2^* P_2$ can be factorised,*

such that

$$P_1^* P_1 + P_2^* P_2 = (EQ)^2 + FQ + G,$$

where $E \in \Psi^{-1}(\Omega)$ *is elliptic,* $Q \in \Psi^1(\Omega)$ *is an operator with principal symbol* $\xi \cdot \boldsymbol{v}^T(x)$ *and* $F, G \in \Psi^{-2}(\Omega)$.

Proof. The full symbol of $P_1^* P_1 + P_2^* P_2$ is given by

$$|\mathfrak{p}_1|^2 + |\mathfrak{p}_2|^2 = \left|\mathfrak{p}_1^{(0)} + \mathfrak{p}_1^{(-1)} + \mathcal{O}(|\xi|^{-2})\right|^2 + \left|\mathfrak{p}_2^{(0)} + \mathfrak{p}_2^{(-1)} + \mathcal{O}(|\xi|^{-2})\right|^2,$$

where $\mathfrak{p}_j^{(-1)}$ denotes the terms of $\mathfrak{p}_j$ that are exactly one order lower than the principal symbol.

Since the principal symbols $\mathfrak{p}_j^{(0)}$ are real, we find that

$$|\mathfrak{p}_1|^2 + |\mathfrak{p}_2|^2 = (\mathfrak{p}_1^{(0)})^2 + (\mathfrak{p}_2^{(0)})^2 + 2\left(\mathfrak{p}_1^{(0)}\mathrm{Re}\left(\mathfrak{p}_1^{(-1)}\right) + \mathfrak{p}_2^{(0)}\mathrm{Re}\left(\mathfrak{p}_2^{(-1)}\right)\right) + \mathcal{O}(|\xi|^{-2}).$$

By the definition of $\boldsymbol{v}$ we know that

$$(\nabla \tilde{u}_j \cdot \boldsymbol{v})^2 = \frac{1}{p}|\nabla \tilde{u}_j|^2 \quad \text{and} \quad (\nabla \tilde{u}_j \cdot \boldsymbol{v}^T)^2 = \left(1 - \frac{1}{p}\right)|\nabla \tilde{u}_j|^2.$$

Since $\{\boldsymbol{v}, \boldsymbol{v}^T\} = \{\boldsymbol{v}(x), \boldsymbol{v}(x)^T\}$ is an orthonormal basis for $\mathbb{R}^2$ we can make the expansions

$$\begin{aligned} |\xi|^2 =& (\xi \cdot \boldsymbol{v})^2 + (\xi \cdot \boldsymbol{v}^T)^2, \\ (\nabla \tilde{u}_j \cdot \xi)^2 =& (\nabla \tilde{u}_j \cdot \boldsymbol{v})^2 (\boldsymbol{v} \cdot \xi)^2 + (\nabla \tilde{u}_j \cdot \boldsymbol{v}^T)^2 (\boldsymbol{v}^T \cdot \xi)^2 \\ &+ 2(\nabla \tilde{u}_j \cdot \boldsymbol{v})(\boldsymbol{v} \cdot \xi)(\nabla \tilde{u}_j \cdot \boldsymbol{v}^T)(\boldsymbol{v}^T \cdot \xi). \end{aligned}$$

This makes it possible to write the principal symbol of P_j as

$$\begin{aligned} \mathfrak{p}_j^{(0)} &= |\nabla \tilde{u}_j|^p \left(1 - p\frac{(\nabla \tilde{u}_j \cdot \xi)^2}{|\nabla \tilde{u}_j|^2 |\xi|^2}\right) \\ &= \frac{|\nabla \tilde{u}_j|^p}{|\xi|^2}\left((2-p)(\boldsymbol{v}^T \cdot \xi)^2 - \frac{2p}{|\nabla \tilde{u}_j|^2}(\nabla \tilde{u}_j \cdot \boldsymbol{v})(\boldsymbol{v} \cdot \xi)(\nabla \tilde{u}_j \cdot \boldsymbol{v}^T)(\boldsymbol{v}^T \cdot \xi)\right) \\ &= \mathfrak{e}_j(\boldsymbol{v}^T \cdot \xi). \end{aligned}$$

Here $\mathfrak{e}_j \in S^{-1}(\Omega \times \mathbb{R}^2)$ is non-zero in a neighbourhood of $(x_0, \boldsymbol{v}(x_0))$, because for $p > 1$ neither $(\nabla \tilde{u}_j \cdot \boldsymbol{v})$ nor $(\nabla \tilde{u}_j \cdot \boldsymbol{v}^T)$ vanishes. The principal symbol

of $P_1^*P_1 + P_2^*P_2$ then takes the simple form

$$\begin{aligned}\left(\mathfrak{p}_1^{(0)}\right)^2 + \left(\mathfrak{p}_2^{(0)}\right)^2 &= (\mathfrak{e}_1^2 + \mathfrak{e}_2^2)(\boldsymbol{v}^T \cdot \xi)^2 \\ &= \mathfrak{e}^2(\boldsymbol{v}^T \cdot \xi)^2,\end{aligned}$$

where $\mathfrak{e} := \sqrt{\mathfrak{e}_1^2 + \mathfrak{e}_2^2} \in S^{-1}(\Omega \times \mathbb{R}^2)$ is also non-zero in a neighbourhood of $(x_0, \boldsymbol{v}(x_0))$. In a similar way we can write

$$\begin{aligned}2\left(\mathfrak{p}_1^{(0)}\mathrm{Re}\left(\mathfrak{p}_1^{(-1)}\right) + \mathfrak{p}_2^{(0)}\mathrm{Re}\left(\mathfrak{p}_2^{(-1)}\right)\right) &= 2\left(\mathfrak{e}_1\mathrm{Re}\left(\mathfrak{p}_1^{(-1)}\right) + \mathfrak{e}_2\mathrm{Re}\left(\mathfrak{p}_2^{(-1)}\right)\right)(\boldsymbol{v}^T \cdot \xi) \\ &= \mathfrak{f}(\boldsymbol{v}^T \cdot \xi),\end{aligned}$$

where $\mathfrak{f} := 2\left(\mathfrak{e}_1\mathrm{Re}\left(\mathfrak{p}_1^{(-1)}\right) + \mathfrak{e}_2\mathrm{Re}\left(\mathfrak{p}_2^{(-1)}\right)\right) \in S^{-2}(\Omega \times \mathbb{R}^2)$. This shows that

$$|\mathfrak{p}_1|^2 + |\mathfrak{p}_2|^2 = \mathfrak{e}^2(\boldsymbol{v}^T \cdot \xi)^2 + \mathfrak{f}(\boldsymbol{v}^T \cdot \xi) + \mathfrak{g},$$

where $\mathfrak{g} \in S^{-2}(\Omega \times \mathbb{R}^2)$. It follows that $P_1^*P_1 + P_2^*P_2$ in a neighbourhood of $(x_0, \boldsymbol{v}(x_0))$ can be written in the form

$$P_1^*P_1 + P_2^*P_2 = (EQ)^2 + FQ + G,$$

where $E \in \Psi^{-1}(\Omega)$ is elliptic, $Q \in \Psi^1(\Omega)$ is an operator with principal symbol $\xi \cdot \boldsymbol{v}^T$ and $F, G \in \Psi^{-2}(\Omega)$. □

The previous theorem implies that the operator $P_1^*P_1 + P_2^*P_2$ is an operator of constant multiplicity because its principal symbol can be written in the form $\left(\mathfrak{e}\left(v^T \cdot \xi\right)\right)^2$. This type of factorisation of $P_1^*P_1 + P_2^*P_2$ also implies that the relevant Levi condition is satisfied; see Lem. 2.28. In turns out that the bicharacteristic curves are similar to those of both P_1 and P_2, as the following theorem shows.

Lemma 4.19. *For $p > 1$, the bicharacteristic curves of EQ are perpendicular to the directions in which ellipticity is lost.*

Proof. The (principal) symbol of EQ is $\mathfrak{e}(\xi \cdot \boldsymbol{v}^T)$ which is clearly of real principal type. We find that

$$\left.\frac{dx(t)}{dt}\right|_{\mathfrak{e}(\xi\cdot\boldsymbol{v}^T)=0} = \left.\frac{\partial}{\partial\xi}\mathfrak{e}(\xi \cdot \boldsymbol{v}^T)\right|_{\mathfrak{e}(\xi\cdot\boldsymbol{v}^T)=0} = \mathfrak{e}\boldsymbol{v}^T.$$

Clearly $x(t)$ is a curve perpendicular to $\boldsymbol{v}$ which defines the direction in which ellipticity is lost. □

As a result of Thm. 2.29, we can therefore finally state the following theorem.

Theorem 4.20. *Let $\Omega \subset \mathbb{R}^2$. If $P_1^* P_1 + P_2^* P_2$ is not elliptic and $p > 1$, then a solution $\delta\sigma$ to the equation*

$$(P_1^* P_1 + P_2^* P_2)\delta\sigma = P_1^*(H_1 - \tilde{H}_1) + P_2^*(H_2 - \tilde{H}_2),$$

has singularities propagating in directions perpendicular to the direction in which ellipticity is lost.

In Sec. 5.4.1, we will see several numerical examples of how the loss of ellipticity for an equivalent boundary value problem, manifest itself as propagating singularities exactly in the directions predicted by this theorem.

4.4.4 The wave front set of the right-hand side

To further investigate how singularities propagate, we need to know the wave front set of the right-hand side of the normal equation for the linearised inverse problem. The following theorem shows how the wave front sets of $P_1^*(H_1 - \tilde{H}_1) + P_2^*(H_2 - \tilde{H}_2)$ and σ are related.

Theorem 4.21. *If $\{|\nabla u_j|\}_{j=1}^2$ are all bounded below by a positive constant in Ω and $\tilde{\sigma}$ is smooth, then*

$$\mathrm{WF}(P_1^*(H_1 - \tilde{H}_1) + P_2^*(H_2 - \tilde{H}_2)) \subseteq \mathrm{WF}(\sigma).$$

Proof. The wave front set of a sum of distributions is at most the union of their respective wave front sets [81, Thm. IX.44]. This implies

$$\mathrm{WF}(P_1^*(H_1 - \tilde{H}_1) + P_2^*(H_2 - \tilde{H}_2)) \subseteq \mathrm{WF}(P_1^*(H_1 - \tilde{H}_1)) \cup \mathrm{WF}(P_2^*(H_2 - \tilde{H}_2)).$$

Because pseudo-differential operators can at most decrease the wave front set of properly supported distributions, see Thm. 2.21, we have the inclusions

$$\mathrm{WF}(P_j^*(H_j - \tilde{H}_j)) \subseteq \mathrm{WF}(H_j), \quad j \in \{1, 2\}. \tag{4.18}$$

Now, since $\sigma \in L_+^\infty(\Omega)$, we have for the operator $L_\sigma := \nabla \cdot \sigma \nabla$ that

$$\mathrm{Char}(L_\sigma) \subseteq \mathrm{WF}(\sigma),$$

which by Thm. 2.21 implies

$$\mathrm{WF}(u_j) \subseteq \mathrm{WF}(\sigma), \quad j \in \{1,2\}. \tag{4.19}$$

Consider the pseudo-differential operator P defined by

$$Pv := \sigma|\nabla v|^p, \quad p > 0, \quad v \in \mathscr{E}'(\Omega).$$

For $|\nabla v|$ uniformly boundary below by a positive constant, P is elliptic away from $\mathrm{WF}(\sigma) \cup \mathrm{WF}(v)$, and it follows from Thm. 2.21 that

$$\mathrm{WF}(Pv) \subseteq \mathrm{WF}(\sigma) \cup \mathrm{WF}(v). \tag{4.20}$$

Note that $H_j = Pu_j = \sigma|\nabla u_j|^p$. Therefore, using (4.19) and (4.20) we get the relation

$$\mathrm{WF}(H_j) \subseteq \mathrm{WF}(\sigma), \quad j \in \{1,2\},$$

which by (4.18) completes the proof. □

4.5 Critical points, partial data, and noise

The main theoretical results of this chapter rely on certain qualitative properties of the solutions to the reference forward problem (1.3). An example is the absence of critical points. Also, the ellipticity condition for the linearised problem, Thm. 4.2, implies that it is not desirable to generate a set of reference solutions with parallel gradients. In this section we will therefore present some results on how the choice of boundary conditions can control such qualitative properties.

As an extension of the mathematical model and analysis, we also redefine the mathematical setting for the linearised inverse problem to cover constrains on either the interior data or on the imposed boundary conditions. This is thought as a simple model of possible practical limitations imposed on the experimental setup. In the end of the section, we also redefine the model of the measurement data to include noise. This will later be used to test the sensitivity of numerical reconstruction methods to such non-systematic errors.

4.5.1 Critical points

A solution to the reference forward problem (1.3) possess several interesting qualitative properties which can be deduced from the ubiquitous nature of second-order divergence form linear elliptic differential operators. In the two dimensional case, the following lemma describes certain properties of the gradient for a specific type of boundary condition.

Lemma 4.22. *Let u_1 and u_2 be solutions of* (1.3)*, with $\Omega \subset \mathbb{R}^2$ and boundary conditions $f_1 = x_1$, $f_2 = x_2$, respectively. Here x_1, x_2 are Cartesian coordinates on Ω. If σ is sufficiently smooth, then u_1, u_2 have no critical points (there is a uniform lower bound for the size of their gradients in $\bar{\Omega}$), and $\nabla u_1, \nabla u_2$ are non-parallel in $\bar{\Omega}$ [7, 74].*

The lemma implies that critical points can be avoided by a simple choice of boundary conditions. Furthermore, it implies that three boundary conditions are sufficient to ensure that the linearised inverse problem is elliptic in two dimensions for any $p > 0$.

Theorem 4.23. *Let $\Omega \subset \mathbb{R}^2$ and $\tilde{\sigma}$ be sufficiently smooth. The boundary conditions $f_1 = x_1$, $f_2 = x_2$, $f_3 = x_1 + x_2$, then generate a set of reference solutions $\tilde{u}_1, \tilde{u}_2, \tilde{u}_3$ for which the ellipticity condition of the linearised inverse problem, given by Thm. 4.2, is satisfied for any p.*

Proof. It is simple consequence of Lem. 4.22, because $\tilde{u}_1, \tilde{u}_2, \tilde{u}_3$ will have no critical points and their gradients are non-parallel in $\bar{\Omega}$ as a result of the linearity of the forward problem. This is clearly sufficient to satisfy the ellipticity condition, given by Thm. 4.2, for any p in two dimensions. □

Remark 4.24. *If $\nabla \tilde{u}_1$ and $\nabla \tilde{u}_2$, corresponding to the imposed boundary conditions f_1 and f_2, are known to be nowhere parallel, then making a third measurement with the boundary condition $f_1 + f_2$ ensures that the linearised inverse problem becomes elliptic in any dimension $n \geq 2$ [13].*

In dimension $n \geq 3$ these results generally does not hold. Actually, it is possible to show that a result similar to Lem. 4.22 cannot exist [14, Prop. 4.4]. However, by a certain mathematical construction, corresponding to choosing boundary conditions as traces of so-called *complex geometric optics* (CGO) solutions, it is possible to show that an open set of boundary conditions give similar qualitative properties for solutions to the reference problem. This is explained in detail by Bal [12, Sec. 5].

4.5.2 Partial data and limited-view data

If we turn the attention to a (pseudo-)physical system modelled by a hybrid inverse problem, it is clear that practical limitations imposed on the measurements correspond to certain constraints on the mathematical model. Such constraints could be of many types and would often be related to the specific application in mind.

It is not our intention consider a specific application, but of interest is a hybrid inverse problem modelling a system, where, say, the interior data acquisition is only possible in subsets of the domain, or only a part of the boundary is available for electrode positioning in the EIT measurements. In this thesis we restrict the attention to these two situations.

The term *partial data* is not a precise description of the latter case, because for a hybrid inverse problem in impedance tomography it gives the impression that not all interior data is available. This is not the case, since the restriction clearly corresponds to a constraint on the chosen boundary conditions in the mathematical model. However, the term is often used in the setting of impedance tomography, where the data is given by a number of boundary data pairs. Here a restriction of the space of boundary conditions is indeed a restriction on the data, such that it becomes *partial*. To avoid any confusion between the two mentioned situations, we use the term *limited-view* to describe the setting in which only a subset of the boundary is available for the electrical measurements.

The only existing treatment of partial and limited-view data, related to hybrid inverse problems in impedance tomography, seems to be the work by Ammari et al [10]. Here a very simple model problem is analysed theoretically using Fourier modes to show invertibility of a normal operator for $p = 2$ for two well-chosen boundary conditions, which, in some sense, corresponds to ellipticity in the pseudo-differential setting.

4.5.2.1 Partial data

Consider the situation where the interior data is only given in a subset of the domain Ω. From an practical perspective, this could model a setting where certain restrictions limit the data acquisition to a point-wise evaluation in parts of the interior.

Let the interior data be given in a simply connected subset of Ω, here denoted by $\Gamma \subset \Omega$ and let its boundary $\partial\Gamma$ be sufficiently smooth. Consider the hybrid

inverse problem with interior data

$$H_j = \sigma |\nabla u_j|^p \quad \text{in } \Gamma, \quad p > 0.$$

To define a mathematical formulation in the partial data setting, we now consider the non-linear data map (3.2) as a map

$$\mathcal{H}_j : L^\infty_+(\Omega) \to L^2(\Gamma).$$

A linearisation of this map is equivalent to the one we presented in Sec. 3.2; the only difference is that the linear equations for the Fréchet derivative of the data map is now restricted to Γ, i.e.

$$\mathrm{d}\,\mathcal{H}_j|_{\tilde{\sigma}}(\delta\sigma) = H_j - \tilde{H}_j \qquad \text{in } \Gamma.$$

In exactly the same way as it was done in Sec. 3.2 and Sec. 4.3, we can then form a system of linear equations and transform it into a first-order system.

In Sec. 5.4.2 we will use this mathematic setting to develop a reconstruction method for the partial data case.

4.5.2.2 Limited-view data

Now, consider a situation where we only have access to a proper subset of the boundary. At the part of the boundary where electrode positioning is not possible, there cannot be any current flux through the boundary. Therefore in the mathematical model, the part of the boundary which is not available, has to be equipped with a homogeneous Neumann boundary condition. If we define this part of the boundary $\Upsilon \subset \partial\Omega$, the forward problems are now of the type

$$\begin{cases} \nabla \cdot \sigma \nabla u_j = 0 & \text{in } \Omega, \\ u_j = f_j & \text{on } \partial\Omega \setminus \Upsilon, \quad 1 \le j \le J. \\ \partial_{\boldsymbol{\nu}} u_j = 0 & \text{on } \Upsilon, \end{cases} \tag{4.21}$$

For such problems, existence of a solution $u_j \in H^1(\Omega)$ is true, if $f \in H^{\frac{1}{2}}(\Omega)$ and $\partial\Omega$ is sufficiently smooth. For the details we refer to the standard reference of Gilbarg and Trudinger [p. 198][37]. That the solution is also unique follows from the fact that for any two solutions u_j and $\breve{u}_j$ to (4.21), the function $v = u_j - \breve{u}_j$

has to be zero. To see this, note that v solves

$$\begin{cases} \nabla \cdot \sigma \nabla v = 0 & \text{in } \Omega, \\ v = 0 & \text{on } \partial\Omega \setminus \Upsilon, \\ \partial_{\boldsymbol{\nu}} v = 0 & \text{on } \Upsilon. \end{cases}$$

Multiplying the top equation by v and integrating by parts gives the relation

$$\int_\Omega \sigma |\nabla v|^2 \, dx = 0,$$

which implies that v is constant in Ω. Since $v = 0$ on $\partial\Omega \setminus \Upsilon$, there is only the possibility that $v = 0$ in Ω.

The forward problem is the only mathematical description that is constrained in the hybrid inverse problem. However, the fact that the qualitative properties of solutions to the constrained forward problem are not covered by Lem. 4.22 and Thm. 4.23, makes it difficult to ensure ellipticity for the inverse problem; at least in a general domain Ω. Also, the possible presence of critical points limits the validity of the presented theorems and is a challenge in the development of reconstruction methods.

We will not conduct a through theoretical analysis of the problem with limited-view data in this thesis, but in Sec. 5.4.2 we present numerical reconstruction results based on a model where only half of the boundary can be equipped with a chosen Dirichlet boundary condition.

4.5.3 Noisy data

Measurement noise is inevitable in any practical application, but the analysis and modelling of physical phenomena, that introduce noise in practical measurements, is often neglected in the mathematical treatment of inverse problems [50]. Therefore, theoretical results are often only stated for the ideal and unrealistic situation of noise-free data.

As explained in Chap. 1, a common challenge in the mathematical treatment of inverse problems is that noisy data is not in the range of the operator that models the physical system. In such situations existence of solutions clearly does not hold, and the development of reconstruction schemes needs to reflect this fact.

In the next chapter we will develop and analyse several iterative reconstruction

methods based on a noise-free interior data model. However, to test the robustness of the methods, we will also try them on interior data contaminated by noise. In this analysis we model the noisy data as

$$\dot{H}_j := H_j(1 + \rho r_j), \quad 1 \leq j \leq J, \tag{4.22}$$

where ρ is the noise level and r_j is a function, which for each point in Ω attains a uniformly random value between -1 and 1. This type of noise has probably no physical meaning, but we choose this model because of the simple mathematical formulation. In Sec. 5.2.5 we will explain how to numerically implement the noise model and in Sec. 5.3.5 we present convergence results for reconstructions based on noisy data. As we will see, the algorithms behave very differently, when the data is contaminated by noise.

Chapter 5

Iterative reconstruction methods for hybrid inverse problems

Most hybrid inverse problems have a mathematical formulation that is based on an underlying non-linear model. To develop a numerical algorithm that finds approximate solutions to such non-linear formulations, we have to decide whether to work directly on the non-linear model or, by symbolic manipulations on the algebraic or PDE level, derive a linear approximation of the original model. In all cases the decision is always based on a compromise between accuracy of the model and the simplicity of the associated analysis and implementation.

Algorithms designed to approximately solve non-linear problems are usually of iterative nature, such that they produce a series of simpler problems that can be solved approximately by applying standard numerical tools. In this chapter we will explain the idea behind a few of such reconstruction algorithms, among which some have been used to solve various hybrid inverse problems in impedance tomography with great success. Based on the theory presented in Chap. 4, we will also explain why some of these methods fail to work in certain cases. It is common feature of all the presented methods, that they are based on a transformation of non-linear mathematical formulations into a series of linear boundary value problems for which the corresponding solutions, under

appropriate conditions, converge to a solution to the original problem.

We will develop algorithms based on two well-known procedures to solve such problems, namely the so-called Picard iterative scheme and the Newton iterative scheme. These schemes are often chosen because they have an intuitive formulation and they can be applied to most types of non-linear problems. In the following chapter, we investigate the properties of the suggested methods, present a numerical implementation, and relate the numerical results to a theoretical classification of the underlying non-linear or linear inverse problems.

Just as different techniques are needed for the theoretical analysis of linear and non-linear PDEs, numerical methods are often designed to perform optimally for a specific class of problems, such that the a priori known distinctive features of solutions are captured. This is true whether the numerical method is based on a linear or non-linear formulation. Our analysis and numerical results are therefore also used to determine the similarities and differences between the proposed algorithms, and to justify that the choice of algorithm should be based on a theoretical analysis of the underlying problem.

Several reconstruction algorithms for problems that fits in the presented mathematical framework already exists in the literature. They all consider a model where the interior data correspond to meaningful physical quantities, because the development of these algorithms was motivated by the wish to solve hybrid inverse problems modelling novel imaging methods. As a consequence of our general formulation of the hybrid inverse problem, we can take a unified reconstruction approach that accounts for both existing modalities and new problems in a single formulation.

As explained in the introduction, when $p = 1$ the interior data model measurements of the interior electrical current density. The mathematical formulation is then identical to the one found in CDII and certain formulations of MREIT. For these problems, reconstruction algorithms have been developed on both the continuous [59, 76] and disctrete level [17]. The cited algorithms are variants of a Picard iterative scheme applied to a non-linear PDE problem. An algorithm based on the minimisation of a non-convex energy functional, has also been suggested and implemented [72]. For a different mathematical formulation of MREIT, where the interior data models a single component of the magnetic flux density vector, several related reconstruction methods have also been developed [78, 84, 86].

For $p = 2$, the interior data model measurements of the interior electrical power density. The inverse problem then coincides with the one from UMEIT. For this problem we find that most existing reconstruction algorithms are of the Newton-type; thus they are based on an linearisation of an underlying non-linear model.

The simplest algorithms consider a single measurement in each iterative step and are based on an approximate inverse to solve a coupled linear system [9, 35]. It is also possible to consider an appropriate least squares functional, which can be minimised among piecewise constant conductivities [22]. Under certain assumptions, symbolic manipulations of the underlying equations can produce a Poisson-type problem for the unknown conductivity which can then be solved numerically [56]. For multiple measurements, the normal form of the linearised problem can also be solved using a so-called Levenberg-Marquardt iterative scheme [16]. We should also mention that there has recently been developed reconstruction algorithms for both $p = 1$ and $p = 2$ when the conductivity is anisotropic [43, 69, 70].

Note that the aforementioned list of algorithms is not complete and several additional reconstruction procedures for hybrid inverse problems have been proposed, among which some have yet to be implemented numerically.

In Sec. 5.2.1, a reconstruction algorithm based on the Picard iterative scheme is developed for the general non-linear mathematical setting and in Sec. 5.3.1 we analyse its performance and explain how this is related to the properties of the underlying PDE formulation. In Sec. 5.2.2-5.2.4 we will develop three iterative algorithms which are based on a successive linearisation of the inverse problem. Two are directly related to the inversion of square linear systems, while the last algorithm is a general inversion framework taking advantage of all available measurements in each iteration. For the last algorithm, the numerical implementation is based on the least squares finite element method (LSFEM). In these settings, the interior data is tacitly assumed to have the necessary regularity.

In Sec. 5.3.2-5.3.4 we analyse the performance of these algorithms and explain how this is related to the properties of the linearised problem. In Sec. 5.3.5 we give a summary of the features of the four developed reconstruction methods and also show convergence results for the situation with noisy interior data. Additional results related to the propagation of singularities, partial data, and limited-view data can be found in Sec. 5.4.

5.1 Iterative schemes for non-linear PDEs and maps

In this section we will derive a family of iterative reconstruction algorithms for the presented inverse problem. In Sec. 5.1.1 we explain how to use the Picard iterative scheme to reformulate the inverse problem and in Sec. 5.2.1,

we develop an iterative reconstruction algorithm and explain the key parts of the corresponding numerical implementation. A theoretical analysis of the reformulated problem is used to predict the performance of this method. We explain the basic idea behind the Newton iterative scheme in Sec. 5.1.2, and in Sec. 5.2.2-5.2.4 we develop three reconstruction algorithms based on an increasing level of mathematical abstraction. Again, a theoretical analysis can predict the performance of these three algorithms. Note that in all cases, the analysis is done on the continuous level.

5.1.1 Picard iteration

A explained in Sec. 3.1, it is possible to recast the hybrid inverse problem as a system of non-linear PDE problems

$$\begin{cases} \nabla \cdot \dfrac{H_j}{|\nabla u_j|^p} \nabla u_j = 0 & \text{in } \Omega, \\ u_j = f_j & \text{on } \partial\Omega, \end{cases} \qquad 1 \leq j \leq J. \tag{5.1}$$

Now, consider the case of a non-linear problem for a function v, expressed in the general algebraic form:

$$\begin{cases} F(q(v), v) = 0 & \text{in } \Omega, \\ v = f & \text{on } \partial\Omega, \end{cases} \tag{5.2}$$

where q is a non-linear functional of v, and F is an operator linear in v. In this setting F could for instance be a partial differential operator on v satisfying one or more boundary conditions and q a non-linear PDE coefficient. It is well-known that there is no general theory for solving such non-linear PDE problems [34]. Note that the general algebraic problem (5.2) corresponds to the problems (5.1) when

$$q_j = \frac{H_j}{|\nabla u_j|^p} \quad \text{and} \quad F(q_j, u_j) = \nabla \cdot q_j \nabla u_j,$$

for functions $\{u_j\}_{j=1}^J$ satisfying the appropriate boundary conditions.

One of the simplest approaches to approximate solutions to a non-linear PDE problem such as (5.2) is to use a standard Picard iterative scheme, also known as the method of successive substitutions [60]. The idea behind the Picard scheme is basically to make an initial guess on the solution v^0 and then use this guess to approximate all non-linear coefficients in the equation. This results in the

series of linear problems

$$F(q(v^k), v^{k+1}) = 0 \quad \text{in } \Omega, \quad k = 0, 1, 2, \ldots,$$

which are then solved successively for v^{k+1} satisfying $v^{k+1} = f$ on $\partial\Omega$. Here we use a notation, where the superscript denotes the iteration number. This means that the solution to the linear problem is used to update the approximation of the non-linear coefficient in each iteration. It is important to notice that the transformation of the non-linear problem into a series of linear problems is *not* a result of any algebraic or symbolic manipulations; it is simply a consequence of a substitution made directly in the non-linear PDE.

The Picard iterations end when some stopping criteria is satisfied. The usual choice is dependent on the tolerance norm $\|v^{k+1} - v^k\|$ in some suitable function space and the iteration number k. However, for problems where the objective is to estimate the PDE coefficient q, and not the function v, it is more natural to choose a stopping criteria based on the tolerance of this coefficient. For a collection of problems that are coupled by a common non-linear coefficient, like the derived non-linear PDE problems (5.1), the scheme can be applied to one equation at a time in a successively manner, where the non-linear coefficient is updated in each step.

The performance of the Picard scheme relies on an initial guess that provides a sufficiently good starting point, such that the successive approximation of the non-linear coefficient is improved in each iteration. In this way one expects that the series of solutions to the linear problems converges to a solution to the original non-linear problem. The convergence properties of the Picard iterative scheme can be studied using contraction maps and the application of the Banach fixed point theorem, however the practicality of applying this theory on a general non-linear PDE problem seems rather limited [60]. Nonetheless, for the case $p = 1$, the convergence properties of the Picard scheme have been analysed [51, 75].

The Picard iterative scheme was the main idea behind one of the first reconstruction algorithms for the hybrid inverse problems expressed in the form of the non-linear PDE problems given by (5.1). In the setting of MREIT ($p = 1$) with two interior measurements ($J = 2$), the non-linear problems were solved approximately by successively applying the Picard procedure to each of the corresponding PDE problems. The resulting algorithm was denoted the *J-substitution algorithm*, due to the fact that the functions H_j models measurements of the magnitude of the current density vector field, often denoted by J [59]. Note that the original formulation of the J-substitution algorithm considered the corresponding Neumann problem. A similar implementation of the Dirichlet problem has also been used to solve the equivalent inverse problem from CDII [75, 76].

In Sec. 4.1, the classification of non-linear PDEs problems showed that each problem is elliptic for $p < 1$, degenerate elliptic for $p = 1$ and hyperbolic for $p > 1$. The expected performance of the reconstruction algorithm is closely linked to this classification. For instance, as we are considering iterative algorithms, a well-performing algorithm cannot successively propagate or amplify errors, and therefore the classification will be important when we analyse the performance of the algorithm in Sec. 5.3.1.

5.1.2 Newton iteration

A different way to reformulate the inverse problem is to ask for a procedure to invert the non-linear data map defined by

$$\mathcal{H} : \sigma \mapsto [H_j]_{j=1}^J.$$

Here we use the notation $[H_j]_{j=1}^J = \big(H_1, \cdots, H_J\big)^T$.

Now, let us step back and consider this problem in the general sense of a non-linear map between certain function spaces:

$$\mathcal{F} : V \to W.$$

For a given function $w \in W$ in the image of $\mathcal{F}$, there is no general theory for finding $v \in V$ such that

$$\mathcal{F}(v) = w.$$

However, it is well-known that Newton's method can be used to approximate solutions to such operator equations. From an initial guess v^0 of the solution v, Newton's method utilises a first-order approximation of the map between $v - v^0$ and $\mathcal{F}(v) - \mathcal{F}(v^0)$ based on a linearisation of $\mathcal{F}$ at v^0.

The first-order approximation in V of $v - v^0$ is a solution δv^0 to the linear operator equation

$$\mathrm{d}\,\mathcal{F}|_{v^0}(\delta v^0) = w - \mathcal{F}(v^0),$$

where $\mathrm{d}\,\mathcal{F}|_{v^0}$ denotes the functional derivative of $\mathcal{F}$ at v_0. Note that if V and W are Banach spaces, the functional derivative should be understood in the sense of the Fréchet derivative; see Sec. 2.1. The Newton iterative scheme is to apply this linearisation in an iterative manner, such that it forms a sequence of linear

problems

$$\mathrm{d}\,\mathcal{F}|_{v^k}(\delta v^k) = w - \mathcal{F}(v^k), \quad k = 0, 1, 2, \ldots,$$

where $v^{k+1} = v^k + \delta v^k$. Under favourable properties of the non-linear map, Newton's method is known to ensure convergence if v^0 is sufficiently close to v [29].

A linearisation of the non-linear data map $\mathcal{H}$ gives the linear equations for $\delta\sigma^k$

$$\mathrm{d}\,\mathcal{H}|_{\sigma^k}(\delta\sigma^k) = [H_j]_{j=1}^J - \mathcal{H}(\sigma^k), \quad k = 0, 1, 2, \ldots. \tag{5.3}$$

As derived in Sec. 3.2, the functional derivative of $\mathcal{H}$ at σ^k in direction $\delta\sigma^k$ is given by

$$\mathrm{d}\,\mathcal{H}|_{\sigma^k}(\delta\sigma^k) = \left[\delta\sigma^k |\nabla u_j^k|^p + p\sigma^k \frac{\nabla u_j^k \cdot \nabla \delta u_j^k}{|\nabla u_j^k|^{2-p}} \right]_{j=1}^J, \tag{5.4}$$

where δu_j^k solves the PDE problem

$$\begin{cases} \nabla \cdot \sigma^k \nabla \delta u_j^k = -\nabla \cdot \delta\sigma^k \nabla u_j^k & \text{in } \Omega, \\ \delta u_j^k = 0 & \text{on } \partial\Omega. \end{cases} \tag{5.5}$$

The equations (5.3), (5.4) and (5.5) form a collection of linear PDE problems for the k'th iterate $(\delta\sigma^k, \{\delta u_j^k\}_{j=1}^J)$, and they can be expressed in the matrix form

$$\boldsymbol{A}\boldsymbol{x} = \boldsymbol{b}, \tag{5.6}$$

where

$$\boldsymbol{A} = \begin{bmatrix} \nabla\cdot([\cdot]\nabla u_1^k) & \nabla\cdot(\sigma^k[\cdot]) & \cdots & 0 \\ \vdots & \vdots & \ddots & \vdots \\ \nabla\cdot([\cdot]\nabla u_J^k) & 0 & \cdots & \nabla\cdot(\sigma^k[\cdot]) \\ |\nabla u_1^k|^p & p\sigma^k \frac{\nabla u_1^k\cdot\nabla[\cdot]}{|\nabla u_1^k|^{2-p}} & \cdots & 0 \\ \vdots & \vdots & \ddots & \vdots \\ |\nabla u_J^k|^p & 0 & \cdots & p\sigma^k \frac{\nabla u_J^k\cdot\nabla[\cdot]}{|\nabla u_J^k|^{2-p}} \end{bmatrix},$$

$$\boldsymbol{x} = \begin{bmatrix} \delta\sigma^k \\ \delta u_1^k \\ \vdots \\ \delta u_J^k \end{bmatrix}, \boldsymbol{b} = \begin{bmatrix} 0 \\ \vdots \\ 0 \\ [H_j]_{j=1}^J - \mathcal{H}(\sigma^k) \end{bmatrix},$$

and homogeneous Dirichlet boundary conditions are imposed on $\{\delta u_j^k\}_{j=1}^J$. Note that this system consists of $2J$ equations and $J+1$ unknowns.

This is equivalent to the linear system that was classified in Sec. 4.2. For instance, by Thm. 4.2, we know that each 2×2 subsystem for $(\delta\sigma^k, \delta u_j^k)$ is DN elliptic if, and only if, $p<1$.

In Sec. 5.2.2-5.2.4 we will develop three different reconstruction algorithms using the presented linearisation. The algorithms are designed to solve the matrix equation (5.6), and they therefore depend on the properties of the governing matrix. The first two algorithms consider a square system of equations. These algorithms are not necessary limited to the case $J=1$, since they can be applied iteratively to square subsystems if the system is not square; thus for $p\geq 1$ they work on a collection of non-elliptic subsystems. To take advantage of all data sets in each iteration, and thereby the possible DN ellipticity of the full system, the third algorithm is designed to find a least squares minimising solution which is suitable in the case of an overdetermined system.

5.2 Iterative reconstruction algorithms

In this section we explain how the presented theory can be applied to construct four iterative reconstruction algorithms for hybrid inverse problems in impedance tomography. The first algorithm is based on Picard iterations, and the next three algorithms are based on Newton iterations. We also present a mathematical formulation of each algorithm, which allows for a numerical

implementation using the finite element method.

5.2.1 Picard-type algorithm

The Picard iterative scheme, presented in Sec. 5.1.1, can be applied directly to the non-linear PDE formulation of the inverse problem to produce the following algorithm:

Algorithm 1 Picard-type algorithm

Define σ^0, maximum number of iterations K and tolerance level T.
Set $k = 0$ and $\varepsilon = 2T$.

while $k < K$ and $\varepsilon > T$ **do**
$j = (k \bmod J) + 1$
Solve for u_j^k in

$$\begin{cases} \nabla \cdot \sigma^k \nabla u_j^k = 0 & \text{in } \Omega, \\ u_j^k = f_j & \text{on } \partial\Omega, \end{cases}$$

and update

$$\sigma^{k+1} = \frac{H_j}{|\nabla u_j^k|^p}.$$

Set $\varepsilon = \|\sigma^{k+1} - \sigma^k\|$ and $k = k + 1$.
end while

We tacitly assume that σ^k is uniformly bounded above and below in Ω for all k, such that the PDE problems for u_j^k are all well-posed. Note that the modulo operation (mod) is used to successively iterate between the J interior measurements, and for each increment in k a single data set is used. As mentioned earlier, for $p = 1$ this algorithm is similar to existing work [59, 75, 76].

Numerical implementation

It is fairly simple to implement Algorithm 1, since each iteration only involves some arithmetic operations on known functions and the solution of a linear PDE problem. We now explain how to derive the mixed weak form of the linear PDE problem which can be implemented using the finite element method.

First, let the imposed boundary conditions be smooth, i.e. $f_j \in C^\infty(\partial\Omega)$. For $\sigma^k \in L^\infty_+(\Omega)$, we want to solve for ∇u_j^k in the linear inhomogeneous problem

$$\begin{cases} \nabla \cdot \sigma^k \nabla u_j^k = 0 & \text{in } \Omega, \\ u_j^k = f_j & \text{on } \partial\Omega. \end{cases} \tag{5.7}$$

We use a mixed formulation, such that we get a problem for the gradient ∇u_j^k, which is crucial for the reconstruction algorithm. In this way, we do not need to numerically differentiate u_j^k, which can introduce additional errors. With the help of the function $v_j^k = u_j^k - F_j$, where F_j denotes the harmonic extension of f_j into Ω, and the vector function $\boldsymbol{w}_j^k$, we can reformulate (5.7) as the homogeneous mixed problem

$$\begin{cases} \nabla \cdot \boldsymbol{w}_j^k = -\nabla \cdot \sigma^k \nabla F_j & \text{in } \Omega, \\ \boldsymbol{w}_j^k = \sigma^k \nabla v_j^k & \text{in } \Omega, \\ v_j^k = 0 & \text{on } \partial\Omega. \end{cases} \tag{5.8}$$

The solution $(v_j^k, \boldsymbol{w}_j^k)$ to (5.8) then defines the pair $(u_j^k, \nabla u_j^k)$ using the definition of v_j^k. The mixed weak formulation of (5.8) is then to find $(v_j^k, \boldsymbol{w}_j^k) \in H_0^1(\Omega) \times H_{\mathrm{div}}(\Omega)$ such that

$$\int_\Omega \left[(\sigma^k)^{-1} \boldsymbol{w}_j^k \cdot \boldsymbol{\psi} + v_j^k \nabla \cdot \boldsymbol{\psi} + \phi \nabla \cdot \boldsymbol{w}_j^k \right] dx = \int_\Omega \sigma^k \nabla F_j \cdot \nabla \phi \, dx, \quad \forall\, (\phi, \boldsymbol{\psi}) \in H_0^1(\Omega) \times H_{\mathrm{div}}(\Omega).$$

This weak form is implemented in a finite dimensional setting with appropriate conforming element functions via the finite element method. Note that ∇F_j should be implemented using its analytical expression, if it is known, to avoid errors from numerical differentiation.

5.2.2 Newton-type algorithm for square subsystems

When the linearised inverse problem (5.6) is a square system of equations, it is most likely not invertible. In the elliptic case ($p < 1$), it is only possible to show optimal stability properties of solutions to the linearised system and uniqueness does not hold in general. This was explained in detail in Chap. 4.

In the following algorithm we treat this problem of non-uniqueness, by asking for a norm minimising solution to the linearised system. As we will show in a

moment, this produces a unique solution, at least in the elliptic case. Also, it works as a motivational factor for the development of the next two algorithms.

Algorithm 2 Newton-type algorithm for square subsystems

Define σ^0, maximum number of iterations K and tolerance level T.
Set $k = 0$ and $\varepsilon = 2T$.

while $k < K$ and $\varepsilon > T$ **do**
$j = (k \bmod J) + 1$
Solve for u_j^k in

$$\begin{cases} \nabla \cdot \sigma^k \nabla u_j^k = 0 & \text{in } \Omega, \\ u_j^k = f_j & \text{on } \partial\Omega. \end{cases}$$

Find a norm minimising solution $(\delta\sigma^k, \delta u_j^k)$ that satisfies

$$\begin{cases} \begin{bmatrix} \nabla \cdot [\cdot] \nabla u_j^k & \nabla \cdot \sigma^k \nabla [\cdot] \\ |\nabla u_j^k|^p & p\sigma^k \frac{\nabla u_j^k \cdot \nabla [\cdot]}{|\nabla u_j^k|^{2-p}} \end{bmatrix} \begin{bmatrix} \delta\sigma^k \\ \delta u_j^k \end{bmatrix} = \begin{bmatrix} 0 \\ H_j - \sigma^k |\nabla u_j^k|^p \end{bmatrix} & \text{in } \Omega, \\ \delta u_j^k = 0 & \text{on } \partial\Omega, \end{cases}$$

and update

$$\sigma^{k+1} = \sigma^k + \delta\sigma^k.$$

Set $\varepsilon = \|\delta\sigma^k\|$ and $k = k + 1$.
end while

Again, we tacitly assume that σ^k is uniformly bounded above and below in Ω for all k, such that the PDE problems for u_j^k are all well-posed. In this algorithm, for each increment in k a single data set is used.

Numerical implementation

To solve for u_j^k we use the implementation that was presented for the Picard iteration in 5.2.1. The only new part in the implementation is therefore to

numerically find a norm minimising solution to the system

$$\begin{cases} \begin{bmatrix} \nabla\cdot[\cdot]\nabla u_j^k & \nabla\cdot\sigma^k\nabla[\cdot] \\ |\nabla u_j^k|^p & p\sigma^k\frac{\nabla u_j^k\cdot\nabla[\cdot]}{|\nabla u_j^k|^{2-p}} \end{bmatrix} \begin{bmatrix} \delta\sigma^k \\ \delta u_j^k \end{bmatrix} = \begin{bmatrix} 0 \\ H_j - \sigma^k|\nabla u_j^k|^p \end{bmatrix} & \text{in } \Omega, \\ \delta u_j^k = 0 & \text{on } \partial\Omega. \end{cases} \tag{5.9}$$

We ask for a solution that is norm minimised in $L^2(\Omega)$ by adding an appropriate Lagrange multiplier term to the weak form. Under the assumption that the linear operator in (5.9) is closed, the solution is then unique [40]. For $p < 1$ it can be shown that this assumption is indeed satisfied [57]. Analysing the appropriate functional setting, multiplying each equation by a test function and integrating by parts, lead to the weak formulation. We want to find $(\delta\sigma^k, \delta u_j^k) \in L^\infty(\Omega) \times H_0^1(\Omega)$ such that

$$\int_\Omega \left[\left(\delta\sigma^k|\nabla u_j^k|^p + p\sigma^k \frac{\nabla u_j^k\cdot\nabla\delta u_j^k}{|\nabla u_j^k|^{2-p}} \right)\phi + \left(\delta\sigma^k\nabla u_j^k + \sigma^k\nabla\delta u_j^k\right)\cdot\nabla\psi + \alpha(\delta\sigma^k\phi + \delta u_j^k\psi) \right] dx = \int_\Omega \left(H_j - \sigma^k|\nabla u_j^k|^p\right)\phi\, dx, \quad \forall\,(\phi,\psi) \in L^\infty(\Omega)\times H_0^1(\Omega).$$

Here α works as a regularisation parameter, that enforces the norm penalty. In our implementation we use a value of $\alpha = 10^{-6}$, but testing with different values in the interval $[10^{-12}, 10^{-3}]$ did not change the qualitative properties of the found solution. This weak form is also implemented in a finite dimensional setting with appropriate conforming element functions via the finite element method.

5.2.3 Newton-type algorithm for square subsystems using an approximate inverse

A different way to overcome the problem of non-uniqueness for solutions to the linearised system, is to derive an analytic expression for an approximate inverse for the matrix equation. In the following paragraph, we will construct such an approximate inverse, based on certain assumptions about the solution.

Each square subsystem of the linearised inverse problem for $(\delta\sigma^k, \delta u_j^k)$ can be

expressed as the scalar operator equation for $\delta\sigma^k$

$$(M_j^k + P_j^k)\delta\sigma^k = H_j - \sigma^k|\nabla u_j^k|^p,$$

where

$$M_j^k[\cdot] = |\nabla u_j^k|^p[\cdot], \quad P_j^k[\cdot] = p\sigma^k \frac{\nabla u_j^k \cdot \nabla \delta u_j^k([\cdot])}{|\nabla u_j^k|^{2-p}},$$

and $\delta u_j^k([\cdot])$ solves

$$\begin{cases} \nabla \cdot \sigma^k \nabla \delta u_j^k([\cdot]) = -\nabla \cdot [\cdot]\nabla u_j^k & \text{in } \Omega, \\ \delta u_j^k = 0 & \text{on } \partial\Omega. \end{cases}$$

We can find an approximation of $\delta\sigma^k$ if we can approximate the operator $(M_j^k + P_j^k)^{-1}$. First note that $(M_j^k)^{-1}$ is well-defined and therefore

$$(M_j^k + P_j^k)^{-1} = (I + (M_j^k)^{-1}P_j^k)^{-1}(M_j^k)^{-1},$$

where I denotes the identity map. Now, we want to construct an approximate inverse of $(I + (M_j^k)^{-1}P_j^k)$. We make the assumption $\sigma^k \nabla \delta u_j^k([\cdot]) \approx -[\cdot]\nabla u_j^k$, which allows us to write

$$(M_j^k)^{-1}P_j^k[\cdot] \approx -p\sigma^k \frac{\nabla u_j^k \cdot \frac{[\cdot]}{\sigma^k}\nabla u_j^k}{|\nabla u_j^k|^2} = -pI[\cdot].$$

For $p \neq 1$ we then have that $\left(I + \frac{1}{p-1}(M_j^k)^{-1}P_j^k\right)(M_j^k)^{-1}$ is an approximate inverse of $M_j^k + P_j^k$ because

$$\begin{gathered} \left(I + \frac{1}{p-1}(M_j^k)^{-1}P_j^k\right)(M_j^k)^{-1}(M_j^k + P_j^k) = \\ \left(I + \frac{1}{p-1}(M_j^k)^{-1}P_j^k\right)(I + (M_j^k)^{-1}P_j^k) = \\ I + \left(1 + \frac{1}{p-1}\right)(M_j^k)^{-1}P_j^k + \frac{1}{p-1}\left((M_j^k)^{-1}P_j^k\right)^2 \approx \\ I\left(1 - \left(1 + \frac{1}{p-1}\right)p + \frac{1}{p-1}p^2\right) = I. \end{gathered}$$

We therefore have that

$$\delta\sigma^k \approx \left(I + \frac{1}{p-1}(M_j^k)^{-1}P_j^k\right)(M_j^k)^{-1}\left(H_j - \sigma^k|\nabla u_j^k|^p\right), \quad p \neq 1.$$

This approximate inverse can be used to construct the following reconstruction algorithm:

Algorithm 3 Newton-type algorithm using an approximate inverse

Define σ^0, maximum number of iterations K and tolerance level T.
Set $k = 0$ and $\varepsilon = 2T$.

while $k < K$ and $\varepsilon > T$ **do**
$j = (k \bmod J) + 1$
Solve for u_j^k in

$$\begin{cases} \nabla \cdot \sigma^k \nabla u_j^k = 0 & \text{in } \Omega, \\ u_j^k = f_j & \text{on } \partial\Omega. \end{cases}$$

Define

$$\tau = \frac{H_j}{|\nabla u_j^k|^p} - \sigma^k.$$

Solve for $\delta u_j^k(\tau)$ in

$$\begin{cases} \nabla \cdot \sigma^k \nabla \delta u_j^k(\tau) = -\nabla \cdot \tau \nabla u_j^k & \text{in } \Omega, \\ \delta u_j^k(\tau) = 0 & \text{on } \partial\Omega, \end{cases}$$

and update

$$\sigma^{k+1} = \frac{H_j}{|\nabla u_j^k|^p} + \frac{p}{p-1}\sigma^k \frac{\nabla u_j^k \cdot \nabla \delta u_j^k(\tau)}{|\nabla u_j^k|^2}.$$

Set $\varepsilon = \|\sigma^{k+1} - \sigma^k\|$ and $k = k + 1$.
end while

Again, we tacitly assume that σ^k is uniformly bounded above and below in Ω for all k, such that the PDE problems for u_j^k are all well-posed. Note that for each increment in k a single data set is used.

This type of algorithm is closely related to, and inspired by, the works of Ammari et al. [8, 9] and Gebauer et al. [35]. They both used a similar algorithm to solve the inverse problem from UMEIT. Up to a sign difference, the algorithms are in fact similar for $p = 2$. Note that for p close to zero, Algorithm 3 is very similar to Algorithm 1.

Numerical implementation

Again, to solve for u_k^j we use the implementation that was presented for the Picard iteration in 5.2.1. Besides some arithmetic operations on known functions, the only new part of this implementation is to numerically solve for $\delta u_j^k(\tau)$ in:

$$\begin{cases} \nabla \cdot \sigma^k \nabla \delta u_j^k(\tau) = -\nabla \cdot \tau \nabla u_j^k & \text{in } \Omega, \\ \delta u_j^k(\tau) = 0 & \text{on } \partial\Omega. \end{cases}$$

We make an implementation based on a mixed formulation because $\sigma^k \nabla \delta u_j^k$ is needed for the approximate inverse. Expressing the PDE as a first-order system for $(\delta u_j^k, \sigma^k \nabla \delta u_j^k)$, multiplying each equation by a test function and integrating by parts, lead to the weak formulation. We want to find $(v, \boldsymbol{w}) \in H_0^1(\Omega) \times H_{\text{div}}(\Omega)$ such that

$$\int_\Omega \left[(\nabla \cdot \boldsymbol{w})\phi + (\sigma^k)^{-1} \boldsymbol{w} \cdot \boldsymbol{\psi} + (\nabla \cdot \boldsymbol{\psi}) v \right] dx = \int_\Omega \tau \nabla u_j^k \cdot \nabla \phi dx, \quad \forall (\phi, \boldsymbol{\psi}) \in H_0^1(\Omega) \times H_{\text{div}}(\Omega).$$

Here, $\sigma^k \nabla \delta u_j^k(\tau)$ is defined by the relation $(\delta u_j^k(\tau), \sigma^k \nabla \delta u_j^k(\tau)) = (v, \boldsymbol{w})$. This weak form is also implemented in a finite dimensional setting with appropriate conforming element functions via the finite element method.

5.2.4 Newton-type algorithm for the full linearised system

When we have access to multiple measurements, the linearised inverse problem (5.6) is not a square system of equations. In this case, it is the standard approach to define a solution of such overdetermined systems using the method of least squares. A least squares solution to the linearised inverse problem (5.6), is a function

$$\boldsymbol{x}^\star = \underset{\boldsymbol{x}}{\text{argmin}} \, \|\boldsymbol{A}\boldsymbol{x} - \boldsymbol{b}\|^2_{L^2(\Omega)},$$

for $\boldsymbol{x}$ satisfying the previously defined homogeneous boundary conditions in appropriate function spaces. With this framework, it is possible to utilise all measurements simultaneously in each step in the Newton algorithm. Thus, for square and overdetermined systems we can define the following algorithm:

Algorithm 4 Newton-type algorithm for the full linearised system

Define σ^0, maximum number of iterations K and tolerance level T.
Set $k = 0$ and $\varepsilon = 2T$.

while $k < K$ and $\varepsilon > T$ **do**
  for $(j = 1, \ldots, J)$
    Solve for u_j^k in

$$\begin{cases} \nabla \cdot \sigma^k \nabla u_j^k = 0 & \text{in } \Omega, \\ u_j^k = f_j & \text{on } \partial\Omega. \end{cases}$$

  end for
  Find

$$\boldsymbol{x}^\star = \underset{\boldsymbol{x}}{\operatorname{argmin}} \, \|\boldsymbol{A}\boldsymbol{x} - \boldsymbol{b}\|^2_{L^2(\Omega)},$$

  and update

$$\sigma^{k+1} = \sigma^k + \delta\sigma^k.$$

  Set $\varepsilon = \|\delta\sigma^k\|$ and $k = k + 1$.
end while

Again, we tacitly assume that σ^k is uniformly bounded above and below in Ω for all k, such that the PDE problems for u_j^k are all well-posed. Note that for each increment in k all J data sets are used.

This algorithm seems to be new, but for $p = 2$ it is related to work by Bal et al. [16], where the so-called Levenberg–Marquardt algorithm is used to find a solution that minimises a regularised residual. It also have some resemblance to work by Capdeboscq et al., where σ is assumed to be piecewise constant [22].

Numerical implementation

Again, to solve for u_j^k we use the implementation that was presented for the Picard iteration in 5.2.1. A straightforward numerical implementation of the least squares problem is not practical, because it turns out that H^2-conforming finite element spaces are necessary to approximate the functions $\{\delta u_j\}_{j=1}^J$. This follows from the fact that $\boldsymbol{A}$ is a second-order operator. H^2-spaces are known to be impractical to implement and as a technical step the matrix equation

$$\boldsymbol{A}\boldsymbol{x} = \boldsymbol{b} \quad \text{in } \Omega,$$

is therefore expressed in the mixed form of a first-order system

$$\begin{cases} \acute{\boldsymbol{A}}\acute{\boldsymbol{x}} = \boldsymbol{b} \ \text{ in } \Omega, \\ \boldsymbol{G}\boldsymbol{x} = \acute{\boldsymbol{x}} \ \text{ in } \Omega, \end{cases} \tag{5.10}$$

where $\boldsymbol{G} = \operatorname{diag}(1, \nabla, \ldots, \nabla)$ and $\acute{\boldsymbol{A}}$ is defined by the relation $\boldsymbol{A} = \acute{\boldsymbol{A}}\boldsymbol{G}$. A simple analysis of the operators $\acute{\boldsymbol{A}}$ and $\boldsymbol{G}$ shows that they act as operators

$$\begin{aligned} \acute{\boldsymbol{A}} &: H^1(\Omega) \times [H_{\mathrm{div}}(\Omega)]^J \to [L^2(\Omega)]^{2J}, \\ \boldsymbol{G} &: H^1(\Omega) \times [H^1(\Omega)]^J \to H^1(\Omega) \times [L^2(\Omega)]^J. \end{aligned}$$

Thus, they specify the appropriate function space setting which satisfies the boundary conditions:

$$(\boldsymbol{x}, \acute{\boldsymbol{x}}) \in H^1(\Omega) \times [H_0^1(\Omega)]^J \times H^1(\Omega) \times [H_{\mathrm{div}}(\Omega)]^J.$$

To this formulation we assign the energy functional

$$I(\boldsymbol{x}, \acute{\boldsymbol{x}}) = \|\acute{\boldsymbol{A}}\acute{\boldsymbol{x}} - \boldsymbol{b}\|^2_{L^2(\Omega)} + \|\boldsymbol{G}\boldsymbol{x} - \acute{\boldsymbol{x}}\|^2_{L^2(\Omega)}.$$

We do not know if this functional admits a unique minimiser. We therefore ask for a function $\boldsymbol{x}^\star$ that is norm minimised in $L^2(\Omega)$ by adding an appropriate Lagrange multiplier term to the weak form. Under the assumption that $\boldsymbol{A}$ is a closed operator, the problem is then known to admit an unique solution, that is equivalent to the one found by applying the continuous form of the Moore–Penrose pseudoinverse to the linear system [40]. When $\boldsymbol{A}$ is DN elliptic, it can be shown that this assumption is indeed satisfied [57]. For a minimiser $(\boldsymbol{x}^\star, \acute{\boldsymbol{x}}^\star)$ of $I(\boldsymbol{x}, \acute{\boldsymbol{x}})$ the first variation vanishes, which means that

$$\begin{gathered} \lim_{t \to 0} \frac{d}{dt} I(\boldsymbol{x}^\star + t\boldsymbol{\phi}, \acute{\boldsymbol{x}}^\star + t\acute{\boldsymbol{\phi}}) = 0, \\ \forall\, (\boldsymbol{\phi}, \acute{\boldsymbol{\phi}}) \in H^1(\Omega) \times [H_0^1(\Omega)]^J \times H^1(\Omega) \times [H_{\mathrm{div}}(\Omega)]^J. \end{gathered}$$

Altogether, this leads to the least squares weak formulation of (5.10). We want to find $(\boldsymbol{x}^\star, \acute{\boldsymbol{x}}^\star) \in H^1(\Omega) \times [H_0^1(\Omega)]^J \times H^1(\Omega) \times [H_{\mathrm{div}}(\Omega)]^J$ such that

$$\begin{gathered} \int_\Omega \left[\acute{\boldsymbol{A}}\acute{\boldsymbol{x}}^\star \acute{\boldsymbol{A}}\acute{\boldsymbol{\phi}} + (\boldsymbol{G}\boldsymbol{x}^\star - \acute{\boldsymbol{x}}^\star)(\boldsymbol{G}\boldsymbol{\phi} - \acute{\boldsymbol{\phi}}) + \alpha \boldsymbol{x}^\star \boldsymbol{\phi} \right] dx = \int_\Omega \boldsymbol{b}\, \acute{\boldsymbol{A}}\acute{\boldsymbol{\phi}}\, dx, \\ \forall\, (\boldsymbol{\phi}, \acute{\boldsymbol{\phi}}) \in H^1(\Omega) \times [H_0^1(\Omega)]^J \times H^1(\Omega) \times [H_{\mathrm{div}}(\Omega)]^J. \end{gathered} \tag{5.11}$$

This is the norm minimising continuous LSFEM weak formulation applied to the first-order system (5.10) with appropriate trial and test functions. We choose the Lagrange multiplier $\alpha = 10^{-6}$, but again testing with different values in the interval $[10^{-12}, 10^{-3}]$ did not change the qualitative properties of the found

solution. Note that the homogeneous Dirichlet boundary conditions for $\{\delta u_j\}_{j=1}^J$ are imposed by the chosen function spaces $H_0^1(\Omega)$. Again, the weak form is also implemented in a finite dimensional setting with appropriate conforming element functions via the finite element method.

The weak formulation implicitly requires that the so-called concomitant of $\acute{\boldsymbol{A}}\acute{\boldsymbol{x}}^\star - \boldsymbol{b}$ and $\acute{\boldsymbol{\phi}}$ vanishes for the weak formulation to be identified with the corresponding normal equation. This is a direct consequence of the LSFEM formulation [18, Rem. 3.12]. As it was shown in Sec. 4.3, a problem of the type (5.11) can be identified with a weak formulation of the normal equation

$$\boldsymbol{A}^*\boldsymbol{A}\boldsymbol{x}^\star = \boldsymbol{A}^*\boldsymbol{b} \text{ in } \Omega,$$

for $\boldsymbol{x}^\star$ satisfying the additional boundary condition

$$\boldsymbol{x}^\star = \boldsymbol{0} \text{ on } \partial\Omega.$$

5.2.4.1 Partial data

Based on the mathematical setting described in Sec. 4.5.2.1, we want to extend the previous algorithm to work on the partial data problem.

Now, in the partial data case we redefine a least squares solution to the linearised first-order problem (4.6), as a minimiser of the least squares functional

$$I(\boldsymbol{x}, \acute{\boldsymbol{x}}) = \|\acute{\boldsymbol{A}}\acute{\boldsymbol{x}} - \boldsymbol{b}\|_V^2 + \|\boldsymbol{G}\boldsymbol{x} - \acute{\boldsymbol{x}}\|_{L^2(\Omega)}^2, \tag{5.12}$$

where

$$V = [L^2(\Omega)]^J \times [L^2(\Gamma)]^{nJ}.$$

By a derivation similar to the one leading to (5.11), we get the least squares weak formulation of (5.12). We want to find $(\boldsymbol{x}^\star, \acute{\boldsymbol{x}}^\star) \in H^1(\Omega) \times [H_0^1(\Omega)]^J \times H^1(\Omega) \times [H_{\mathrm{div}}(\Omega)]^J$ such that

$$\int_{\Omega,\Gamma} \acute{\boldsymbol{A}}\acute{\boldsymbol{x}}^\star \acute{\boldsymbol{A}}\acute{\boldsymbol{\phi}}\, dx + \int_\Omega \left[(\boldsymbol{G}\boldsymbol{x}^\star - \acute{\boldsymbol{x}}^\star)(\boldsymbol{G}\boldsymbol{\phi} - \acute{\boldsymbol{\phi}}) + \alpha \boldsymbol{x}^\star \boldsymbol{\phi}\right] dx = \int_{\Omega,\Gamma} \boldsymbol{b}\, \acute{\boldsymbol{A}}\acute{\boldsymbol{\phi}}\, dx,$$
$$\forall\, (\boldsymbol{\phi}, \acute{\boldsymbol{\phi}}) \in H^1(\Omega) \times [H_0^1(\Omega)]^J \times H^1(\Omega) \times [H_{\mathrm{div}}(\Omega)]^J.$$

Here, what we mean by $\int_{\Omega,\Gamma}$ is that the integration is over Ω for the top J equations, over Γ for the bottom nJ equations. Again, we choose the Lagrange multiplier $\alpha = 10^{-6}$, and the weak form can be implemented in a finite dimensional setting with appropriate conforming element functions via the finite

element method.

By a suitable definition of the adjoint $\acute{\boldsymbol{A}}^*$ it is possible to show a correspondence between solutions to the normal form and the weak form of the least squares formulation, if, for example, $\delta\sigma^k$ and $\{\delta u_j^k\}_j^J$ vanishes on $\partial\Omega$, and $\delta\sigma^k$ and $\{\nabla\delta u_j^k\}_j^J$ vanishes on $\partial\Gamma$. This can be seen by a calculation similar to the one performed in the proof of Lem. 4.7.

5.2.4.2 Limited-view data

The mathematical setting for limited-view data was explained in Sec. 4.5.2.2. Here we present a way to redefine the numerical implementation of the forward problem to cover this situation.

In the problem with limited-view data, we need to solve a forward problem of the type

$$\begin{cases} \nabla\cdot\sigma\nabla u = 0 & \text{in } \Omega, \\ u = f & \text{on } \partial\Omega\setminus\Upsilon, \\ \partial_{\boldsymbol{\nu}} u = 0 & \text{on } \Upsilon. \end{cases} \tag{5.13}$$

First, we transform (5.13) into the first-order system

$$\begin{cases} \nabla\cdot\boldsymbol{w} = 0 & \text{in } \Omega, \\ \boldsymbol{w} = \sigma\nabla u & \text{in } \Omega, \\ u = f & \text{on } \partial\Omega\setminus\Upsilon, \\ \partial_{\boldsymbol{\nu}} u = 0 & \text{on } \Upsilon. \end{cases} \tag{5.14}$$

Since we are dealing with mixed boundary conditions, we cannot formulate the problem in a corresponding homogeneous form, as we did in Sec. 5.2.1. Instead we use integration by parts to write up the weak form, and treat the Dirichlet condition as a *natural* condition; that is, it is included in the weak form, and treat the Neumann condition as a *strong* condition that is enforced on the solution space. The mixed weak formulation of (5.14) is then to find $(u,\boldsymbol{w})\in H_0^1(\Omega)\times H_{\mathrm{div}}(\Omega)$ such that

$$\int_\Omega \left[\sigma^{-1}\boldsymbol{w}\cdot\boldsymbol{\psi} + u\nabla\cdot\boldsymbol{\psi} + \phi\nabla\cdot\boldsymbol{w}\right] dx = \int_{\partial\Omega\setminus\Upsilon} f\partial_{\boldsymbol{\nu}}\phi\, ds,$$
$$\forall\,(\phi,\boldsymbol{\psi})\in H^1(\Omega)\times H_{\mathrm{div}}(\Omega),$$

for (u, ϕ) satisfying a homogeneous Neumann boundary condition on Υ. Again, the weak form can be implemented in a finite dimensional setting with appropriate conforming element functions via the finite element method.

5.2.5 Noise model

To test the robustness of the presented reconstruction methods, we want to analyse the convergence properties of the four algorithms when the measurements are corrupted by noise.

For this, we use the simple noise model that was introduced in Sec. 4.5.3. In the numerical finite element setting, we denote by $\boldsymbol{H}_j$ the vector of discrete values of H_j and denote its noisy counterpart by $\dot{\boldsymbol{H}}_j$, which is defined by the relation

$$\dot{\boldsymbol{H}}_j = \boldsymbol{H}_j + \rho \boldsymbol{r}_j^T \boldsymbol{H}_j, \quad 1 \leq j \leq J. \tag{5.15}$$

Here $\boldsymbol{r}_j$ is a vector of uniformly distributed random numbers between -1 and 1. For the results in the next section, we the use the two noise levels $\rho = 0.1$ and $\rho = 0.5$. Note that the random vectors $\boldsymbol{r}_j$ are generated before the analysis begins, such that exactly the same noisy measurements are used in all computations.

5.3 Numerical results

In this section, we apply the four presented iterative reconstruction methods to the class of non-linear inverse problems and analyse their performance. The implementation of the discrete finite dimensional weak formulation of the linear problem for u_j, the linearised inverse problem and all numerical operations have been done using The FEniCS Project [65].

For the numerical analysis we consider $\Omega = \mathbb{D}$, the unit disc in the plane. Meshing is done automatically in FEniCS. For this work we use a uniform mesh of 6084 elements, because it provides a good compromise between the finite element methods ability to capture local phenomena and the computational cost. It should, however, be noted that the interior measurements $\{H_j\}_{j=1}^J$ are calculated on a different mesh with 6400 elements and afterwards projected onto the mesh of 6084 elements. This is done to avoid committing an inverse crime. For all visualising purposes we use the open-source visualisation software Paraview [42].

As a phantom we use the function σ shown in Fig. 5.1, which is based on the MATLAB code for the *heart-and-lungs phantom* [73]. It has a background value of 1.0 that is perturbed in two ellipses where the value is 0.5 and in a circular region where the value is 2.0. A smoothing layer around each perturbation is defined using quintic Hermite blending functions, such that $\sigma \in C^2(\Omega)$ [39]. For the initial guess on σ, we use $\sigma^0 = 1$. In all the plots of reconstructions we will use the same colorbar as the one shown in Fig. 5.1.

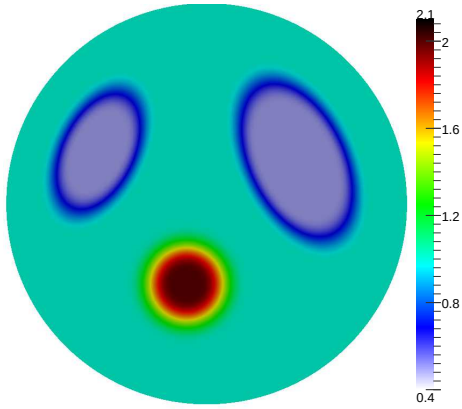

Figure 5.1: The phantom σ.

For the presented algorithms of the noise-free and full data problem, we consider five values of p corresponding to two elliptic ($p = 0.5$ and $p = 0.75$), one degenerate elliptic ($p = 1$) and two hyperbolic ($p = 1.5$ and $p = 2$) problems. In all reconstructions the boundary conditions $f_1 = x/2$ and $f_2 = (x+y)/(2|x+y|)$ are used, such that the linearised systems are all DN elliptic when $J = 2$. This is easy to conclude for the initial iteration, but by a visual inspection of the directions of the computed gradients $\nabla u_1^k, \nabla u_2^k$ it seems that the systems indeed stay DN elliptic for all the presented results. The factor $1/2$ in the boundary conditions is chosen to reduce the successive amplification of errors. For the stopping criteria we use a fixed number of ten iterations.

In Sec. 5.3.1-5.3.4 will go though the results from the four algorithms one by one and in Sec. 5.3.5 we give a summery of the findings and also show convergence results using noisy data. Additional results in Sec. 5.4 show reconstructions that visualise how the loss of ellipticity for the linearised problem manifest itself as propagating singularities in the reconstruction, exactly as explained by theory. We also present additional reconstructions based on the partial data and limited-view data models.

5.3.1 Picard-type algorithm

Fig. 5.2 shows four plots of the reconstructions for $p = 0.5$ and $p = 1$ after ten Picard iterations (Algorithm 1), utilising a single measurement (Fig. 5.2a - 5.2b) and two measurements (Fig. 5.2c - 5.2d). For $p = 0.5$, the algorithm provides a nearly perfect reconstruction. When $p = 1$ we get a reconstruction where we can identify the three perturbations in the domain, but the contrast is too low when we only use a single measurement. Utilising a second interior measurement increases the contrast and the reconstruction is very good.

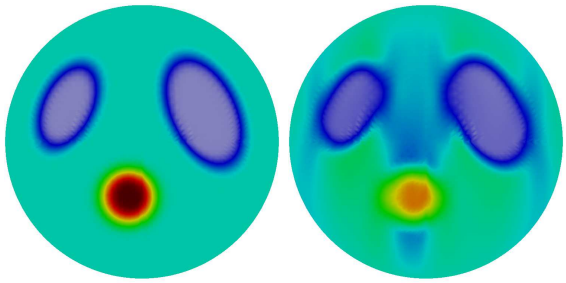

(a) $p = 0.5, J = 1$ **(b)** $p = 1, J = 1$

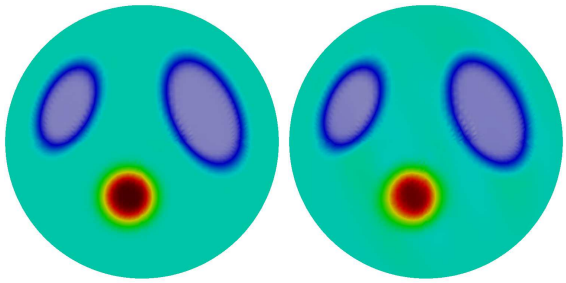

(c) $p = 0.5, J = 2$ **(d)** $p = 1, J = 2$

Figure 5.2: Plots of reconstructions of σ after ten Picard iterations, with a single interior measurement ($J = 1$) and two interior measurements ($J = 2$).

On Fig. 5.3 we have plotted the relative $L^2(\Omega)$ error in the reconstruction as a function of the iteration number. This clearly depends on the parameter p. For the chosen values of $p \leq 1$, the algorithm seems to converge, however the convergence rate is slow for $p = 1$. Note that the convergence rate increases when we utilise a second interior measurement. Also note that the error does not seem to converge to zero for $p = 0.5$, which is expected since the inverse problem is not solved on the same mesh as the one we use to generate the interior measurements. The four reconstructions for $p = 0.5$ and $p = 0.75$ have pairwise

similar convergence plots simply because the problems are already elliptic when $J = 1$, and the additional measurement is in some sense redundant. However, the convergence rate is improved slightly. For $p = 1.5$ and $p = 2$ we do not get convergence for this algorithm.

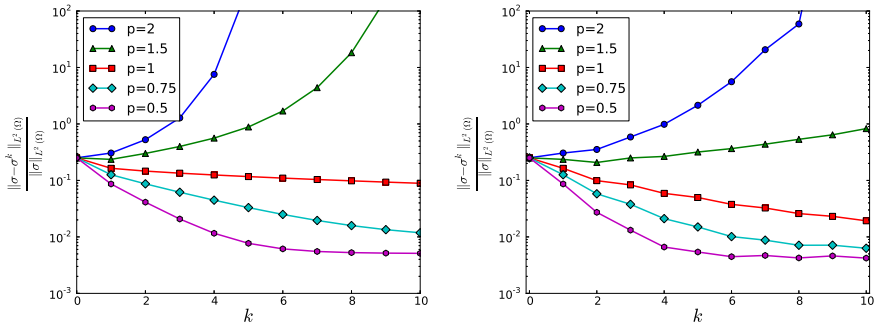

(a) $J = 1$ **(b)** $J = 2$

Figure 5.3: Convergence plots for the Picard iterations with one and two interior measurements. Note how the convergence rate depends on the parameter p.

In Sec. 4.1 we classified the non-linear PDE problems. When we apply the Picard scheme, we expect that the solution found in each iteration has properties that are related to the solutions of the non-linear PDE problems. Based on the classification as elliptic, degenerate elliptic and hyperbolic, and the known associated properties of solutions to such PDE problems, it seems reasonable that the Picard iteration works best in the elliptic case ($p = 0.5$ and $p = 0.75$) and does not converge when we have hyperbolic problems ($p = 1.5$ and $p = 2$). In the degenerate elliptic case ($p = 1, J = 1$), it was shown in the proof of Thm. 4.1, that the non-linear problem (3.1) is degenerate in the direction of ∇u_1 [12]. For the chosen set (σ, f_1), the degeneracy is therefore close to being horizontal. This most likely accounts for the low contrast and what looks like vertical smoothing, especially near the boundaries of the perturbations where the normal is also horizontal. When the algorithm iterates between two degenerate elliptic problems that do not share degenerate directions ($p = 1, J = 2$), we see that the reconstruction has no visible artifacts.

The Picard iteration is not only simple to implement, it is also computationally inexpensive. We use a standard laptop for the computations, and each iteration takes around 1.0 second.

5.3.2 Newton-type algorithm for square subsystems

Fig. 5.4 shows four plots of the reconstructions for $p = 0.5$ and $p = 1$ after ten Newton iterations (Algorithm 2), utilising a single measurement (Fig. 5.4a - 5.4b) and two measurements (Fig. 5.4c - 5.4d). Again, we see that the algorithm gives a nearly perfect reconstruction for $p = 0.5$. For $p = 1, J = 1$, we get a reconstruction that has some artifacts, but the contrast is better than the reconstruction obtained with the Picard iteration. For $p = 1, J = 2$, the reconstruction is improved, but the Picard iteration gives a reconstruction with less artifacts.

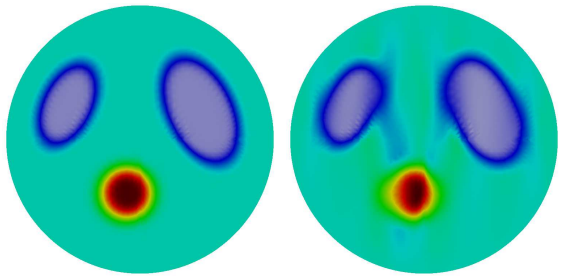

(a) $p = 0.5, J = 1$ **(b)** $p = 1, J = 1$

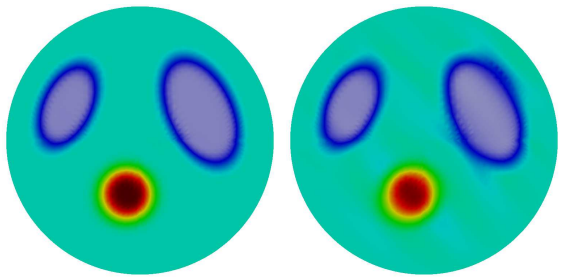

(c) $p = 0.5, J = 2$ **(d)** $p = 1, J = 2$

Figure 5.4: Plots of reconstructions of σ after ten Newton iterations, with a single interior measurement ($J = 1$) and two interior measurements ($J = 2$).

Looking at the convergence plots in Fig. 5.5, we see that after just two iterations the reconstruction error is almost constant for $p \leq 1$. Also note that the use of an additional data set ($J = 2$) does not seem to improve the reconstruction error or the convergence rate very much for the elliptic problems ($p < 1$). For $p = 1.5$ and $p = 2$, again we have an algorithm that does not converge.

This algorithm is based on a linearisation of the underlying non-linear hybrid

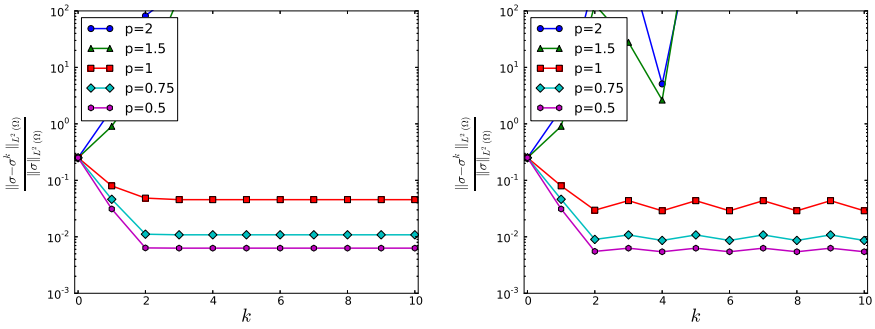

(a) $J = 1$ **(b)** $J = 2$

Figure 5.5: Convergence plots for the Newton iterations with one and two interior measurements.

inverse problem, and we know exactly how to classify this linearised system. This implies that the stability properties and possible non-uniqueness of the problem is captured by this method. When $p < 1$ we have uniqueness up to smoothing terms for the linearised problem, and this can explain the good reconstruction. For the degenerate elliptic case ($p = 1, J = 1$), we showed in Sec. 4.2 that the linearised problem (5.6) is degenerate elliptic in the direction of ∇u_1^k. Again, this most likely accounts for the vertical smoothing, especially near the boundaries of the perturbations where the normal is horizontal. When $p = 1.5$ and $p = 2$, we have a hyperbolic system, only equipped with Dirichlet boundary data, that permits propagation of singularities and this can also explain why the algorithm does not converge.

This Newton type algorithm is a bit more computational expensive than the Picard algorithm (Algorithm 1), since it requires solving a coupled PDE system in each iteration. In our case, each iteration takes around 1.3 seconds.

5.3.3 Newton-type algorithm for square subsystems using an approximate inverse

Fig. 5.6 shows four reconstructions produced after ten Newton iterations using an approximate inverse (Algorithm 3), again utilising a single measurement (Fig. 5.6a - 5.6b) and two measurements (Fig. 5.6c - 5.6d). The approximate inverse is only defined for $p \neq 1$, thus we do not consider the case $p = 1$.

In all four reconstructions we see that the three perturbations are clearly visible.

In the elliptic case ($p = 0.5$) the reconstructions and the convergence plot is very similar to the ones for the Picard algorithm and the Newton algorithm presented in the last sections. For $p = 2$ we now have what appears to be a converging algorithm, but in the case of a single measurement we have several visible artifacts in the reconstruction. This is due to the hyperbolic nature of the problem. We will give a finer characterisation of such artifacts in Sec. 5.4.1, where we also explain the link to the theoretical result of Thm. 4.17.

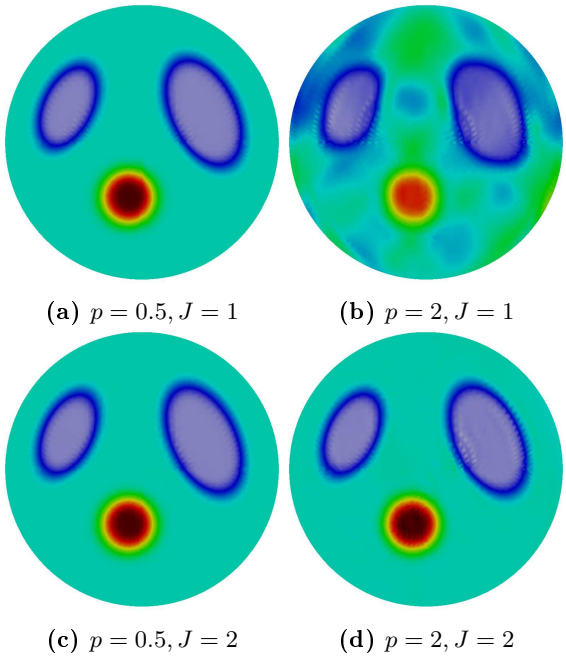

(a) $p = 0.5, J = 1$ **(b)** $p = 2, J = 1$

(c) $p = 0.5, J = 2$ **(d)** $p = 2, J = 2$

Figure 5.6: Plots of reconstructions of σ after ten Newton iterations using an approximate inverse, with a single interior measurement ($J = 1$) and two interior measurements ($J = 2$).

By looking at the convergence plots in Fig. 5.7, we see that the use of an additional data set does not change much when $p < 1$, but decrease the reconstruction error significantly when $p > 1$. For $p < 1, J = 2$ the error reaches a almost constant level after three iterations. Again, the classification of the linearised inverse problem can explain why the reconstructions for $p < 1$ are better than the ones produced when $p > 1$. When the linear system is (DN) elliptic ($p < 1$ or $J = 2$) the reconstruction errors after ten iterations are comparable. Also, note that the algorithm seems to perform best for $p = 0.5$ and $p = 2$ when $J = 2$. A possible explanation, is that the norm of the approximate inverse increases when p approaches 1. Thus, for values of p close to 1, errors are to a certain extend amplified more in the iterative scheme.

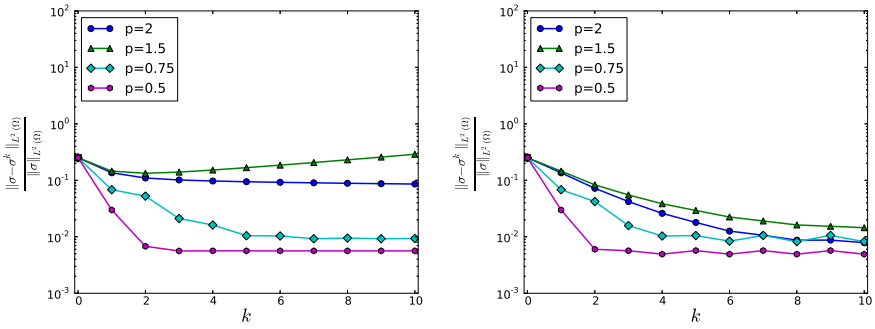

(a) $J = 1$ (b) $J = 2$

Figure 5.7: Convergence plots for the Newton iterations using an approximate inverse with one and two interior measurements.

Compared to the previous algorithm, the use of an approximate inverse really simplifies the implementation, but the computational complexity is higher, because of the additional arithmetic operations. In our case, each iteration takes around 3.0 seconds.

5.3.4 Newton-type algorithm for the full linearised system

Fig. 5.8 shows plots of the reconstructions produced after ten iterations using the norm minimising LSFEM formulation (Algorithm 4). Again we make reconstructions using a single measurement (Fig. 5.8a - 5.8c) and two measurements (Fig. 5.8d - 5.8f).

In all six reconstructions we see that the three perturbations are clearly visible. For $p = 0.5$ we get good reconstructions, which are comparable with all the other algorithms. Again, since the problem only needs a single measurement to be elliptic, the additional measurement is in some way redundant. For $p = 1$ we get reconstructions that are comparable to ones we got using the Newton algorithm for square subsystems and for $p = 2$ they are comparable to the ones we got using an approximate inverse. Again, the artifacts that are visible for $p = 1, J = 1$ and $p = 2, J = 1$ can be explained by the fact that we solve a non-elliptic problem; see also Sec. 5.4.1.

On the convergence plots in Fig. 5.9, we see how the algorithm converges for all ten problems. When $p < 1$, the convergence rate is similar to the two other algorithms for the linearised inverse problems, and when $J = 1$ we now get

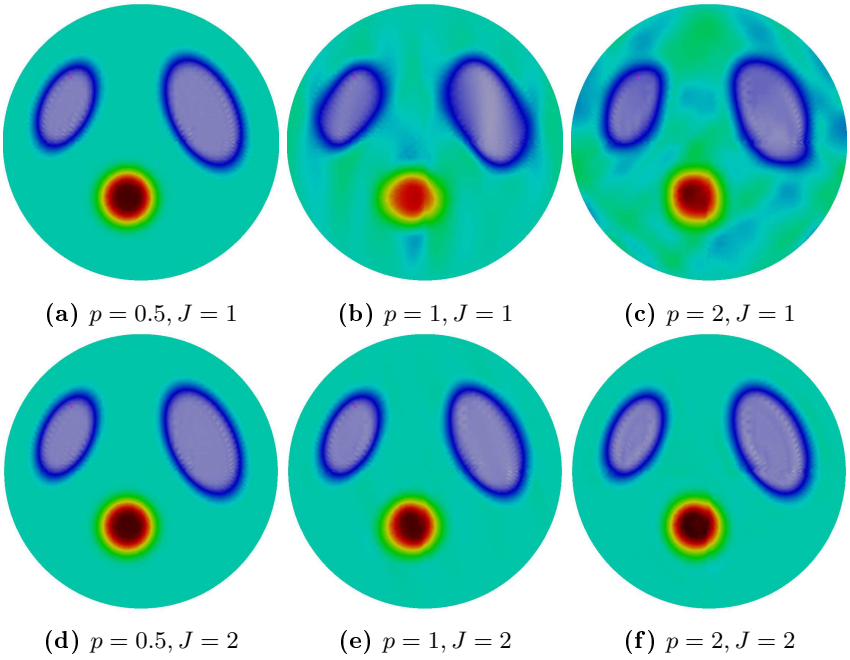

(a) $p = 0.5, J = 1$ **(b)** $p = 1, J = 1$ **(c)** $p = 2, J = 1$

(d) $p = 0.5, J = 2$ **(e)** $p = 1, J = 2$ **(f)** $p = 2, J = 2$

Figure 5.8: Plots of reconstructions of σ after ten norm minimising least squares iterations, with a single interior measurement ($J = 1$) and two interior measurements ($J = 2$).

convergence for all five values of p. For $J = 2$ the reconstructions are comparable to the ones we got using the approximate inverse. For $p = 1$ the convergence is comparable to the ones we got using Newton method for square subsystems. In some sense, this reconstruction method captures the best features of both methods. However, a drawback is that it is computationally more expensive. In our case, each iteration takes around 8 seconds when $J = 1$ and around 25 seconds when $J = 2$.

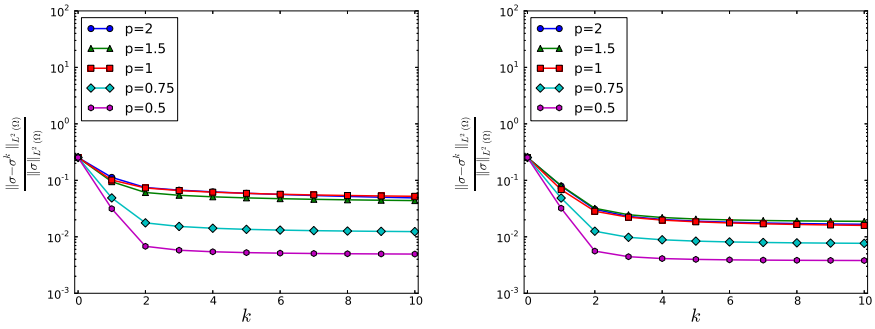

(a) $J = 1$ (b) $J = 2$

Figure 5.9: Convergence plots for the norm minimising least squares algorithm with one and two interior measurements.

5.3.5 Comparison of reconstruction methods and noisy data

In this section we present a summery of the numerical results, along with results for noisy data; see Tab. 2-5.

For each of the four algorithms we list the relative $L^2(\Omega)$-error after ten iterations, for noise-free data and when the data is corrupted by noise using the presented noise model (5.15). All errors in the tables are rounded to four decimal places. If no number is present is the table, it means that the algorithm was not converging, which here is defined by the criteria, that the relative error after ten iterations is larger than the initial relative error. We also list the classification of the problem for a given p and J. This should be understood, as the classification of the inverse problem that the algorithm solves in each iteration.

As we see from Tab. 2-5, Algorithm 1 and Algorithm 3 perform well on the problems that they were initially designed to solve, that is $p = 1, J = 2$ and $p = 2, J = 2$, respectively. This is also true when the data is corrupted by noise. Algorithm 2 only performs well for elliptic problems. Algorithm 4 seems to be very robust and is the only algorithm that convergences for all the presented cases. Also, in most cases, the relative error is the lowest of all the algorithms. For a more comprehensive analysis of the performance of each algorithm, we refer to the previous sections.

Table 2: Summary for Algorithm 1

p	J	Classification	Rel. err.	Rel. err. ($\rho = 0.1$)	Rel. err. ($\rho = 0.5$)
0.5	1	Elliptic	0.0051	0.0332	
0.75	1	Elliptic	0.0118	0.0424	
1	1	Deg. elliptic	0.0889		
1.5	1	Hyperbolic			
2	1	Hyperbolic			
0.5	2	Elliptic	0.0042	0.0271	0.1353
0.75	2	Elliptic	0.0063	0.0302	0.1508
1	2	Deg. elliptic	0.0205	0.0401	0.1896
1.5	2	Hyperbolic			
2	2	Hyperbolic			
Approx. time per iteration: 1.0 s.					

Table 3: Summary for Algorithm 2

p	J	Classification	Rel. error	Rel. error ($\rho = 0.1$)	Rel. error ($\rho = 0.5$)
0.5	1	Elliptic	0.0063	0.0378	0.1876
0.75	1	Elliptic	0.0108	0.0456	0.2286
1	1	Deg. elliptic	0.0455	0.0981	
1.5	1	Hyperbolic			
2	1	Hyperbolic			
0.5	2	Elliptic	0.0054	0.0361	0.1793
0.75	2	Elliptic	0.0086	0.0429	0.2132
1	2	Deg. elliptic	0.0289	0.0811	
1.5	2	Hyperbolic			
2	2	Hyperbolic			
Approx. time per iteration: 1.3 s.					

Table 4: Summary for Algorithm 3

p	J	Classification	Rel. error	Rel. error ($\rho = 0.1$)	Rel. error ($\rho = 0.5$)
0.5	**1**	**Elliptic**	**0.0056**	**0.0385**	**0.1928**
0.75	**1**	**Elliptic**	**0.0093**	**0.0478**	
1.5	**1**	**Hyperbolic**			
2	**1**	**Hyperbolic**	**0.0859**	**0.0963**	
0.5	**2**	**Elliptic**	**0.0049**	**0.0402**	**0.2016**
0.75	**2**	**Elliptic**	**0.0082**	**0.0773**	
1.5	**2**	**Hyperbolic**	**0.0145**	**0.0774**	
2	**2**	**Hyperbolic**	**0.0079**	**0.0360**	**0.1840**

Approx. time per iteration: 3 s.

Table 5: Summary for Algorithm 4

p	J	Classification	Rel. error	Rel. error ($\rho = 0.1$)	Rel. error ($\rho = 0.5$)
0.5	**1**	**Elliptic**	**0.0049**	**0.0383**	**0.1818**
0.75	**1**	**Elliptic**	**0.0124**	**0.0459**	**0.1942**
1	**1**	**Deg. elliptic**	**0.0521**	**0.0681**	**0.1884**
1.5	**1**	**Hyperbolic**	**0.0438**	**0.0634**	**0.1712**
2	**1**	**Hyperbolic**	**0.0488**	**0.0589**	**0.1458**
0.5	**2**	**DN elliptic**	**0.0038**	**0.0265**	**0.1273**
0.75	**2**	**DN elliptic**	**0.0077**	**0.0304**	**0.1339**
1	**2**	**DN elliptic**	**0.0159**	**0.0354**	**0.1315**
1.5	**2**	**DN elliptic**	**0.0188**	**0.0389**	**0.1232**
2	**2**	**DN elliptic**	**0.0167**	**0.0327**	**0.1023**

Approx. time per iteration: 8 s. ($J = 1$) **and** 25 s. ($J = 2$)

5.4 Additional numerical results

In this section we present some additional numerical results based on Algorithm 4. In Sec. 5.4.1 we give a finer characterisation of the artifacts the appear when we solve the non-elliptic linearised inverse problem, and relate this to the theretical results on the prorogation of singularities. In Sec. 5.4.2 and 5.4.3 we present reconstructions based on the inverse problem with partial data and limited-view data, respectively.

5.4.1 Propagation of singularities

We have already seen examples of artifacts in the presented reconstructions that are related to the loss of ellipticity. Algorithm 1,2, and 4 all showed artifacts in the reconstruction for the degenerate elliptic problem, which is closely related to the direction in which the problems are degenerate; see Fig. 5.2b, 5.4b, and 5.8b. However, this situation is not covered by the theoretical results on the propagation of singularities.

In this section we will visualise how the propagation of singularities aligns with the directions predicted by theory. In Fig. 5.10 we have plotted reconstructions after ten iterations with Algorithm 4 for four values of p which renders the linearised inverse problem hyperbolic. In all reconstructions we use a single boundary condition, such that the gradient of the solution to the reference problem is in the horizontal direction, at least for the first iteration.

According to the results of Thm. 4.14 and 4.20, the propagation should happen along curves for which the angle between the curve and the gradient of the reference potential should be $\sin^{-1}(p^{-1/2})$. For the four chosen values of p, $1.1, 1.5, 2$ and 3, this corresponds to curves at angles about $72°, 55°, 45°$ and $35°$ to the horizontal axis, respectively. Therefore, on each plot in Fig. 5.10 we have added arrows which show two directions in which the theoretical results state that singularities propagate. We clearly see that the artifacts seem to align in exactly these directions.

Thm. 4.21 implies that the wave front set of the right-hand of the governing equation at most includes the points in the smoothing layer around the perturbations and the associated singular directions, which in this case are normals to this layer. The propagation of singularities should then happen from points, for which the direction of the singularity aligns with the loss of ellipticity. Indeed, on the plots we see that the artifacts seem to be curves that are tangent to the perturbations, exactly at points for which the normal is $\cos^{-1}(p^{-1/2})$ to the horizontal axis.

The propagation of singularities is a distinct nature of the inverse problem and not related to the chosen reconstruction method. For instance, note that the reconstruction made by Algorithm 3 for $p = 2, J = 1$ (Fig. 5.6b) shows artifacts that seem to align at angles about $45°$ to horizontal. This algorithm is based on the original formulation of the square linearised system, and these artifacts are therefore explained by the results of Thm. 4.13 and 4.17.

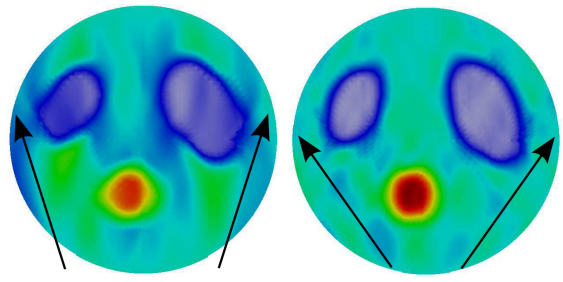

(a) $p = 1.1, J = 1$ (b) $p = 1.5, J = 1$

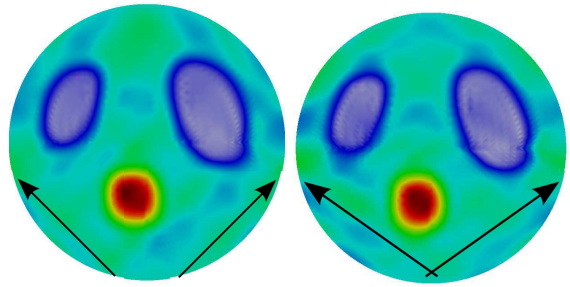

(c) $p = 2, J = 1$ (d) $p = 3, J = 1$

Figure 5.10: Plots of reconstructions of σ after ten norm minimising least squares iterations, with a single interior measurement ($J = 1$) and four different values of p. The arrows visualise directions in which the theoretical results state that singularities propagate.

5.4.2 Partial data

For the numerical test with partial data we define Γ as a disc with radius 0.5 centred at the point $(0.1, 0)$; see Fig. 5.11.

In Fig. 5.12 we show six reconstructions produced with ten norm minimising least squares iterations in the partial data case. We see that elliptic problems ($p = 0.5$ or $J = 2$) allow for a good reconstruction in Γ. In the non-elliptic case, it seems that the reconstruction captures the presence of the two perturbations in Γ, but the contrast and shape is not precise. When $p = 1$ the reconstructions seem to have a lower contrast than the reconstructions for $p = 2$. This was also the case for the problem with full data; see Fig. 5.9.

The reconstruction in the domain outside Γ is very blurred, however it seems that there are low values in the top left area, most likely due to the top left perturbation in the phantom. Also, when $J = 1$ the blurring seems to be in

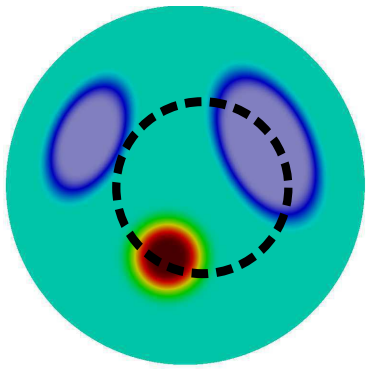

Figure 5.11: The partial data in only availavle within the disc shaped area Γ whose boundary is visualised by the dashed circle.

the horizontal direction, most likely due to the fact that ∇u_1 is close to being horizontal. For $J = 2$ the blurring seems to be from the center towards the boundary of the domain. Since no interior data is available outside Γ, the mathematical formulation is in this area limited to the Fréchet derivative of the solution operator for the problem (1.3); see Lem. 3.2. The blurring outside Γ is most likely a result of (1.3) being an elliptic problem.

On Fig. 5.13 we present convergence plots for the partial data problem. Note that the relative errors on these plots are calculated in Γ, and that the second axis is different from the one used on the previous convergence plots. We see that the relative errors for the non-elliptic problems $p \geq 1, J = 1$ seem to increase after a few iterations. When the problem is (DN) elliptic, we see that the relative error becomes smaller, and the method seem to convergence for any p. In this case, we see that the reconstruction algorithm is able to provide a reasonable reconstruction in the area where the partial data is given.

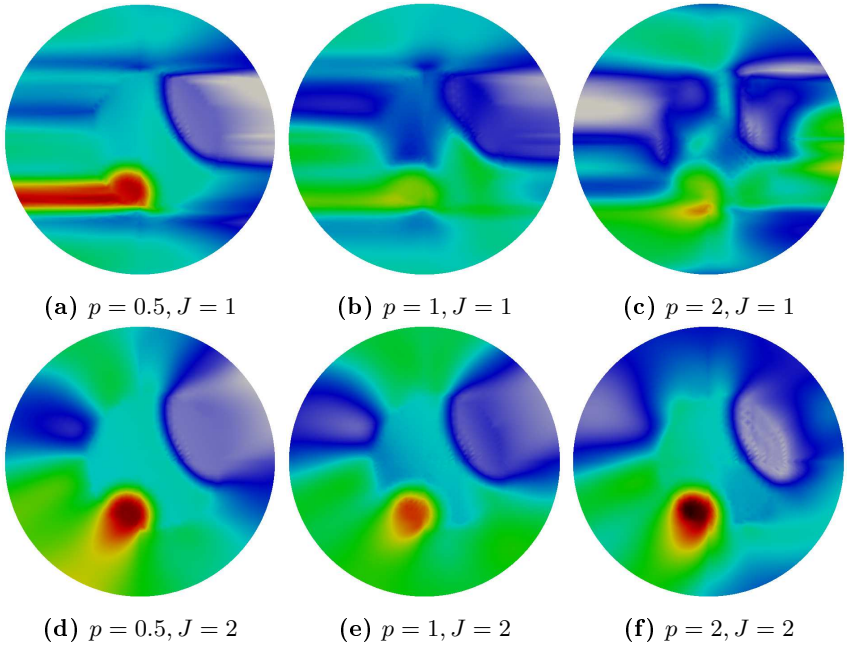

(a) $p = 0.5, J = 1$ (b) $p = 1, J = 1$ (c) $p = 2, J = 1$

(d) $p = 0.5, J = 2$ (e) $p = 1, J = 2$ (f) $p = 2, J = 2$

Figure 5.12: Plots of reconstructions of σ after ten norm minimising least squares iterations with partial data.

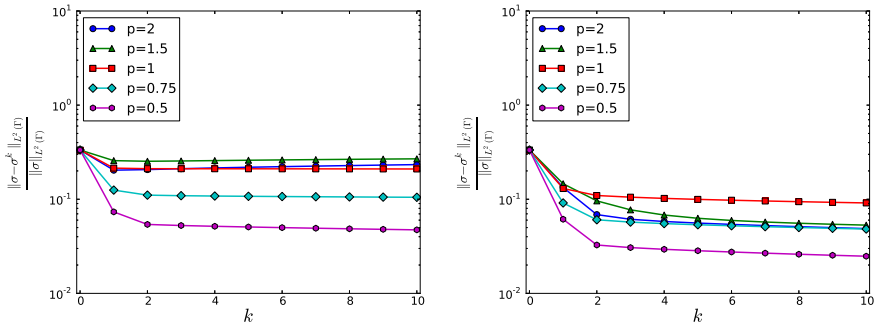

(a) $J = 1$ (b) $J = 2$

Figure 5.13: Convergence plots for the norm minimising least squares algorithm with one and two interior measurements using partial data. Note that the relative error is calculated only in the domain where the partial is available.

5.4.3 Limited-view data

We end the numerical analysis with the case of limited-view data. Here we restrict the imposed boundary conditions to the top half of the boundary. In this analysis we use the set of boundary conditions

$$f_1 = \sin(\theta) \quad \text{and} \quad f_2 = \sin(2\theta), \quad \theta \in [0, \pi],$$

where θ denotes the usual polar angle. On the bottom part of the boundary, we impose a homogeneous Neumann condition, as explained in Sec. 4.5.2.

On Fig. 5.14 we show plots of six reconstructions using limited-view data. We see that for $p = 0.5$ we get a nearly prefect reconstruction. For $p = 1$ we get a good reconstruction in the top part of the domain, and adding a second data set results in a much better reconstruction in the lower part. For $p = 2$ we have a similar behaviour, but the overall quality of the reconstruction is not as good.

A visual inspection of ∇u_1^k and ∇u_2^k reveals that both are small in magnitude and nearly horizontal in the lower part of the domain. Therefore, for $p \geq 1$ the system is close to being non-elliptic in the lower part of the domain, and this can explain why the reconstructions clearly have artifacts in this area. Also, u_1^k seems to have a critical point at the bottom, near $(0, -1)$. This can explain the high values in the reconstruction near the bottom for $p = 2, J = 1$. To a less extend, the critical point also seems to affect the reconstitution for $p = 1, J = 1$. The visual inspection also reveals that u_2^k probably has critical points at $(\pm 1, 0)$, but this does not seem to affect the reconstructions; most likely because ∇u_1^k does not vanish at the same points. Note that both Algorithm 1 and 3 would fail to work for this problem, because they rely on a division by $|\nabla u_j^k|^p$ in each iteration.

On the convergence plots in Fig. 5.15, we see that convergence seems to be limited to the cases where $p < 1$ or $J = 2$. For $p > 1, J = 2$ we get slow convergence, most likely due to the fact that ∇u_1^k and ∇u_2^k are nearly parallel in the lower part of Ω and the problem is therefore close to not being DN elliptic. Note that for $p = 1.5$, the use of an additional data set does not improve the relative error after ten iterations.

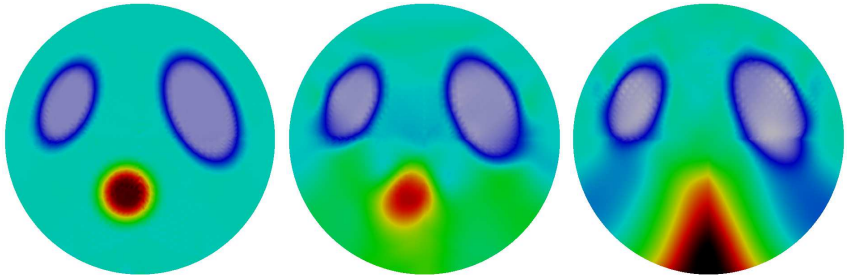

(a) $p = 0.5, J = 1$ (b) $p = 1, J = 1$ (c) $p = 2, J = 1$

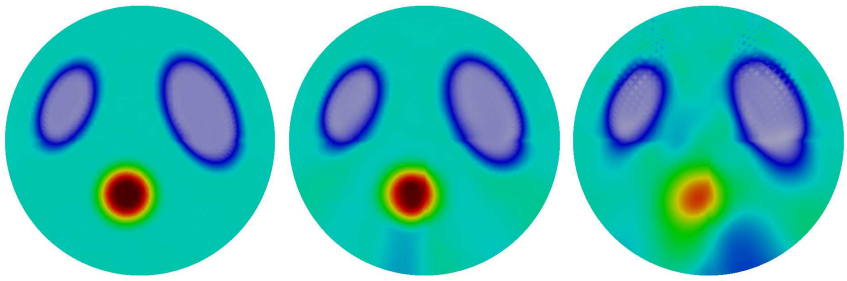

(d) $p = 0.5, J = 2$ (e) $p = 1, J = 2$ (f) $p = 2, J = 2$

Figure 5.14: Plots of reconstructions of σ after ten norm minimising least squares iterations with limited-view data.

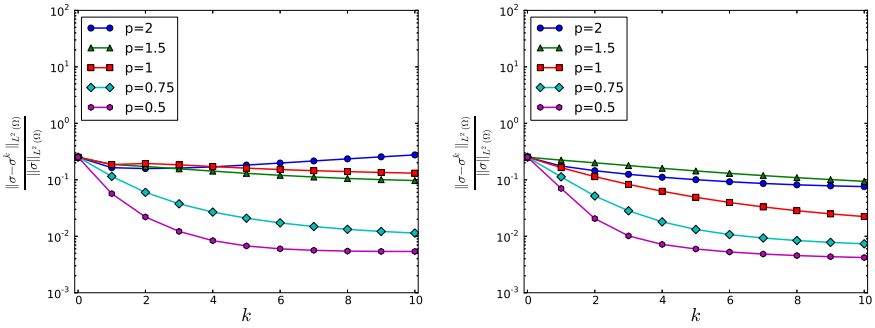

(a) $J = 1$ (b) $J = 2$

Figure 5.15: Convergence plots for the norm minimising least squares algorithm with one and two interior measurements using limited-view data.

Chapter 6

Contributions, limitations, and perspectives

Hybrid inverse problems are mathematical descriptions of imaging procedures that utilise multiple existing imaging techniques to recover an interior physical property. In this thesis we studied a general hybrid inverse problem in impedance tomography. Mathematically, the inverse problem was the reconstruction of a coefficient in a linear elliptic partial differential equation from non-linear interior data given as a point-wise functional dependent on the coefficient and the solution to a corresponding boundary value problem. From reading the previous chapters, it should be apparent to the reader that a theoretical analysis, based on pseudo-differential operator theory, gives important insight into the qualitative properties of solutions to such hybrid inverse problems, and as a natural implication, closely connected is the design and performance of the related iterative reconstruction methods.

In this final chapter we summarise the thesis in a broader context, and discuss the most important results and observations from the previous chapters. This is done on several levels. First we list the most important contributions and results, and discuss their implications. We will then reflect on certain limitations in the mathematical model and treatment, and give ideas on how to extent or modify the analysis. Finally, we shortly discuss the perspectives and guidelines for related research within the field of hybrid inverse problems.

6.1 Contributions

The individual contributions are discussed in their specific context in the previous chapters. In addition, we give here a more general discussion of the contributions in a wider context.

The purpose of the study was to describe the qualitative properties of solutions to a class of hybrid inverse problems in impedance tomography, and relate these finding with the development and performance of iterative reconstruction methods. Additionally, the ambition was to extend the analysis to examples with partial and limited-view data.

The main theoretical contributions are Thm. 4.17 and 4.20. Here we presented novel result regarding the propagation of singularities for the linearised hybrid inverse problem and a similar result for the corresponding normal form, both expressed as scalar pseudo-differential operator equations. The latter result is based on the theory for operators of constant multiplicity. To the author's knowledge, this is the first time that such an analysis has been conducted and therefore these are the first precise results about the distinctive features of the solutions to a non-elliptic linearised hybrid inverse problem.

The classification of the linearised hybrid inverse problem, Thm. 4.2, is consistent with that of Kuchment and Steinhauer [57] and Bal [13], who both found similar results. The associated stability results for the (DN) elliptic problem, Thm. 4.5, were derived using theory for determined and overdetermined systems of linear partial differential equations, and the related boundary value problems. This is much inspired by the work of Bal [13], yet our approach treated a more general type of interior data and some parts of the analysis is explained a bit more in depth; an example is the proof that the Lopatinskii condition is satisfied for the elliptic problem, see Thm. 4.3 and Rem. 4.4. Kuchment and Steinhauer [57] showed similar stability results relying entirely on theory from pseudo-differential calculus, but we think that this approach is less elegant, since boundary conditions cannot be included in the pseudo-differential analysis in an obvious way. The equivalent ellipticity and stability results for the first-order system and the scalar operator, found in Thm. 4.6, 4.11, 4.13 and 4.14 seem to be new, or at least generalisations of previous work, but they are not that surprising, since they are concerned with a reformulation of the original second-order differential system.

In Chap. 5, we presented a thorough analysis of iterative reconstruction methods for hybrid inverse problem in impedance tomography. To the authors knowledge, this is the first time that this has been done. It was explained how mathematical theory can be used to design reconstruction methods for inverse

problems described by non-linear PDEs or maps. Based on this theory, we developed four iterative reconstruction algorithms for a general class of hybrid inverse problems in impedance tomography and explained how these could be implemented using the finite element method. One algorithm was also extended to the cases of partial and limited-view data. Some of the numerical methods are inspired by existing work, but they were all redefined on the general class of hybrid inverse problems. The only exception was the Newton-type algorithm using an approximate inverse, which is not defined for $p = 1$.

The numerical results verified that a theoretical analysis of the inverse problem can predict the performance of the developed iterative reconstruction methods. For $p < 1$, all algorithms performed well, due to the optimal stability properties associated with ellipticity. In the non-elliptic case, some algorithms did not converge, while others produced reconstructions with clearly visible propagating singularities. This aligned perfectly with the results from the theoretical part. Of the presented methods, we would like to point out the Newton-type algorithm for the full linearised system, based on the least squares finite element method. It gave the best reconstructions in all of the non-elliptic cases, and it is a general reconstruction framework which is defined independently on the number of measurements. It is the first time this type of algorithm has been developed for, and used on, the general inverse problem; yet some related methods have previously been used on the inverse problem from UMEIT [16, 22]. In the final part of Chap. 5, we also presented novel numerical results using partial and limited-view data. The qualitative features of these reconstructions could also be explained by theoretical considerations.

A common thread in this thesis has been the attempt to explain the close connection between the theoretical and numerical analysis of such problems; in particular the connection between the classification of the inverse problem and the performance of related iterative reconstruction algorithms. There has been a need for such an analysis, because several reconstruction algorithms for hybrid inverse problems have been developed and implemented in the last few years, but the motivation behind the choice of method and the choice of implementation is often not entirely accounted for. Furthermore, the qualitative features of the produced reconstructions are not always explained in relation to the mathematical problem it tries to solve.

6.2 Limitations

Although the study has successfully demonstrated several connections between the theoretical and numerical results, the presented work has a number of

limitations that need to be mentioned and addressed in future studies. It is important to be aware of such limitations, because it means that the results and observations need to be interpreted accordingly.

First of all, the presented mathematical model for electrical impedance tomography is way too simple to model any real physical system. A two-dimensional model of electric fields is clearly a simplification, since it is well-known that electric fields propagate in three dimensions. The assumption that conductivity is an isotropic property is also false, at least for tissues that have an anisotropic physical structure [20].

As mentioned in the introduction, the interior data functional is a generalisation of a functional that models a physical property. Even when the hybrid inverse problem is related to a imaging method, such as MREIT or UMEIT, it is only theoretically possible to obtain this interior data, and an exact point-wise data acquisition without any noise relies on an unrealistic experimental set-up. An example is the data acquisition model for UMEIT, which is explained in Sec. 1.2.2. Here one of the assumptions is that any type of plane ultrasonic wave can be generated. In any application, there is of course practical limitations on the ultrasonic wave, which in this data acquisition model correspond to a certain filtering of the interior data. For instance, the magnitude of the wave number has a practical upper bound, and as a result the interior data will always be low-pass filtered.

Many of the theoretical results that relies on pseudo-differential calculus, requires the PDE coefficients of the linearised hybrid inverse problem to be sufficiently smooth. It is not difficult to satisfy this requirement, by choosing a smooth reference conductivity, but when an iterative reconstruction method is applied to a problem, the smoothness requirement is most likely not satisfied after the first iteration. Therefore, it would be interesting to investigate in which way non-smooth PDE coefficients change the theoretical and numerical results.

In this thesis, the intention has been to consider a simple inverse problem and simple algorithms. This also means that the numerical implementations merely works as proofs-of-concept, and they could definitely be improved. One could certainly make a more advanced finite element implementation by a different choice of element functions, different meshing, fine-tuning parameters for the linear solver and so on. However, since the hybrid inverse problem is based on a very simplified model of reality, it only seem relevant to improve the numerical implementation if a more realistic mathematical model is used.

For the iterative methods, we have also not been concerned with a theoretical analysis of the associated convergence properties. It is probably very difficult to obtain general convergence results, that does not depend on a sufficiently

good choice of reference conductivity. However, for practical applications within applied mathematics it seems that many iterative algorithms are used with great success, even when there does not exist any theoretical justification for the observed convergence.

6.3 Perspectives

Advances in the field of hybrid imaging within the last decade, have resulted in many interesting problems, both related to mathematical and practical challenges. Some hybrid methods, such as Photoacoustic Tomography [97] and MREIT [84], look promising as future imaging techniques. Other methods are less likely to work in practise, often because the underlying physical model is inadequate or based on wrong assumptions. Nevertheless, there is an increasing need for safe, cheap and efficient imaging techniques, which is a motivational factor for the continuous development of hybrid imaging methods and the corresponding formulation, analysis and numerical implementation of hybrid inverse problems.

The findings of this study have a number of possibly important implications for future practice and we have gone some way towards enhancing our understanding of hybrid inverse problems in impedance tomography. As mentioned previously, we have focused on simplicity throughout the theoretical and numerical analysis. This implies that most of the presented results and observations are general, and the ideas and techniques can most likely be used on similar problems described by PDEs or maps between Banach spaces.

Many mathematical problems from hybrid imaging are closely related. Often the description is based on a PDE model of the physical system and additional interior data expressed by a point-wise functional of one or more PDE coefficients and the corresponding solution to the PDE problem. In this case, the presented analysis work as an example of how to treat such problems. For instance, it seems natural to try to extend the analysis of the propagation of singularities to the inverse problems from Quantitative Elastography and Ultrasound Modulated Optical Tomography, for which the reconstruction considers several PDE coefficients. For these inverse problems, ellipticity and stability have already been analysed [15, 96].

It is still the author's opinion, that the analysis should be systematic, kept simple, and not be too focused on specific applications. However, there is still room to reformulate the inverse problem to include a better model of the physical system. In relation to EIT, a choice could be to use a model that takes

into account the presence of boundary electrodes and contact impedances; for example the so-called complete electrode model [90]. Also, the three-dimensional case should be treated numerically.

If the hybrid inverse problem is related to a physical coupling, the interior data acquisition is related to a certain experimental procedure. It is often difficult, if not impossible, to find information about exactly what can be measured in such experiments. Real experimental data would of course be of finite precision and include measurement noise, and from a practical perspective, it would also be interesting to include this in the mathematical model. This could be based on both empirical and non-empirical reasoning, but it should be done in a systematic way. In relation the UMEIT, we have already mentioned several examples of the impracticability of the data acquisition model. A better understanding and modelling of the acoustic-electric effect and the ultrasonic wave propagation is therefore an important topic for future research in relation to this modality.

Appendix A

Notation and symbols

The following appendix contains a brief review of the notation used in the previous chapters. Most notation is standard, but we include it here for completeness.

We use lower case bold letters for vectors and vector functions (such as $\boldsymbol{u}$); the only exceptions being x (the spatial variable in Ω), k (the wave number), and ξ (the Fourier variable). Calligraphic upper case fonts are often used for maps and operators (such as $\mathcal{L}$) and upper case bold letters for matrices (such as $\boldsymbol{A}$). In the numerical treatment, the latter is also used for matrices of operators.

The tilde accent ($\tilde{}$) is used to denote mathematical objects associated to the reference problem, see also p. 36, and the acute accent ($\acute{}$) to denote mathematical objects associated to the first order boundary value problem; see also (4.4). All constants are generally denoted by c, including subscripts when necessary.

List of symbols

$\boldsymbol{A}$	Matrix of operators in the linearised inverse problem; see (5.6).
$\boldsymbol{b}$	Right-hand side in the linearised inverse problem; see (5.6).
$\mathcal{B}$	Boundary operator in the linearised inverse problem; see (3.12).
$\acute{\mathcal{B}}$	Boundary operator in the first order linearised inverse problem; see (4.4).
$C^\infty(\Omega)$	Smooth functions on Ω.
$C_0^\infty(\Omega)$	Smooth functions with compact support on Ω. Also denoted the test functions.
$C_+^\infty(\Omega)$	Smooth functions on Ω uniformly bounded below by a positive constant.
D^α	Differential operator for a multi-index α defined by $$D^\alpha u := (-i)^{\lvert\alpha\rvert}\frac{\partial^{\lvert\alpha\rvert}u(x)}{\partial x_1^{\alpha_1}\cdots\partial x_n^{\alpha_n}} = (-i)^{\lvert\alpha\rvert}\partial_{x_1}^{\alpha_1}\cdots\partial_{x_n}^{\alpha_n}u,$$ where i denotes the imaginary unit.
$đ\xi$	Measure used in the Fourier transform, $đ\xi := (2\pi)^{-n}d\xi$.
$\mathscr{D}'(\Omega)$	Distributions on Ω.
$\mathrm{d}\,\mathcal{F}\vert_u$	Fréchet derivative of $\mathcal{F}$ at u; see Def. 2.1.
$\mathscr{E}'(\Omega)$	Distributions with compact support in Ω.

f_j	Boundary condition for the forward problem; see (1.3).
$\boldsymbol{f}$	Right-hand side in the linearised inverse problem; see (3.12).
$\acute{\boldsymbol{f}}$	Right-hand side in the first order linearised inverse problem; see (4.4).
H_j	Interior data; see (1.4).
$\dot{H}_j$	Noisy counterpart of H_j; see (4.22).
$\boldsymbol{H}_j$	Discrete representation of H_j.
$\dot{\boldsymbol{H}}_j$	Noisy counterpart of $\boldsymbol{H}_j$; see (5.15).
$H_0^1(\Omega)$	Functions in the Sobolev space $H^1(\Omega)$ with zero trace.
$H_{\mathrm{div}}(\Omega)$	Hilbert space of vector functions in $[L^2(\Omega)]^n$ for which the divergence is also an $L^2(\Omega)$ function; see [92, Chap. 20].
J	Number of boundary conditions and measurements.
k	Iteration number.
$[\cdot]^k$	The k'th iterate of $[\cdot]$.
$L_+^\infty(\Omega)$	Functions on Ω uniformly bounded below and above by positive constants.
$\mathcal{L}$	Linear operator in the linearised inverse problem; see (3.12).
$\acute{\mathcal{L}}$	Linear operator in the first order linearised inverse problem; see (4.4).
$\acute{\mathcal{L}}^*$	Adjoint of $\acute{\mathcal{L}}$; see Def. 4.7.
mod	Modulo operator.
$\mathfrak{p}(x,\xi)$	Symbol of the pseudo-differential operator $P(x,D)$.
$\mathfrak{p}^{(0)}(x,\xi)$	Principal symbol of the classical pseudo-differential operator $P(x,D)$.
p	Exponent in the interior data; see (1.4).
$S^m(\Omega\times\mathbb{R}^n)$	Class of classical symbols of degree m; see Def. 2.7.
$S^m_{1,0}(\Omega\times\mathbb{R}^n)$	Standard class of symbols of degree m and type $1,0$; see Def. 2.3.
$\operatorname{sing\,supp} u$	Singular support of $u\in\mathscr{D}'(\Omega)$; see Def. 2.17.

$\mathscr{S}(\mathbb{R}^n)$	Schwartz space of functions with rapidly decreasing derivatives; see [38, Chap. 5].
$\hat{u}$	Fourier transform of the function $u \in \mathscr{S}(\Omega)$; see (2.2).
u_j	Solution to the forward problem; see (1.3).
$\acute{\boldsymbol{u}}$	Solution to the first order linearised inverse problem; see (4.4).
$\boldsymbol{u}$	Solution to the linearised inverse problem; see (3.12).
$W^{k,p}(\Omega)$	Sobolev space on Ω; see e.g. Adams [2]. For non-integer order spaces, these spaces should be understood as Bessel potential spaces [1].
$\mathrm{WF}(u)$	Wave front set of $u \in \mathscr{D}'(\Omega)$; see Def. 2.19.
x	Spatial variable, $x \in \Omega$.
$\boldsymbol{x}$	Solution to the linearised inverse problem; see (5.6).
$\partial\Omega$	The boundary of Ω.
$\partial_{\boldsymbol{\nu}}$	The normal derivative, i.e. $\partial_{\boldsymbol{\nu}} u := \boldsymbol{\nu} \cdot \nabla u$.
$\boldsymbol{\nu}$	Exterior normal to $\partial\Omega$.
Ω	An open subset of $\mathbb{R}^n$, $n = 2, 3$.
$\Psi^m(\Omega)$	The class of classical pseudo-differential operators of order m.
$\Psi^m_{1,0}(\Omega)$	The class of pseudo-differential operators of order m and type $1, 0$.
ρ	The noise level; see (4.22) and (5.15).
σ	Function modelling the conductivity.
Γ	Simply connected subset of Ω. The data is limited to Γ in the partial data setting.
ξ	Fourier variable, $\xi \in \mathbb{R}^n$.
Υ	The part of $\partial\Omega$ which is not available in the limited-view setting.

Bibliography

[1] D.R. Adams and L.I. Hedberg. *Function Spaces and Potential Theory*. Die Grundlehren der mathematischen Wissenschaften in Einzeldarstellungen. Springer, 1996.

[2] R.A. Adams and J.J.F. Fournier. *Sobolev Spaces*. Pure and Applied Mathematics. Elsevier Science, 2003.

[3] S. Agmon, A. Douglis, and L. Nirenberg. Estimates near the boundary for solutions of elliptic partial differential equations satisfying general boundary conditions. I. *Communications on Pure and Applied Mathematics*, 12(4):623–727, Nov 1959.

[4] S. Agmon, A. Douglis, and L. Nirenberg. Estimates near the boundary for solutions of elliptic partial differential equations satisfying general boundary conditions II. *Communications on Pure and Applied Mathematics*, 17(1):35–92, Feb 1964.

[5] M.S. Agranovich. Elliptic singular integro-differential operators. *Russian Mathematical Surveys*, 20(5):1–121, 1965.

[6] M.S. Agranovich and M.A. Shubin. *Partial Differential Equations IX: Elliptic Boundary Value Problems*. Encyclopaedia of Mathematical Sciences. Springer, 1997.

[7] G. Alessandrini and V. Nesi. Univalent σ-harmonic mappings. *Archive for Rational Mechanics and Analysis*, 158(2):155–171, 2001.

[8] H. Ammari. *An Introduction to Mathematics of Emerging Biomedical Imaging*. Mathématiques et Applications. Springer, 2008.

[9] H. Ammari, E. Bonnetier, Y. Capdeboscq, M. Tanter, and M. Fink. Electrical impedance tomography by elastic deformation. *SIAM Journal on Applied Mathematics*, 68(6):1557–1573, 2008.

[10] H. Ammari, J. Garnier, and W. Jing. Resolution and stability analysis in acousto-electric imaging. *Inverse Problems*, 28(8):084005, Aug 2012.

[11] S.R. Arridge and O. Scherzer. Imaging from coupled physics. *Inverse Problems*, 28(8):080201, 2012.

[12] G. Bal. Hybrid inverse problems and internal functionals. *Inverse Problems and Applications: Inside Out II*, 60:325–368, 2012.

[13] G. Bal. Hybrid inverse problems and redundant systems of partial differential equations. *arXiv preprint arXiv:1210.0265*, 2012.

[14] G. Bal. Cauchy problem for ultrasound-modulated EIT. *Analysis & PDE*, 6(4):751–775, 2013.

[15] G. Bal and S. Moskow. Local inversions in ultrasound-modulated optical tomography. *Inverse Problems*, 30(2):025005, Feb 2014.

[16] G. Bal, W. Naetar, O. Scherzer, and J. Schotland. The Levenberg–Marquardt iteration for numerical inversion of the power density operator. *Journal of Inverse and Ill-Posed Problems*, 21(2):265–280, 2013.

[17] Ö. Birgül, B.M. Eyüboglu, and Y.Z. Ider. Current constrained voltage scaled reconstruction (CCVSR) algorithm for MR-EIT and its performance with different probing current patterns. *Physics in medicine and biology*, 48(5):653, 2003.

[18] P.B. Bochev and M.D. Gunzburger. *Least-Squares Finite Element Methods*. Applied Mathematical Sciences. Springer, 2009.

[19] L. Borcea. Electrical impedance tomography. *Inverse Problems*, 18(6):R99–R136, Dec 2002.

[20] J.D. Bronzino. *Medical Devices and Systems*. The Biomedical Engineering Handbook, Third Edition. Taylor & Francis, 2006.

[21] R.B. Buxton. *Introduction to Functional Magnetic Resonance Imaging: Principles and Techniques*. Introduction to Functional Magnetic Resonance Imaging: Principles and Techniques. Cambridge University Press, 2009.

[22] Y. Capdeboscq, J. Fehrenbach, F. de Gournay, and O. Kavian. Imaging by modification: Numerical reconstruction of local conductivities from corresponding power density measurements. *SIAM J. Imaging Sci.*, 2(4):1003–1030, 2009.

[23] J. Chazarain. Opérateurs hyperboliques à caractéristiques de multiplicité constante. *Annales de l'institut Fourier*, 24(1):173–202, 1974.

[24] J. Chazarain. Propagation des singularités pour une classe d'opérateurs à caractéristiques multiples et résolubilité locale. *Annales de l'institut Fourier*, 24(1):203–223, 1974.

[25] O. Christensen. *Functions, Spaces, and Expansions: Mathematical Tools in Physics and Engineering*. Applied and Numerical Harmonic Analysis. Birkhäuser Boston, 2010.

[26] D. Colton, J. Coyle, and P. Monk. Recent developments in inverse acoustic scattering theory. *SIAM Rev.*, 42(3):369–414, Jan 2000.

[27] C. Cosner. On the definition of ellipticity for systems of partial differential equations. *Journal of Mathematical Analysis and Applications*, 158(1):80–93, 1991.

[28] I.J.D. Craig and J.C. Brown. *Inverse problems in astronomy: A guide to inversion strategies for remotely sensed data*. A. Hilger, 1986.

[29] P. Deuflhard. *Newton Methods for Nonlinear Problems: Affine Invariance and Adaptive Algorithms*. Springer Series in Computational Mathematics. Springer, 2011.

[30] F.A. Duck, A.C. Baker, and H.C. Starritt. *Ultrasound in Medicine*. Series in Medical Physics and Biomedical Engineering. Taylor & Francis, 2002.

[31] J.J. Duistermaat and L. Hörmander. Fourier integral operators. II. *Acta mathematica*, 128(1):183–269, 1972.

[32] H.W. Engl, M. Hanke, and A. Neubauer. *Regularization of Inverse Problems*. Mathematics and Its Applications. Springer, 2000.

[33] H.W. Engl, A.K. Louis, and W. Rundell, editors. *Inverse Problems in Medical Imaging and Nondestructive Testing*. Springer Vienna, 1997.

[34] L.C. Evans. *Partial Differential Equations*. Graduate Studies in Mathematics. American Mathematical Society, 2010.

[35] B. Gebauer and O. Scherzer. Impedance-acoustic tomography. *SIAM Journal on Applied Mathematics*, 69(2):565–576, 2008.

[36] M. Giaquinta and G. Modica. *Mathematical Analysis: An Introduction to Functions of Several Variables*. Mathematical analysis. Birkhäuser Boston, 2009.

[37] D. Gilbarg and N.S. Trudinger. *Elliptic Partial Differential Equations of Second Order*. Die Grundlehren der mathematischen Wissenschaften in Einzeldarstellungen. Springer-Verlag, 1977.

[38] G. Grubb. *Distributions and Operators*. Graduate Texts in Mathematics. Springer, 2009.

[39] H. Hagen. *Curve and Surface Design*. Society for Industrial and Applied Mathematics, 1992.

[40] R. Hagen, S. Roch, and B. Silbermann. *C* - Algebras and Numerical Analysis*. Chapman & Hall/CRC Pure and Applied Mathematics. Taylor & Francis, 2000.

[41] P.C. Hansen. *Discrete Inverse Problems: Insight and Algorithms*. Fundamentals of Algorithms. Society for Industrial and Applied Mathematics, 2010.

[42] A. Henderson. *The ParaView guide*. Kitware, Clifton Park, NY, 2004.

[43] N. Hoell, A. Moradifam, and A. Nachman. Current density impedance imaging of an anisotropic conductivity in a known conformal class. *arXiv preprint arXiv:1302.7044*, 2013.

[44] D.S. Holder. *Electrical Impedance Tomography: Methods, History and Applications*. Series in Medical Physics and Biomedical Engineering. Taylor & Francis, 2010.

[45] L. Hörmander. *The Analysis of Linear Partial Differential Operators I - IV*. Classics in Mathematics. Springer, 2009.

[46] J. Hsieh. *Computed Tomography: Principles, Design, Artifacts, and Recent Advances*. Progress in Biomedical Optics and Imaging. SPIE Press, 2003.

[47] P.G. Huray. *Maxwell's Equations*. John Wiley & Sons, 2011.

[48] V. Isakov. *Inverse Problems for Partial Differential Equations*. Springer, 1998.

[49] J. Jossinet, B. Lavandier, and D. Cathignol. The phenomenology of acousto-electric interaction signals in aqueous solutions of electrolytes. *Ultrasonics*, 36(1):607–613, 1998.

[50] J. Kaipio and E. Somersalo. *Statistical and Computational Inverse Problems*. Applied Mathematical Sciences. Springer, 2006.

[51] Y.J. Kim, O. Kwon, J.K. Seo, and E.J. Woo. Uniqueness and convergence of conductivity image reconstruction in magnetic resonance electrical impedance tomography. *Inverse Problems*, 19(5):1213–1225, 2003.

[52] A.I. Komech and A. Shubin. *Elements of the Modern Theory of Partial Differential Equations*. Springer, 1999.

[53] C.S. Kubrusly. *Spectral Theory of Operators on Hilbert Spaces*. Springer, 2012.

[54] P. Kuchment. Mathematics of hybrid imaging: A brief review. In *The Mathematical Legacy of Leon Ehrenpreis*, pages 183–208. Springer, 2012.

[55] P. Kuchment and L. Kunyansky. Synthetic focusing in ultrasound modulated tomography. *IPI*, 4(4):665–673, Sep 2010.

[56] P. Kuchment and L. Kunyansky. 2D and 3D reconstructions in acousto-electric tomography. *Inverse Problems*, 27(5):055013, 2011.

[57] P. Kuchment and D. Steinhauer. Stabilizing inverse problems by internal data. *Inverse Problems*, 28(8):084007, 2012.

[58] O. Kwon, H. Pyo, J.K. Seo, and E.J. Woo. Mathematical framework for B_z-based MREIT model in electrical impedance imaging. *Computers & Mathematics with Applications*, 51(5):817–828, 2006.

[59] O. Kwon, E.J. Woo, J.R. Yoon, and J.K. Seo. Magnetic resonance electrical impedance tomography (MREIT): Simulation study of J-substitution algorithm. *Biomedical Engineering, IEEE Transactions on*, 49(2):160–167, 2002.

[60] H.P. Langtangen. *Computational Partial Differential Equations: Numerical Methods and Diffpack Programming*. Texts in Computational Science and Engineering. Springer, 2003.

[61] B. Lavandier, J. Jossinet, and D. Cathignol. Experimental measurement of the acousto-electric interaction signal in saline solution. *Ultrasonics*, 38(9):929 – 936, 2000.

[62] C.L. Lawson and R.J. Hanson. *Solving Least Squares Problems*. Classics in Applied Mathematics. Society for Industrial and Applied Mathematics, 1995.

[63] L.P. Lebedev and I.I. Vorovich. *Functional Analysis in Mechanics*. Springer Monographs in Mathematics. Springer, 2003.

[64] P. Lindqvist. Notes on the p-Laplace equation. Lecture note, 2006.

[65] A. Logg, K.-A. Mardal, and G. Wells. *Automated Solution of Differential Equations by the Finite Element Method: The FEniCS Book*. Lecture Notes in Computational Science and Engineering. Springer, 2012.

[66] P.W. Macfarlane, A. van Oosterom, O. Pahlm, P. Kligfield, M. Janse, and J. Camm. *Comprehensive Electrocardiology*. Comprehensive Electrocardiology. Springer, 2010.

[67] N.G. Meyers. An L^p-estimate for the gradient of solutions of second order elliptic divergence equations. *Annali della Scuola Normale Superiore di Pisa-Classe di Scienze*, 17(3):189–206, 1963.

[68] D. Miklavčič, N. Pavšelj, and F.X. Hart. Electric properties of tissues. *Wiley encyclopedia of biomedical engineering*, 2006.

[69] F. Monard and G. Bal. Inverse anisotropic diffusion from power density measurements in two dimensions. *Inverse Problems*, 28(8):084001, 2012.

[70] F. Monard and G. Bal. Inverse anisotropic conductivity from power densities in dimension $n \geq 3$. *Communications in Partial Differential Equations*, 38(7):1183–1207, 2013.

[71] C. Montalto and P. Stefanov. Stability of coupled-physics inverse problems with one internal measurement. *Inverse Problems*, 29(12):125004, 2013.

[72] A. Moradifam, A. Nachman, and A. Timonov. A convergent algorithm for the hybrid problem of reconstructing conductivity from minimal interior data. *Inverse Problems*, 28(8):084003, 2012.

[73] J.L. Mueller and S. Siltanen. *Linear and Nonlinear Inverse Problems with Practical Applications*. Computational Science and Engineering. SIAM, 2012.

[74] A. Nachman, A. Tamasan, and A. Timonov. Conductivity imaging with a single measurement of boundary and interior data. *Inverse Problems*, 23(6):2551, 2007.

[75] A. Nachman, A. Tamasan, and A. Timonov. Recovering the conductivity from a single measurement of interior data. *Inverse Problems*, 25(3):035014, 2009.

[76] A. Nachman, A. Tamasan, and A. Timonov. Current density impedance imaging. *Tomography and Inverse Transport Theory. Contemp. Math*, 559:135–150, 2011.

[77] F. Natterer. *The Mathematics of Computerized Tomography*. Classics in Applied Mathematics. Society for Industrial and Applied Mathematics, 2001.

[78] S.H. Oh, B.I. Lee, E.J. Woo, S.Y. Lee, M.H. Cho, O. Kwon, and J.K. Seo. Conductivity and current density image reconstruction using harmonic B_z algorithm in magnetic resonance electrical impedance tomography . *Physics in Medicine and Biology*, 48(19):3101–3116, Oct 2003.

[79] C. Park, O. Kwon, E.J. Woo, and J.K. Seo. Electrical conductivity imaging using gradient B_z decomposition algorithm in magnetic resonance electrical impedance tomography (MREIT). *Medical Imaging, IEEE Transactions on*, 23(3):388–394, 2004.

[80] J.N. Reddy. *An Introduction to Continuum Mechanics.* An Introduction to Continuum Mechanics. Cambridge University Press, 2013.

[81] M. Reed and B. Simon. *Fourier Analysis, Self-Adjointness.* Number II in Methods of Modern Mathematical Physics. Academic Press, 1975.

[82] W. Rudin. *Functional Analysis.* International series in pure and applied mathematics. McGraw-Hill, 2006.

[83] O. Scherzer. *Handbook of Mathematical Methods in Imaging: Vol. 1.* Springer Reference. Springer, 2011.

[84] J.K. Seo and E.J. Woo. Magnetic Resonance Electrical Impedance Tomography (MREIT). *SIAM Rev.*, 53(1):40–68, Jan 2011.

[85] J.K. Seo, J.-R. Yoon, E.J. Woo, and O. Kwon. Reconstruction of conductivity and current density images using only one component of magnetic field measurements. *Biomedical Engineering, IEEE Transactions on*, 50(9):1121–1124, 2003.

[86] J.K. Seo, J.-R. Yoon, E.J. Woo, and O. Kwon. Reconstruction of conductivity and current density images using only one component of magnetic field measurements. *IEEE Transactions on Biomedical Engineering*, 50(9):1121–1124, Sep 2003.

[87] A. Shubin. *Pseudodifferential Operators and Spectral Theory.* Pseudodifferential Operators and Spectral Theory. Springer, 2001.

[88] R. Snieder and J. Trampert. *Inverse problems in geophysics.* Springer, 1999.

[89] V.A. Solonnikov. Overdetermined elliptic boundary-value problems. *J Math Sci*, 1(4):477–512, 1973.

[90] E. Somersalo, M. Cheney, and D. Isaacson. Existence and uniqueness for electrode models for electric current computed tomography. *SIAM Journal on Applied Mathematics*, 52(4):pp. 1023–1040, 1992.

[91] R.S. Strichartz. *A Guide to Distribution Theory and Fourier Transforms.* World Scientific, 2003.

[92] L. Tartar. *An Introduction to Sobolev Spaces and Interpolation Spaces.* Lecture notes of the Unione Matematica Italiana. Springer, 2007.

[93] M.E. Taylor. *Pseudodifferential Operators and Nonlinear PDE*. Birkhäuser Boston, 1991.

[94] M.E. Taylor. *Partial Differential Equations III: Nonlinear Equations*. Applied Mathematical Sciences. Springer, 2010.

[95] F. Treves. *Introduction to Pseudodifferential and Fourier Integral Operators*. Springer, 1980.

[96] T. Widlak and O. Scherzer. Stability in the linearized problem of quantitative elastography. *arXiv preprint arXiv:1406.0291*, 2014.

[97] M. Xu and L.V. Wang. Photoacoustic imaging in biomedicine. *Review of scientific instruments*, 77(4):041101, 2006.

[98] H. Zhang and L.V. Wang. Acousto-electric tomography. In *Biomedical Optics 2004*, pages 145–149. International Society for Optics and Photonics, 2004.